Alma Mater Studiorum - Università di Bologna

School of Science
Department of Physics and Astronomy
Master Degree Programme in Astrophysics and Cosmology

Stellar Density Profile and Central Black Hole Mass in Globular Clusters

Graduation Thesis

Presented by:
Filippo Bucci

Supervisor:
Chiar.mo Prof. Carlo Nipoti

Co-supervisor:
Chiar.mo Prof. Luca Ciotti

Academic year 2024-2025
Graduation date III

To know what you know and to know what you do not know, that is true wisdom.

Confucius

Abstract

One of the most puzzling open issues in modern astrophysics is the paucity of evidence for the existence of intermediate-mass black holes (IMBHs). These are black holes (BHs) lying in the mass range between 10^2 and 10^5 $M_\odot$. While the astrophysical community is virtually certain of the existence of stellar-mass BHs ($< 10^2$ $M_\odot$) and of supermassive BHs ($10^5 - 10^{10}$ $M_\odot$), the search for BHs in the remaining gap of the mass spectrum has provided very few definitive results so far. Globular clusters (GCs) are among the best candidates for hosting IMBHs: extrapolating Magorrian's relation down to GCs' masses, BHs of $10^2 - 10^3$ $M_\odot$ are expected to be found at their centres. Although many observational efforts have been employed to find them, only very debated detections have been made, thus far.

On the theoretical side, one way to support this search is to study models for spherical, isotropic, one-component stellar systems with a central Keplerian potential. These systems represent a zeroth-order approximation of GCs hosting central IMBHs. A basic requirement for a model to be physically acceptable is the phase-space consistency, i.e., that its distribution function (DF) is everywhere non-negative. The simplicity of spherical, isotropic models permits an easy computation of the DF, once a stellar density profile is assumed, through the well-known Eddington's formula. Therefore, determining their phase-space consistency is straightforward. As a compelling consequence, one can say which density profiles *cannot* host a central BH of a given mass, if the velocity distribution is isotropic. This can help in ruling out some GCs as possible hosts of IMBHs, or at least in placing upper limits on the putative BHs' masses.

This thesis explores a variety of models of this kind, using not only direct computations of the DF, but also some sufficient or necessary conditions for the consistency. These conditions proved particularly powerful for γ-models with a dominant BH, constraining their consistency over nearly the entire parameter space. Numerical evaluations of the DF completed the work, showing that isotropic γ-models with $\gamma \geq 1/2$ are consistent, while those with $\gamma < 1/2$ are not, independently of the BH's mass, confirming previous findings.

I provide alternative proofs, in special cases, of a theorem proven by An & Evans (2006), showing that no spherical, isotropic model with a central density profile flatter than $r^{-1/2}$ can host a central BH. My theorems highlight that the inconsistency arises

at high relative energies, and were used to rule out the consistency of Sérsic models with Sérsic index $n < 2$, Einasto models, Plummer models and King models, when they are isotropic and a BH is present. In contrast, a direct inspection of the DF shows that isotropic Sérsic models with $n \geq 2$ are consistent for all BH masses.

King models are often used to describe the surface brightness profiles of GCs, so I discussed under what circumstances they could be used to constrain IMBHs' masses based on inconsistency arguments. To understand how close to the centre observations should go to accomplish this, I constructed models that resemble King profiles, but have a $r^{-7/4}$ cusp in the innermost regions. Then, I computed the minimum size of the cusp to prevent inconsistency as a function of the BH-to-stellar mass ratio. I estimated that these models may be used to exclude the presence of BHs more massive than about 0.5% of the host cluster's mass in the closest and most massive systems.

This thesis is a first, preparatory analysis of the consistency of models for GCs with central IMBHs, and of its observational implications. It provides a solid basis for future consistency analyses of more complex and realistic models, including, e.g., orbital anisotropy or multiple mass components, which can help constrain the existence of IMBHs at the centres of GCs. Studies of this kind can complement dynamical modelling of GCs based on the Jeans equations, as the phase-space consistency of the solutions of these equations is not guaranteed.

Contents

Acronyms

BH black hole 1–3, 12–28, 31–45, 47–50, 52–71, 73–81, 83–85

BWK Bahcall-Wolf-King 45, 47–50, 52–56, 63, 69–71

CBE *collisionless Boltzmann equation* 7

DF *distribution function* 6–16, 18–28, 31–37, 40–45, 47–50, 52, 54, 55, 60–63, 65–71, 73–79, 81

DM dark matter 4, 6, 13, 27, 28

ELT *Extremely Large Telescope* 3, 41

GC globular cluster 3–7, 12–14, 16, 28–30, 33, 38, 40, 41, 44, 45, 48, 52–54, 56, 61–64, 66–71

HST *Hubble Space Telescope* 16, 41

IMBH intermediate-mass black hole 2–4, 13, 14, 44, 52, 54, 63

JWST *James Webb Space Telescope* 3, 41

LHS left-hand side 84

LISA *Laser Interferometer Space Antenna* 2

NC necessary condition 11, 19, 26, 78, 82, 83, 85

OM Osipkov-Merritt 10, 11, 16, 19, 20, 27, 64, 65, 78, 82–85

RHS right-hand side 47, 76, 84, 85

SSC strong sufficient condition 12, 19–22, 26

WSC weak sufficient condition 11, 12, 19, 20, 26, 83–85

List of Figures

List of Tables

Chapter 1

Introduction

In this chapter, I provide a brief overview of the current knowledge regarding the existence of the so-called intermediate-mass black holes and their presence in globular clusters, besides highlighting their astrophysical importance (Section 1.1). Furthermore, in Section 1.2, I recall the main theoretical concepts of stellar dynamics that will be used in the following chapters, and I introduce the notation. In Section 1.3, I describe the main assumptions adopted in this work and discuss their validity. Finally, I dedicate Section 1.4 to a summary of the main contents of the thesis.

1.1 The Scientific Case

1.1.1 Intermediate-Mass Black Holes

Einstein's theory of general relativity predicts that any object moves according to the curvature of the spacetime. Photons are no exception to this, and, in the presence of a sufficient curvature, they can be trapped, with no hope of reaching anyone's eyes. The objects that would be able, if they exist, to provide such a strong gravitational influence were called black holes (BHs). The first theoretical description of a BH came from Schwarzschild (1916), but it took nearly 50 years to obtain the first observational evidence for their existence, with the discovery of X-ray binaries (Giacconi et al. 1962) and quasi-stellar objects (Schmidt 1963).

Today, the astrophysical community is virtually certain of the existence of *stellar-mass BHs* (with mass $M_\bullet \lesssim 100\ \mathrm{M}_\odot$), which are the endpoints of the evolution of massive stars, and of *supermassive BHs* ($10^5\ \mathrm{M}_\odot \lesssim M_\bullet \lesssim 10^{10}\ \mathrm{M}_\odot$), found at the centres of most galaxies (e.g., Merritt 2013, Genzel et al. 2024). Our current understanding of supermassive BH formation suggests that at least some of these objects did not form

as they are, but they grew out of lighter seed BHs. However, stellar-mass BHs are too light to explain the formation of 10^{10} $M_\odot$ BHs in the first billion years of the Universe (e.g., Wu et al. 2015). If this picture is correct, intermediate-mass black holes (IMBHs) with 100 $M_\odot \lesssim M_\bullet \lesssim 10^5$ $M_\odot$ should have existed, at some point in the past. Since the current observations are not able to directly probe them at high redshift, we can look in the local universe for those that failed to grow into supermassive BHs (see Mezcua 2017, and references therein). Possible sites hosting them are dwarf galaxies, globular clusters and the halos or spiral arms of large galaxies, where ultraluminous X-ray sources are sometimes detected (Mezcua 2017). Despite the intensive searches of the last decades, the only relatively secure detections of IMBHs came from a couple of gravitational wave observations of BH-BH mergers, still probing only the low mass end of the IMBH range (Abbott et al. 2020; The LIGO Scientific Collaboration et al. 2025). As of yet, no claimed detection of an IMBH with other methods has been confirmed (Greene et al. 2020; see also, e.g., Paynter et al. 2021, Della Croce et al. 2024, Häberle et al. 2024, Bañares-Hernández et al. 2025 for more recent observational studies).

1.1.2 Importance of Intermediate-Mass Black Hole Searches

As mentioned above, IMBHs are thought to be the seeds for the supermassive BHs that reside at the centres of a large fraction of galaxies. Hence, the detection of IMBHs could constrain the possible seed formation mechanisms, providing also insights into the BH-galaxy co-evolution. This can be done, for example, by extending known scaling relations to lower BH masses and by estimating IMBH occupation fractions in various environments (Greene et al. 2020). In the future, more direct evidence of the early seeding mechanisms will be provided by gravitational wave experiments like the *Laser Interferometer Space Antenna* (LISA), sensitive to IMBH-IMBH mergers up to redshift $z \approx 20$ (e.g., Sesana et al. 2011).

Several studies have also shown that IMBHs can play an important role in the dense stellar systems, if any, where they formed (e.g., Baumgardt et al. 2005; Trenti et al. 2007; Giersz et al. 2015).

Finally, some galaxies have been found to host off-nuclear X-ray sources with luminosities above the Eddington limit for BHs of about 10 $M_\odot$ (Mezcua 2017). Many of these ultraluminous X-ray sources have been recently associated with super-Eddington accreting stellar-mass BHs or neutron stars, but the debate is still open, especially for the most luminous ones (Greene et al. 2020). Their identification as IMBHs may shed light on the spectral features of accreting IMBHs, thus helping constrain the impact of mini-quasars on the Universe's reionisation (e.g., Madau & Haardt 2015).

1.1.3 Intermediate-Mass Black Holes in Globular Clusters

The most valuable candidates for hosting IMBHs are globular clusters (GCs), dwarf galaxies and ultraluminous X-ray sources. This thesis focuses on the aspects regarding the search for IMBHs in GCs. The motivations for expecting this class of BHs to reside at their centres are various.

- A simplistic extrapolation of the Magorrian et al. (1998) relation between the central BH's mass and the host spheroid's mass holding for galaxies suggests that GCs with total stellar mass $M_{\rm GC} \approx 10^5 - 10^6$ $\rm M_\odot$ should contain central BHs of $10^2 - 10^3$ $\rm M_\odot$.

- Several mechanisms have been proposed for the formation of IMBHs in dense environments such as the central regions of GCs. These include slow accretion of a stellar-mass BH by subsequent mergers (Miller & Hamilton 2002) and rapid formation through gravitational runaway merging of massive stars (Portegies Zwart & McMillan 2002).

- Some GCs are thought to be the disrupted nuclei of dwarf galaxies, where an IMBH may have previously formed via galaxy evolution processes (e.g., Freeman 1993).

Intensive observational campaigns have been carried out in the last decades with the aim of finding BHs of intermediate mass within the Galactic GCs and a few others in the Local Group. Despite the many claimed detections, none have been confirmed yet (Greene et al. 2020, Sec. 3.5; the recent detection by Häberle et al. 2024 in the cluster ω Centauri has recently been questioned by Bañares-Hernández et al. 2025). Moreover, no significant accretion signature has been identified, allowing Tremou et al. (2018) to place a $10 - 15\%$ upper limit on the occupation fraction of 10^3 $\rm M_\odot$ BHs within the Galactic GCs. However, the absence of radio or X-ray emission does not yield definitive proof of the absence of an IMBH, due to the many uncertainties regarding the accretion rate, the gas density, the radiative efficiency, and so on.

One of the main limitations concerning dynamical studies is the small size of the sphere of influence of a putative IMBH in a GC, no more than $1'' - 2''$ (see Section 2.5.3). However, the situation might improve in the next years. First of all, the outstanding sensitivity of the recently-launched *James Webb Space Telescope* (JWST), combined with its sub-arcsecond resolution, may increase the number of stars detected close to the clusters' centres. Moreover, the upcoming *Extremely Large Telescope* (ELT) will

reach an unprecedented angular resolution, allowing us to probe the innermost regions of the Galactic GCs, despite the highly crowded fields.

The current state of the art and the future perspectives thus motivate my thesis work, whose main objective is to understand which features of the stellar density profiles are a signature of the *absence* of an IMBH in a GC. But before being more specific, let me recall the relevant aspects of stellar dynamics and introduce the notation.

1.2 Concepts of Stellar Dynamics

A *stellar system*, in a broad sense, is an assembly of point masses that interact through gravity (Binney & Tremaine 2008). Stars (and stellar remnants) can indeed be treated as point masses for many astrophysical applications, and physical collisions between them are so rare that their motion is only determined by their mutual gravitational attraction (e.g., see Ciotti 2021, Exercise 1.1). In the following, I will refer to the particles composing a stellar system as stars, for simplicity. Still, my results hold for any system that falls within the definition of stellar system, e.g., a dark matter (DM) halo.

In the vast majority of applications (and in the current one), relativistic effects are not important, and the behaviour of stellar systems is dictated by Newton's laws of motion and Newton's law of gravitation. This behaviour is studied by the field of *stellar dynamics*.

Since we are dealing only with gravitational forces, implying that the particles' orbits are independent of their mass, in the following, when I mention quantities such as the energy (total and kinetic) and the angular momentum, I mean their analogues per unit mass, if not otherwise stated.

1.2.1 The Smooth Potential

The gravitational field (force per unit mass) acting on the i-th particle of a system of N point particles of mass m_j at positions $\boldsymbol{x}_j$ in an inertial reference frame S_0 is

$$\boldsymbol{g}_{\rm true}(\boldsymbol{x}_i) = -G \sum_{j=1;\, j\neq i}^{N} m_j \frac{\boldsymbol{x}_i - \boldsymbol{x}_j}{\|\boldsymbol{x}_i - \boldsymbol{x}_j\|^3}, \tag{1.1}$$

where $G \simeq 6.67 \times 10^{-8}\ \mathrm{cm^3\,s^{-2}\,g^{-1}}$ is the universal gravitational constant and $\|\ldots\|$ is the standard Euclidean norm. The associated equations of motion in S_0 are

$$\frac{\mathrm{d}^2\boldsymbol{x}_i}{\mathrm{d}t^2} = \boldsymbol{g}_{\mathrm{true}}(\boldsymbol{x}_i), \quad i = 1, \ldots, N, \tag{1.2}$$

where the independent variable t represents time. The problem of solving this system of ordinary differential equations is commonly known as the N-body problem. In general, this problem is not solvable analytically for $N > 2$, as is the case of the stellar systems we wish to study (e.g., for a GC, $N \approx 10^5 - 10^6$). Moreover, computing $\boldsymbol{g}_{\mathrm{true}}$ for each timestep of a time integration for the large number of particles we are considering would be computationally expensive.

Fortunately, it can be shown that in many situations the true gravitational field $\boldsymbol{g}_{\mathrm{true}}$ can be substituted with a field $\boldsymbol{g}$ produced by a continuous mass density distribution $\rho(\boldsymbol{x}, t)$, taken to be a good description of the true 'granular' mass density distribution. The (smooth) gravitational potential is the scalar function $\Phi(\boldsymbol{x}, t)$ such that $\boldsymbol{g} = -\nabla\Phi$, which is related to the density producing the field $\boldsymbol{g}$ by Poisson's equation

$$\triangle\Phi(\boldsymbol{x}, t) = 4\pi G\rho(\boldsymbol{x}, t), \tag{1.3}$$

where $\triangle$ is the Laplace operator.

The orbit of a test star moving in the smooth potential is a good approximation of the true orbit for timescales much shorter than (Binney & Tremaine 2008; Ciotti 2021)

$$t_{\mathrm{2b}} \approx \frac{0.1N}{\ln N} t_{\mathrm{cross}}, \tag{1.4}$$

where the subscript '2b' stands for *two-body relaxation*, the process driving the diffusion of a star's velocity due to the gravitational encounters with the other stars in the system. In Eq. (1.4), $t_{\mathrm{cross}} \approx R/v$ is the crossing time, where R is the size of the system and v is the typical velocity of a star. A stellar system with an age much smaller than t_{2b} is said to be *collisionless*.

In a GC, $t_{\mathrm{cross}} \approx 0.5$ Myr and $N \approx 10^5 - 10^6$ (e.g., see Table 1.3 of Binney & Tremaine 2008), so $t_{\mathrm{2b}} \approx 10^8 - 10^9$ yr, which is smaller than the typical age of these systems, about 10 Gyr. Thus, evolutionarily speaking, two-body relaxation plays an important role in shaping the appearance of a GC. However, their evolution occurs on timescales much larger than t_{cross}, so they can be modelled as evolving through a series of stationary, collisionless states, because the potential is approximately constant and smooth along a star's orbit (e.g., Hamilton et al. 2018).

In addition, the collisionless approximation is thought to be valid for systems made by non-baryonic DM particles, for which weak interactions between the particles are negligible and N is extremely large, in any astrophysical context.

1.2.2 The Distribution Function

When modelling a stellar system such as a GC, it is impractical to follow the orbit of each star, even in the collisionless approximation. It is more useful to describe the system on statistical grounds, introducing the one-particle phase-space distribution function $f(\boldsymbol{x}, \boldsymbol{v}, t)$, or simply the *distribution function* (DF), as the mass density of stars at the point $(\boldsymbol{x}, \boldsymbol{v})$ of the one-particle phase space at time t. By one-particle phase space, I mean the 6-dimensional position-velocity space of one particle (henceforth, I will refer to this as the *phase space*).

This definition is equivalent to others given in the literature by a simple rescaling of f. For example, let us assume that all N stars have the same mass. Given that

$$M = \int_{\mathbb{R}^6} f \mathrm{d}^3\boldsymbol{v} \mathrm{d}^3\boldsymbol{x} \tag{1.5}$$

is the total stellar mass of the system, the function $f(\boldsymbol{x}, \boldsymbol{v}, t)/M$ gives the probability density of finding a star at $(\boldsymbol{x}, \boldsymbol{v})$, while $f(\boldsymbol{x}, \boldsymbol{v}, t)N/M$ gives the number density of stars in the phase space.

A one-component (or single-component) stellar system is constituted by N identical point particles of mass m. In general, a stellar system can be made of more mass components (e.g., stars of different masses, metallicities, ages, etc.), each containing identical point masses. In such cases, we talk about a multi-component stellar system. For the sake of simplicity, in this thesis, we will restrict ourselves to the case of one-component systems.

The conservation of mass in the phase space implies that, along any given orbit, f must obey Boltzmann's equation

$$\frac{\partial f}{\partial t} + \langle \boldsymbol{v}, \nabla_{\boldsymbol{x}} f \rangle - \langle \nabla_{\boldsymbol{x}} \Phi_{\mathrm{T}}, \nabla_{\boldsymbol{v}} f \rangle = C[f], \tag{1.6}$$

where $\langle \ldots, \ldots \rangle$ is the usual inner product in $\mathbb{R}^3$, $\nabla_{\boldsymbol{x}}$ and $\nabla_{\boldsymbol{v}}$ are the Cartesian gradient operators with respect to $\boldsymbol{x}$ and $\boldsymbol{v}$, respectively, and $\Phi_{\mathrm{T}} = \Phi + \Phi_{\mathrm{ext}}$, with $\Phi_{\mathrm{ext}}(\boldsymbol{x}, t)$ being a smooth external potential not produced by the mass distribution of the stellar system described by f. The *collision term* $C[f]$ appears to account for the phase-space diffusion of the particles moving in the true potential rather than in the smoothed one. Eq. (1.6) is quite complicated, but fortunately, we can make some simplifying

assumptions.

The first is that the system is collisionless, so $C[f] = 0$. As argued above, this is not strictly true for GCs, but it provides a good (and widely used) approximation when studying their 'instantaneous' structure, since gravitational encounters are negligible over the timescale of a stellar orbit $t_{\rm cross}$ (e.g., Meylan & Heggie 1997). Hence, Eq. (1.6) reduces to the *collisionless Boltzmann equation* (CBE)

$$\frac{\partial f}{\partial t} + \langle \boldsymbol{v}, \nabla_{\boldsymbol{x}} f \rangle - \langle \nabla_{\boldsymbol{x}} \Phi_{\rm T}, \nabla_{\boldsymbol{v}} f \rangle = 0. \tag{1.7}$$

The minimum requirement for a model to be acceptable is the *consistency*. A collisionless, single-component stellar system is said to be consistent if and only if its DF satisfies Eq. (1.7) and

$$f(\boldsymbol{x}, \boldsymbol{v}, t) \geq 0, \quad \forall (\boldsymbol{x}, \boldsymbol{v}) \in \mathbb{R}^6, \ \forall t \in \mathbb{R}, \tag{1.8}$$

$$\triangle \Phi(\boldsymbol{x}, t) = 4\pi G \rho(\boldsymbol{x}, t), \tag{1.9}$$

where

$$\rho(\boldsymbol{x}, t) = \int_{\mathbb{R}^3} f(\boldsymbol{x}, \boldsymbol{v}, t) \mathrm{d}^3 \boldsymbol{v}, \tag{1.10}$$

is the stellar mass density distribution of stars in real space. A model that does not satisfy the above requirements must be rejected as unphysical. If a stellar system is self-gravitating (i.e., $\Phi_{\rm ext} = 0$) and consistent, it is said to be *self-consistent*.

The second assumption we adopt is that of equilibrium. In other words, $\partial f / \partial t = 0$. Thus, all quantities derived from f (and $\Phi_{\rm ext}$) are independent of time. Because of the fairly short crossing time of GCs, stars inside them have completed many revolutions since the clusters formed, suggesting that a (nearly) stationary distribution has been reached (e.g., Meylan & Heggie 1997). Eq. (1.7) thus reduces to the CBE for a stationary system

$$\langle \boldsymbol{v}, \nabla_{\boldsymbol{x}} f \rangle - \langle \nabla_{\boldsymbol{x}} \Phi_{\rm T}, \nabla_{\boldsymbol{v}} f \rangle = 0. \tag{1.11}$$

A theorem first stated by Jeans (1915) restricts the possible forms for the DF of a stationary, collisionless stellar system (e.g., see Binney & Tremaine 2008, Ciotti 2021).

Theorem 1.1 (Jeans' theorem)**.** *Any steady-state solution of the CBE depends on the phase-space coordinates only through global, regular integrals of motion in the total potential, and any function of such integrals of motion is a solution of the stationary CBE.*

A global integral of motion in the potential $\Phi_{\rm T}$ is a function $I(\boldsymbol{x}, \boldsymbol{v})$ which is conserved

along any orbit $[\boldsymbol{x}(t), \boldsymbol{v}(t)]$ in Φ_{T}. An integral of motion is said to be regular if it is continuous and has continuous first-order partial derivatives. In the following, we will exploit this theorem to build models where the DF depends on the integrals of motion arising from the assumed (spatial and temporal) symmetries of the total potential.

1.2.3 Moments of the Distribution Function

In this subsection, I summarise the main velocity moments of the DF relevant for our purposes.

First, the stellar mass density $\rho(\boldsymbol{x}, t)$, defined in Eq. (1.10), is the zeroth-order moment of f. It represents the mass density of stars in a volume element centred in the position $\boldsymbol{x}$ at time t.

The first-order moments are obtained by multiplying $f(\boldsymbol{x}, t)$ by the i-th components (in an orthogonal coordinate system) of the velocity, and integrating over the velocity space. This, divided by $\rho(\boldsymbol{x}, t)$, gives the i-th component of the mean stellar velocity at position $\boldsymbol{x}$ at time t:

$$\overline{v}_i(\boldsymbol{x}, t) = \frac{1}{\rho(\boldsymbol{x}, t)} \int_{\mathbb{R}^3} f(\boldsymbol{x}, \boldsymbol{v}, t) v_i \, \mathrm{d}^3\boldsymbol{v}. \tag{1.12}$$

The mean stellar velocity is then $\overline{\boldsymbol{v}} = (\overline{v}_1, \overline{v}_2, \overline{v}_3)$, and indicates the velocity of *streaming motions* in the stellar system.

The second-order velocity moments relevant for us are the components of the so-called *velocity dispersion tensor*, namely,

$$\sigma_{ij}^2(\boldsymbol{x}, t) = \frac{1}{\rho(\boldsymbol{x}, t)} \int_{\mathbb{R}^3} f(\boldsymbol{x}, \boldsymbol{v}, t)(v_i - \overline{v}_i)(v_j - \overline{v}_j) \, \mathrm{d}^3\boldsymbol{v}. \tag{1.13}$$

This tensor quantifies the dispersion of the stellar velocities about the mean velocity along each direction, at given position $\boldsymbol{x}$ and time t.

1.2.4 Spherical Systems

Consider a stationary, collisionless stellar system in a spherically symmetric total gravitational potential $\Phi_{\mathrm{T}}(r)$, where $r \equiv \|\boldsymbol{x}\|$. The symmetries of the potential tell us it admits four global integrals of motion: the energy (per unit mass) $E = \Phi_{\mathrm{T}} + v^2/2$, where $v \equiv \|\boldsymbol{v}\|$, and the components of the (specific) angular momentum $\boldsymbol{L} = \boldsymbol{x} \times \boldsymbol{v}$, where $\times$ denotes the cross product. From Jeans' theorem, we know that we can use them as arguments of the DF.

In fact, it is more convenient to work with the *relative* energy

$$\mathcal{E} \equiv -E = \Psi_{\rm T} - \frac{v^2}{2}, \tag{1.14}$$

where $\Psi_{\rm T} = \Psi + \Psi_{\rm ext} \equiv -\Phi_{\rm T}$ is the total relative potential, $\Psi \equiv -\Phi$ is the stellar relative potential and $\Psi_{\rm ext} \equiv -\Phi_{\rm ext}$ is the external relative potential. Throughout this work, I will adopt the convention for which $\Phi(\boldsymbol{x}) \to 0$ as $\|\boldsymbol{x}\| \to \infty$, which is valid for all models that will be treated.[1] Therefore, the relative potentials are always positive, and gravitationally bound stars have $\mathcal{E} > 0$. In addition, stars with higher $\mathcal{E}$ are more tightly 'bound' to the stellar system.

The most general form for the DF of a stationary, collisionless stellar system in a spherically symmetric potential is $f = f(\mathcal{E}, \boldsymbol{L})$ (Lynden-Bell 1960, 1962a). However, I restrict the analysis to systems that have complete spherical symmetry (and are thus non-rotating). The possible choices left for the DF are $f = f(\mathcal{E})$ or $f = f(\mathcal{E}, L)$, with $L \equiv \|\boldsymbol{L}\|$ (Binney & Tremaine 2008). In the following, I shall sometimes refer to such systems simply as *spherical systems*, meaning that they are spherically symmetric in all properties.

Another concept that is useful to introduce here is the cumulative mass profile, namely, the mass enclosed within a radius r. For a spherical system, this is readily given by

$$M(r) = 4\pi \int_0^r \rho(\xi)\xi^2 \mathrm{d}\xi. \tag{1.15}$$

Ergodic Spherical Systems

When the DF depends only on the relative energy, it is said to be *ergodic*. We refer to systems with such a DF as ergodic systems. In order to consider only gravitationally bound stars, we define $f(\mathcal{E}) = h(\mathcal{E})\theta(\mathcal{E}-\mathcal{E}_{\rm t})$, where $\theta(x)$ is the Heaviside step function and $\mathcal{E}_{\rm t} \geq 0$ is the truncation relative energy.[2] Consequently, $f(\mathcal{E}) = 0$ for $\mathcal{E} \leq \mathcal{E}_{\rm t}$. If $\mathcal{E}_{\rm t} > 0$, the system is spatially truncated beyond the truncation radius $r_{\rm t}$ at which $\Psi_{\rm T} = \mathcal{E}_{\rm t}$. This is because a star with relative energy $\mathcal{E}$ has $\Psi_{\rm T}(r) = \mathcal{E} + v^2/2 \geq \mathcal{E} \equiv \Psi_{\rm T}(r_{\mathcal{E}})$, implying that the star is confined within a distance $r_{\mathcal{E}}$ from the system's centre, since $\Psi_{\rm T}$ is necessarily a decreasing function of radius, from Newton's second theorem. Consequently, all stars are confined within the radius $r_{\rm t} \equiv r_{\mathcal{E}_{\rm t}}$. Note that $r_{\rm t} = \infty$, if $\mathcal{E}_{\rm t} = 0$, so the system is spatially untruncated.

[1] This can be done whenever the density distribution producing the potential Φ decreases faster than $\|\boldsymbol{x}\|^{-2}$, as $\|\boldsymbol{x}\| \to \infty$ (e.g., see Ciotti 2021, Sec. 2.1).

[2] The truncation relative energy is chosen to be non-negative to get $f = 0$ for unbound stars, which have $\mathcal{E} \leq 0$.

Ergodic systems have no streaming motions, and their velocity dispersion tensor is isotropic. In other words, $\overline{\boldsymbol{v}}(r) = 0$ and $\sigma_{ij}^2(r) = \sigma^2(r)\delta_{ij}$ everywhere, with δ_{ij} being the Kronecker's delta. Hereafter, I will sometimes refer to systems with such a velocity dispersion tensor as *isotropic systems*.

Remarkably, each pair $[\rho(r), \Psi_{\rm T}(r)]$ has a unique ergodic DF, given by Eddington's formula (Eddington 1916):

$$h(\mathcal{E}) = \frac{1}{\sqrt{8}\pi^2}\frac{\mathrm{d}}{\mathrm{d}\mathcal{E}}\int_{\mathcal{E}_{\rm t}}^{\mathcal{E}}\frac{\mathrm{d}\rho}{\mathrm{d}\Psi_{\rm T}}\frac{\mathrm{d}\Psi_{\rm T}}{\sqrt{\mathcal{E}-\Psi_{\rm T}}} \tag{1.16a}$$

$$= \frac{1}{\sqrt{8}\pi^2}\int_{\mathcal{E}_{\rm t}}^{\mathcal{E}}\frac{\mathrm{d}^2\rho}{\mathrm{d}\Psi_{\rm T}^2}\frac{\mathrm{d}\Psi_{\rm T}}{\sqrt{\mathcal{E}-\Psi_{\rm T}}} + \frac{\mathrm{d}\rho/\mathrm{d}\Psi_{\rm T}\,|_{\Psi_{\rm T}=\mathcal{E}_{\rm t}}}{\sqrt{8}\pi^2\sqrt{\mathcal{E}-\mathcal{E}_{\rm t}}}\,, \tag{1.16b}$$

where $\rho(\Psi_{\rm T})$ is the density computed at the radius at which the total relative potential is $\Psi_{\rm T}$.[3] Eq. (1.16b) can be obtained from Eq. (1.16a) by integrating by parts and then differentiating with respect to $\mathcal{E}$. Using this result, if the stellar density and the total potential are specified, one can recover (analytically or numerically) the ergodic DF.

As we will shortly see, Eq. (1.16) can be generalised to some classes of spherical, anisotropic systems.

Spherical Anisotropic Systems

In general, if $f = f(\mathcal{E}, L)$, the velocity dispersion tensor is not isotropic. Nonetheless, it is diagonal in spherical coordinates, with components $\sigma_r^2 \neq \sigma_\theta^2 = \sigma_\varphi^2$. The coordinates θ and φ are the polar angle and the azimuthal angle, respectively. Even in this case, there are no streaming motions.

The only way to have $\sigma_r^2 = \sigma_\theta^2 = \sigma_\varphi^2$ everywhere, is that f does not depend on L. Hence, a spherical, non-rotating, stationary, collisionless stellar system is isotropic if and only if it has an ergodic DF. When I talk about spherical, isotropic stellar systems, I mean ergodic spherical systems, while systems where $f = f(\mathcal{E}, L)$ will be addressed as spherical, anisotropic systems.

A special class of models amenable to density inversion to recover f are the Osipkov-Merritt (OM) models (Osipkov 1979; Merritt 1985). In these models, $f = h(Q)\theta(Q - Q_{\rm t})$, where $Q \equiv \mathcal{E} - L^2/(2r_{\rm a}^2)$ and $Q_{\rm t} \geq 0$.[4] The free parameter $r_{\rm a}$ is called the *anisotropy*

[3] This can always be done because, from Newton's second theorem, $\mathrm{d}\Psi_{\rm T}/\mathrm{d}r = -GM(r)/r^2$, so $\Psi_{\rm T}(r)$ is a strictly monotonic decreasing function of r; thus it is invertible.

[4] Since $Q = \mathcal{E} - L^2/(2r_{\rm a}^2)$, the minimum relative energy of stars with a given Q is $\mathcal{E}_{\rm min}(Q) = Q$. Therefore, systems with a given $Q_{\rm t}$ have a truncation relative energy $\mathcal{E}_{\rm t} = Q_{\rm t}$. This is why $Q_{\rm t} \geq 0$ (see Footnote 2).

radius. Defining the *anisotropy parameter*

$$\beta(r) \equiv 1 - \frac{\sigma_\theta^2(r)}{\sigma_r^2(r)}, \tag{1.17}$$

one can show that

$$\beta(r) = \frac{1}{1 + (r_\mathrm{a}/r)^2}, \tag{1.18}$$

for OM models. In general, a radially biased velocity distribution ($\sigma_r^2 > \sigma_\theta^2$) implies $\beta > 0$, a tangentially biased velocity distribution ($\sigma_r^2 < \sigma_\theta^2$) implies $\beta < 0$, and an isotropic velocity distribution leads to $\beta = 0$. It is evident that OM models are nearly isotropic for $r \ll r_\mathrm{a}$ and radially anisotropic for $r \gtrsim r_\mathrm{a}$.

The spherical, isotropic models can be recovered as a special case of the OM models posing $r_\mathrm{a} \to \infty$. Therefore, all the results presented here will apply to ergodic spherical systems as well, in the appropriate limit.

First, a generalisation of Eddington's formula exists:

$$h(Q) = \frac{1}{\sqrt{8}\pi^2} \frac{\mathrm{d}}{\mathrm{d}Q} \int_{Q_\mathrm{t}}^{Q} \frac{\mathrm{d}\varrho}{\mathrm{d}\Psi_\mathrm{T}} \frac{\mathrm{d}\Psi_\mathrm{T}}{\sqrt{Q - \Psi_\mathrm{T}}} \tag{1.19a}$$

$$= \frac{1}{\sqrt{8}\pi^2} \int_{Q_\mathrm{t}}^{Q} \frac{\mathrm{d}^2\varrho}{\mathrm{d}\Psi_\mathrm{T}^2} \frac{\mathrm{d}\Psi_\mathrm{T}}{\sqrt{Q - \Psi_\mathrm{T}}} + \frac{\mathrm{d}\rho/\mathrm{d}\Psi_\mathrm{T}\,|_{\Psi_\mathrm{T}=Q_\mathrm{t}}}{\sqrt{8}\pi^2\sqrt{Q - Q_\mathrm{t}}}, \tag{1.19b}$$

where $\varrho \equiv \rho(1 + r^2/r_\mathrm{a}^2)$ is the *augmented density* of the stellar component. Clearly, this reduces to Eq. (1.16) as $r_\mathrm{a} \to \infty$.

Eq. (1.19) allows one to determine the sign of f (and so the model's consistency) by explicitly evaluating it. However, this is often a non-trivial task, and it can sometimes be skipped by using some analytic consistency conditions.

As presented in Chapter 14 of Ciotti (2021), some necessary and sufficient conditions for the consistency of the OM models can be found without a direct inspection of the DF, if the stellar density and the total potential are known (Ciotti & Pellegrini 1992). In particular, there are a necessary condition (NC)

$$\frac{\mathrm{d}\varrho}{\mathrm{d}r} \leq 0\,, \quad \forall r \in [0, \infty[\,, \tag{1.20}$$

a weak sufficient condition (WSC)

$$\frac{\mathrm{d}}{\mathrm{d}r}\left[\frac{\mathrm{d}\varrho}{\mathrm{d}r}\frac{r^2}{M_\mathrm{T}(r)}\right] \geq 0\,, \quad \forall r \in [0, \infty[\,, \tag{1.21}$$

and a strong sufficient condition (SSC)

$$\frac{\mathrm{d}}{\mathrm{d}r}\left[\frac{\mathrm{d}\varrho}{\mathrm{d}r}\frac{r^2\sqrt{\Psi_{\mathrm{T}}(r)}}{M_{\mathrm{T}}(r)}\right] \geq 0\,, \quad \forall r \in [0,\infty[\,, \tag{1.22}$$

holding, in this form, for spatially untruncated systems ($\mathcal{E}_{\mathrm{t}} = 0$). Eq. (1.21) is called *weak* sufficient condition because the set of consistent models satisfying it is a subset of the set of consistent models satisfying the *strong* sufficient condition. This follows from the fact that Eq. (1.21) implies Eq. (1.22), so all models satisfying the WSC satisfy the SSC as well.

If we are interested in isotropic systems (as in the majority of this work), we can set $r_{\mathrm{a}} \to \infty$, so that $\varrho = \rho$. It is then evident that Eq. (1.20) entails that any consistent spherical model with an ergodic DF must have a radially decreasing density profile, independently of the total potential in which the stars move. This criterion is satisfied by all models discussed throughout this thesis.

1.3 Models' Assumptions

Here, I specify the assumptions I will adopt in the following chapters and discuss their validity in the scientific context of interest.

The main objective of this thesis is to understand which stellar density profiles for GCs are compatible with the presence of a central BH of various masses. This task will be accomplished, under the assumptions listed below, by constructing models through a 'ρ-to-f' approach. This means assuming a given density distribution and recovering the DF that produces such a density distribution in the given total potential. This method has the advantage of having quite direct control of the observables (e.g., the surface brightness distribution), but the inversion is only possible under special assumptions on the symmetry and the kinematic structure of the system. Still, we can exploit this technique to analyse the consistency of particular models with a central BH, and reject as unphysical those that lead to a somewhere negative underlying DF.

The central BH, of mass $M_\bullet$, is modelled as a point particle sourcing an external potential $\Phi_{\mathrm{ext}} = -GM_\bullet/r$. There are no particular assumptions made on the BH's mass, in general, but for this model to be realistic, we need the BH to be much heavier than the individual stars, so that it is approximately fixed at the centre of the system (e.g., see Merritt 2013, Sec. 5.4). For a typical GC with a (non-binary) 10^3 $\mathrm{M}_\odot$ central BH, we can safely neglect its motion, for our purposes (Lin & Tremaine 1980).

I point out that there may be degeneracy between a central, spherically symmetric

sub-cluster of dark stellar remnants and a central BH, as long as it is not resolvable (e.g., van der Marel & Anderson 2010; Zocchi et al. 2019). Therefore, models that result in being inconsistent rule out the presence of both these components, or, more generally, of any sufficiently small spherical mass distribution.

I neglect any other source of gravitational field, such as gas or DM, since they do not contribute significantly to the total mass budget in normal GCs. Their inclusion in the external potential could be used, for instance, to extend the present work to the study of dwarf galaxies with central IMBHs.

As mentioned in the previous section, I consider only spherical, non-rotating, single-component, collisionless stellar systems in equilibrium, for which Jeans' theorem holds and a smooth potential can be used. In particular, in Chapters 2 and 3, I analyse models with an ergodic DF, and thus with an isotropic velocity dispersion tensor.

The fact that GCs should be quite dynamically old suggests that they should have relatively little rotation and a shape close to spherical. Observations confirm this, as a rough approximation, although signatures of flattening (e.g., White & Shawl 1987) and of ordered rotation (e.g., Bianchini et al. 2013, 2018; Kamann et al. 2018) are being detected in an increasing number of cases.

The two-body relaxation might justify the assumption of an ergodic DF in the context of GCs, since this process tends to isotropise the stellar orbits. However, isotropy might have been attained only in the central regions, where $t_{2\mathrm{b}}$ is shorter, and this is still not guaranteed (e.g., Zocchi et al. 2016a). Nonetheless, I stick with this assumption, for simplicity, and I postpone the inclusion of orbital anisotropy to a brief discussion in Chapter 4 and future works.

The relatively rapid dynamical evolution of GCs can also produce a significant *mass segregation*, where more massive stars and remnants sink to the central regions (e.g., Meylan & Heggie 1997). Hence, in some cases, the spatial distributions of stars with different masses can differ significantly, and multi-component models are required (e.g., Gieles & Zocchi 2015). I do not delve into this problem here, but I note that the present work could be extended to systems with multiple components f_k, as the consistency of such systems stems from the consistency of the individual components in the total potential $\Phi_{\mathrm{T}} = \sum_k \Phi_k + \Phi_{\mathrm{ext}}$ (Ciotti & Pellegrini 1992; Ciotti 2021).

1.4 Outline of the Thesis

As stated above, in this thesis, I study the consistency of models for spherical, isotropic stellar systems in the potential produced by a central point mass, which are meant to

represent GCs with central IMBHs. I do this by recovering their DF, numerically or analytically, through Eddington's formula (Eq. 1.16), and by exploiting some analytic consistency conditions, such as those presented in Eqs. (1.20)–(1.22). This work might pave the way for future techniques to rule out the presence of central IMBHs in GCs: if the observed properties match a model that does not admit a central BH, the mass of the putative BH can be constrained, according to our capability to resolve its sphere of influence. This could provide independent upper limits on central BHs' masses found in other studies (e.g., Della Croce et al. 2024, Bañares-Hernández et al. 2025). Models that recover the full phase-space distribution – i.e., the DF – of the stellar populations, could be particularly viable to improve the dynamical studies based on the Jeans equations (e.g., van der Marel & Anderson 2010; Kamann et al. 2016; Mann et al. 2019). These involve only the velocity moments of the DF, so the requirement that their solutions exist is weaker than the requirement of phase-space consistency.

In Chapter 2, I choose some well-known potential-density pairs and, adding the BH's contribution to the total potential, I assess the consistency of the resulting models with an isotropic dynamical structure. I confirm the general finding that a central density cusp[5] at least as steep as $r^{-1/2}$ is needed for these models to be consistent (Tremaine et al. 1994; An & Evans 2006; see also Appendices A.1 and A.2). In the light of this, in Chapter 3, I construct some new model density profiles, starting from centrally flat profiles of common use for GCs, and adding a central cusp. Then, I investigate how the size of this cusp and the mass of the BH affect the models' consistency.

Finally, in Chapter 4, I present the possible extensions of this work, also discussing the effects of orbital anisotropy on the consistency of spherical systems with central BHs, and I summarise the main findings of the thesis.

In addition, I devote Appendix A to show extended proofs of some results that I use in the main body of the thesis.

[5]The term 'cusp' refers to the cusp-like appearance of a radial density profile on linear scales that diverges at the centre.

Chapter 2

Spherical Isotropic Systems with a Central Black Hole

In this chapter, I present the analysis of the consistency of several models of stellar systems that are spherical, non-rotating and with isotropic velocity dispersion. I include, as an 'external' source of gravitational potential, a central point particle of mass $M_\bullet$, representing a central BH. The models are built starting from some known potential-density pairs. The sign of the underlying ergodic DF is then determined by explicitly computing it or through some consistency conditions.

In Section 2.1, I provide a thorough analysis of the consistency of γ-models with a central BH, giving also a comparison between the outcomes of the consistency conditions in Eqs. (1.20)–(1.22) and of the numerical evaluation of f through Eddington's formula (Eq. 1.16).

In Section 2.2, I consider Plummer models with a central BH. The original self-consistent model is derived from a given DF, but here I take its resulting density profile and compute a new DF that can reproduce such a profile in the presence of a central BH. In particular, I focus on the BH-dominated case as a representative example where the DF has an analytic expression.

In Section 2.3, I argue that the Einasto density profiles are incompatible with a central BH, if the orbits are isotropic, based on a result found for γ-models (Tremaine et al. 1994; see also Appendix A.1) and generalised in Theorem A.1 (but see An & Evans 2006 for an even more general theorem).

In Section 2.4, I repeat a similar analysis to that for γ-models, though more concise, considering the Sérsic density profiles. There, I define a characteristic relative energy beyond which the DFs with $M_\bullet > 0$ deviate from the self-consistent ones.

Finally, in Section 2.5, I provide an in-depth discussion concerning a family of density profiles that proved to be quite successful in reproducing the surface brightness profiles of GCs, namely, the King density profiles. I build the models following a similar procedure to that presented in Section 2.2, and I find that such models are inconsistent in the presence of a central BH. Then, I estimate under which conditions the BH's effect might be observationally relevant.

2.1 Isotropic γ-Models with a Central Black Hole

Below, I provide a thorough analysis of the consistency of the so-called γ-models, in the presence of a central BH. These models were independently introduced by Dehnen (1993) and Tremaine et al. (1994) with the main aim of describing the central density cusps of elliptical galaxies and of bulges of spiral galaxies observed with the *Hubble Space Telescope* (HST). Despite them not being much useful for the modelling of GCs, I use the γ-models as a simple test case that shows how the consistency analysis can be carried out and how a central BH affects, in general, the properties of the DF of a spherical, isotropic stellar system. In addition, the parameter γ sets the central logarithmic density slope of these models, which makes them ideal to analyse the relation between this property of the density profile and the sign of the DF, when a central BH is present.

In this section, I report and re-derive several results already obtained by Tremaine et al. (1994) and Baes et al. (2005), for completeness, but I also address the consistency problem with other techniques.

2.1.1 The Models

The γ-models form a family of one-parameter models for spherical, isotropic stellar systems (with two additional parameters setting the physical scales, M and a). The stellar mass density distribution of these models is

$$\rho(r) = \frac{3-\gamma}{4\pi a^3} \frac{M}{(r/a)^{\gamma}\,(1+r/a)^{4-\gamma}}\,, \quad \gamma \in [0,3[\,, \tag{2.1}$$

where r is the spherical radial coordinate. Here, M is the total *stellar* mass (always finite for $\gamma < 3$), and a is a scale radius. The density profiles of the γ-models are characterised by a $r^{-\gamma}$ central profile and go as r^{-4} for $r \gg a$. From Eq. (2.1), it can be shown that systems with $\gamma \geq 3$ have a divergent cumulative mass profile $M(r)$ at all radii, while systems with $\gamma < 0$ are inconsistent, if the velocity dispersion is isotropic (Tremaine et al. 1994; see also the necessary condition for the consistency of OM models

in Eq. 1.20). The gravitational potential Φ of the γ-models is obtained by substituting Eq. (2.1) into Poisson's equation (Eq. 1.3).

It is convenient to consider dimensionless quantities. Thus, I normalise all radii, mass densities and gravitational potentials in the following way:

- $r/a \to r$;
- $\rho/\left(Ma^{-3}\right) \to \rho$;
- $-\Phi/\left(GM/a\right) \to \Psi$;

where Ψ is the dimensionless stellar relative potential (the dimensionless total relative potential is denoted with the subscript 'T' and has the same normalisation). In other words, the unit of mass is M, the unit of length is a, and the unit of velocity is $\sqrt{GM/a}$. In these units, the scale radius a, the total stellar mass M and the universal gravitational constant G are all unity, and Eq. (2.1) simplifies as

$$\rho(r) = \frac{3-\gamma}{4\pi}\frac{1}{r^{\gamma}(1+r)^{4-\gamma}}\,, \quad \gamma \in [0,3[\,. \tag{2.2}$$

This results in a dimensionless cumulative stellar mass profile (Eq. 1.15)

$$M(r) = \left(\frac{r}{1+r}\right)^{3-\gamma}\,, \tag{2.3}$$

and a dimensionless stellar relative potential

$$\Psi(r) = \begin{cases} \frac{1}{2-\gamma}\left[1-\left(\frac{r}{1+r}\right)^{2-\gamma}\right], & \gamma \neq 2, \\ \ln\left(1+\frac{1}{r}\right), & \gamma = 2. \end{cases} \tag{2.4}$$

We then reduced to a one-parameter family of dimensionless models. In the following, I will always consider dimensionless quantities, if not otherwise stated. The physical value of a quantity that has dimensions of $(\text{mass})^l(\text{length})^m(\text{velocity})^n$ can be recovered by multiplying its dimensionless value by $M^l a^m (\sqrt{GM/a})^n$, expressed in the desired physical units.

We are mostly interested in studying systems with a central BH, so I also add the potential of a central point particle of mass $M_\bullet \equiv \mu M$. I will refer to μ as the BH-to-stellar mass ratio. Hence, the total cumulative mass profile becomes

$$M_{\rm T}(r) = \left(\frac{r}{1+r}\right)^{3-\gamma} + \mu\,, \tag{2.5}$$

and the total relative potential is

$$\Psi_{\rm T}(r) = \begin{cases} \frac{1}{2-\gamma}\left[1-\left(\frac{r}{1+r}\right)^{2-\gamma}\right]+\frac{\mu}{r}, & \gamma \neq 2, \\ \ln\left(1+\frac{1}{r}\right)+\frac{\mu}{r}, & \gamma = 2. \end{cases} \tag{2.6}$$

2.1.2 The Distribution Function in the High Relative Energy Limit

We assume that the DF is ergodic, so the velocity dispersion tensor is isotropic, and that the system is untruncated, so $f(\mathcal{E}) = h(\mathcal{E})\theta(\mathcal{E})$, where $\theta(x)$ is the Heaviside step function. Therefore, the DF can be obtained from Eq. (1.16), i.e., Eddington's formula, with $\mathcal{E}_{\rm t} = 0$.

Following the considerations of Tremaine et al. (1994), I report the noticeable result that isotropic γ-models with a central BH *can* be consistent only for $\gamma \in [1/2, 3[$. Indeed, as shown in Appendix A.1, in the limit as $\mathcal{E} \to \infty$, where the integral in Eq. (1.16) is dominated by stars close to the central BH,[1] the DF has the asymptotic behaviour

$$f(\mathcal{E}) \sim \frac{(3-\gamma)\gamma \mathrm{B}(\gamma, 1/2)}{4\pi\mu^{\gamma}}\left(\gamma-\frac{1}{2}\right)\mathcal{E}^{\gamma-3/2}, \tag{2.7}$$

where $\mathrm{B}(x,y)$ is the Euler Beta function, which is always non-negative for positive x and y. Therefore, the DF becomes asymptotically negative at the centre if $\gamma \in [0, 1/2[$ in γ-models with a central BH of arbitrary mass. Such models are then inconsistent and must be rejected.[2]

In Theorem A.1, I provide a generalisation of Eq. (2.7) to any spherical system with an ergodic DF with stellar density that goes as $r^{-\gamma}$, as $r \to 0$. Moreover, An & Evans (2006) found an even more general necessary condition for the consistency of spherical models with central BHs, including the possibility of orbital anisotropy (Eq. A.14).

2.1.3 Black Hole-Dominated Systems

First of all, we can study BH-dominated models, which are simpler models that can help understand more realistic systems with non-dominating BHs. This limiting case should highlight the effects of a central BH on the systems' properties.

In BH-dominated systems ($\mu \gg 1$), the stellar mass, and so also the stellar potential, are negligible with respect to the mass and the potential of the BH, so the total

[1] Recall that $\mathcal{E} = \Psi_{\rm T} - v^2/2$, and that $\Psi_{\rm T} \sim \mu/r \to \infty$, as $r \to 0$.

[2] Note, however, that $\mathrm{B}(x,y)$ diverges for $x = 0$, so Eq. (2.7) is not valid for $\gamma = 0$. Also, the leading term of the expansion of the DF in Eq. (2.7) vanishes for $\gamma = 1/2$. See Appendix A.1 for a discussion of these two cases.

cumulative mass profile and the total potential become

$$M_{\rm T}(r) = \mu\,, \quad \Psi_{\rm T}(r) = \frac{\mu}{r}\,. \tag{2.8}$$

Consistency Conditions

As anticipated in Section 1.2.4, Eqs. (1.20)–(1.22) can be used to infer the consistency of a given OM model without a direct inspection of the DF. We can reduce to isotropic systems by setting $r_{\rm a} \to \infty$. In this case, $\varrho = \rho(1 + r^2/r_{\rm a}^2) = \rho$, and, from Eq. (2.2), it is clear that the necessary condition (NC) in Eq. (1.20) is satisfied for all values of $\gamma \in [0, 3[$. Hence, based only on the NC, we can say that all isotropic γ-models *can* be consistent, independently of the mass of the BH.

To find BH-dominated systems that are consistent, I exploited the weak (WSC) and strong (SSC) sufficient conditions (Eqs. 1.21 and 1.22, respectively). The former is satisfied by models with $\gamma \in {\rm WSC}_\gamma \equiv [1, 3[$, while the latter by models with $\gamma \in {\rm SSC}_\gamma \equiv [36/65, 3[$. As expected, ${\rm WSC}_\gamma \subseteq {\rm SSC}_\gamma$. Since $36/65 \simeq 0.554$, and considering that Eq. (2.7) rules out the consistency of models with $\gamma < 1/2$, we were able to determine the consistency or the inconsistency of almost all BH-dominated γ-models through analytic calculations and without computing the DF, the only exceptions being the models with $\gamma \in [1/2, 36/65[$.

The Distribution Function

The consistency conditions and the high relative energy limit of the DF (Section 2.1.2) fail to assess the consistency of BH-dominated γ-models with $\gamma \in [1/2, 36/65[$; a direct inspection of the DF is then needed.

For the numerical evaluation of the DFs, I exploited the AGAMA library[3] (Vasiliev 2018), which allows the computation of the DFs of spherical, isotropic models, once provided the density and total potential profiles, through numerical calculation of Eddington's formula in the form of Eq. (1.16b), so that $f(\mathcal{E}) = h(\mathcal{E})\theta(\mathcal{E})$ is recovered. The AGAMA algorithm computes the density derivatives through finite difference methods and uses an 8-point Gauss-Legendre quadrature method for the numerical integration.

I report my results in Figs. 2.1 and 2.2. In the first figure, I show the DFs for values of γ in the unconstrained interval $[1/2, 36/65 \simeq 0.554[$, assuming $\mu = 10^3$. In all cases, the DFs tend to zero at high relative energies, but do not become negative in the considered $\mathcal{E}$ range. It is worth pointing out that the gap between the $\gamma = 1/2$ curve and the others is due to a discontinuity in the logarithmic slope of the DF as

[3] Library hosted at https://github.com/GalacticDynamics-Oxford/Agama.

$\mathcal{E} \to \infty$. Indeed, from Eq. (2.7), we see that $\mathrm{d}\ln f/\mathrm{d}\ln\mathcal{E} \sim \gamma - 3/2 \to -1$, as $\mathcal{E} \to \infty$ and $\gamma \to 1/2$. However, for $\gamma = 1/2$, Eq. (2.7) is not valid because the $(\gamma - 1/2)$ term vanishes, and Eq. (A.13) shows that, in this case, $\mathrm{d}\ln f/\mathrm{d}\ln\mathcal{E} \sim -5/2$.

In Fig. 2.2, I show the DFs for integer and half-integer values of γ between 0 and 5/2, computed assuming a total relative potential as in Eq. (2.8), with $\mu = 10^3$. While at low relative energies the DFs for all values of γ have a very similar behaviour, there is a clear separation at $\mathcal{E} > \mathcal{E}_{\rm crit} \approx 10^3$ (in units of GM/a). Since $\Psi_{\rm T} = \mathcal{E} + v^2/2 \geq \mathcal{E}$, all stars with $\mathcal{E} = \mathcal{E}_{\rm crit}$ are at radii where $\Psi_{\rm T}(r) \geq \mathcal{E}_{\rm crit}$. This means that they are at radii $r \leq r_{\rm crit}$, where $\Psi_{\rm T}(r_{\rm crit}) \equiv \mathcal{E}_{\rm crit}$, because $\Psi_{\rm T}$ is a decreasing function of radius. Thus, $r_{\rm crit}$ is the maximum radius at which a star with energy $\mathcal{E}_{\rm crit}$ can be found, and all stars with $\mathcal{E} \geq \mathcal{E}_{\rm crit}$ are within $r_{\rm crit}$. In other words, *a star of given relative energy is always confined within the sphere where the total potential is larger than or equal to the star's relative energy.*

From Eq. (2.8), we have that $r_{\rm crit} = \mu/\mathcal{E}_{\rm crit} \approx 1$, since $\mu = 10^3$, which is, indeed, the dimensionless scale radius at which $\rho(r)$ in Eq. (2.2) changes slope from $r^{-\gamma}$ to r^{-4}. Thus, the DFs with different values of γ have different slopes at $\mathcal{E} > \mathcal{E}_{\rm crit} \approx 10^3$ according to their different *density* slopes in the 'corresponding' spatial region $r < r_{\rm crit} \approx 1$. Note also that, as expected from Eq. (A.12), the $\gamma = 0$ model is inconsistent, as its DF is negative for $\mathcal{E} \gtrsim 5 \times 10^4$. For $\gamma = 1/2$ and $\gamma = 1$ the DFs become decreasing functions of $\mathcal{E}$ for $\mathcal{E} \gtrsim \mathcal{E}_{\rm crit}$, in agreement with Eqs. (2.7) and (A.13), but they do not become negative, at least in the considered relative energy range. At $\mathcal{E} \gtrsim \mathcal{E}_{\rm crit}$, the $\gamma = 3/2$ model is asymptotically constant, while the other models are increasing functions of $\mathcal{E}$, as expected from Eq. (2.7).

2.1.4 Systems with Finite Black Hole Mass

Consistency Conditions

It is possible to show that, in general, a one-component OM model satisfies the WSC in the self-gravitating case and in the presence of a central BH of arbitrary finite mass *if and only if* the WSC is satisfied by that model in the BH-dominated case (Theorem A.4). In other words, a density profile that satisfies the WSC in the BH-dominated case satisfies the same condition for *all* finite (and null) values of μ, and vice versa. This proves that γ-models with $\gamma \geq 1$ are consistent for all $\mu \in [0, \infty[$, as they satisfy the WSC in the BH-dominated case (see Section 2.1.3).

To get wider constraints, I determined whether the SSC in Eq. (1.22) is satisfied for values of μ ranging between 10^{-6} and 100 and for γ in the range $[0, 1[$. I found that for any fixed μ there is a critical value $\gamma_{\rm crit}(\mu)$ such that all models with $\gamma \geq \gamma_{\rm crit}(\mu)$

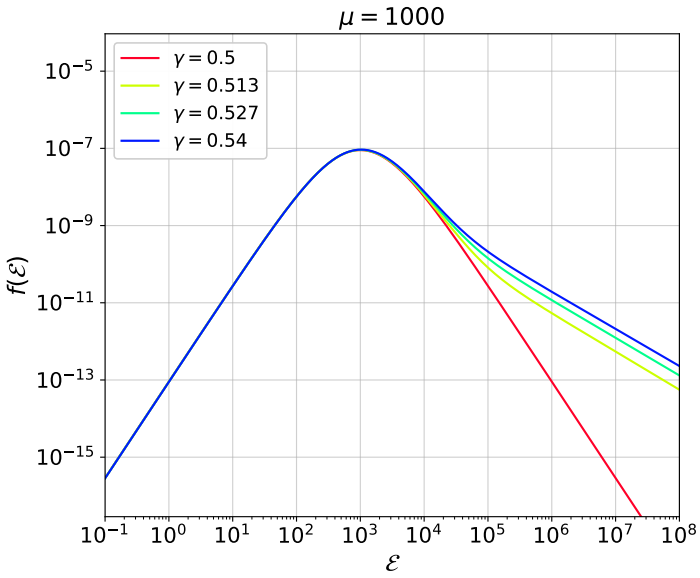

Figure 2.1. DFs of BH-dominated γ-models for a selection of values of γ within the interval $[1/2, 36/65[$, which is the range for which the SSC (Eq. 1.22) and Theorem A.1 fail to constrain the non-negativity of the DF. Here, Eddington's formula (Eq. 1.16b) is computed assuming that the total relative potential is given by Eq. (2.8), with $\mu = 10^3$. The DF is in units of $(MG^3a^3)^{-1/2}$, while the relative energy $\mathcal{E}$ is in units of GM/a, where M is the total stellar mass and a is the scale length of the models (Eq. 2.1).

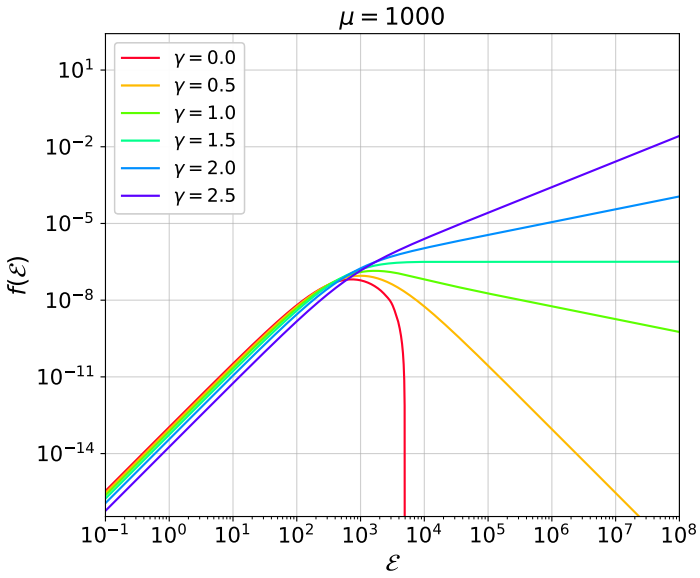

Figure 2.2. DFs of BH-dominated γ-models for a selection of values of γ. The total relative potential used to compute these DFs is given by Eq. (2.8), where I substituted $\mu = 10^3$. The DF is in units of $(MG^3a^3)^{-1/2}$, while the relative energy $\mathcal{E}$ is in units of GM/a, where M is the total stellar mass and a is the scale length of the models (Eq. 2.1).

satisfy the SSC, while the others do not. I show the results in Fig. 2.3.[4] The function $\gamma_{\rm crit}(\mu)$ is monotonically decreasing, and the maximum value reached in the considered μ range is $\gamma_{\rm crit} \simeq 0.984$ for $\mu = 10^{-6}$. For values of $\mu \gtrsim 1$, $\gamma_{\rm crit}(\mu)$ flattens approaching $\gamma_{\rm crit}(\infty) = 36/65$, which is the value of $\gamma_{\rm crit}$ found in the BH-dominated case. Therefore, in this example, the SSC establishes the consistency of a wider set of models as μ increases.

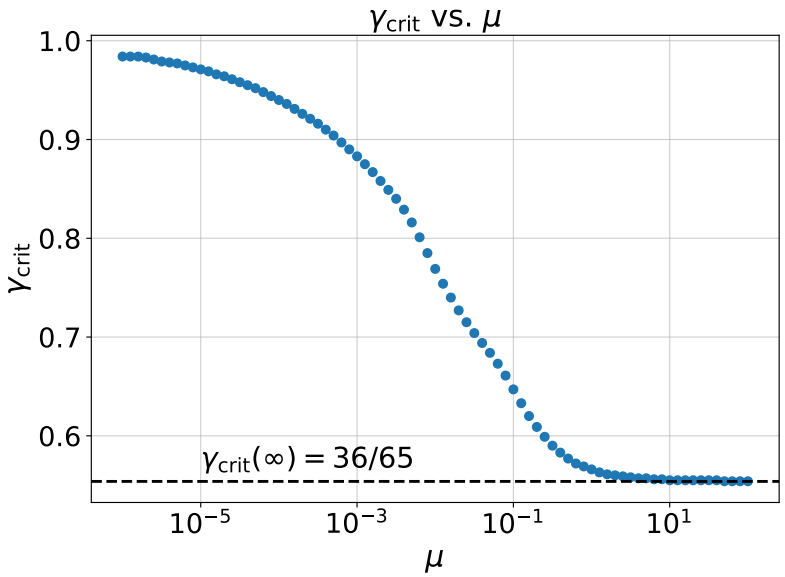

Figure 2.3. Minimum value of γ for which the SSC (Eq. 1.22) is satisfied by γ-models with central BH as a function of the BH-to-stellar mass ratio μ. The horizontal line indicates the value of $\gamma_{\rm crit}$ for BH-dominated models (see Section 2.1.3).

The Distribution Function

To assess the consistency of γ-models with a central BH of finite mass that do not satisfy the SSC, I numerically computed the DFs over a reasonably wide relative energy range, using again the AGAMA software (see Section 2.1.3). I also considered models for which the consistency or the inconsistency has already been established, in order to have an insight into the characteristics of their DFs.

Fig. 2.4 shows the DFs of the γ-models for a selection of values of γ in the self-gravitating case and for a few values of $\mu \in [10^{-4}, 1]$. The DF is always non-negative in the self-gravitating case ($\mu = 0$) and, in the models with $\gamma \geq 1/2$, even in the presence

[4] Calculations performed with *Wolfram Mathematica* (Wolfram Research, Inc., *Mathematica*, Version 14.2, Champaign, IL, 2025).

of a BH, confirming the results obtained in the BH-dominated case (see Section 2.1.3). For $\gamma < 2$, the self-consistent DF has a vertical asymptote at $\mathcal{E} = (2-\gamma)^{-1}$, because this is the maximum value reached by $\Psi_\mathrm{T} = \Psi$ in Eq. (2.4), while for $\gamma \geq 2$ there is no maximum relative energy. In agreement with Eq. (A.12), which is the limit as $\gamma \to 0$ of Eq. (2.7), the $\gamma = 0$ models with central BH are inconsistent; their DFs become negative at increasingly higher $\mathcal{E}$ for increasing values of μ. As a general trend, the DFs of the models with $\mu \in]0, 1[$ deviate from the corresponding self-consistent DFs at higher $\mathcal{E}$ for lower μ. Instead, the $\mu = 1$ models always lie below the self-consistent DF because, even at very large radii (low $\mathcal{E}$), the BH is relevant. It is evident that the BH, for fixed μ, modifies more significantly the DFs of the self-consistent models with lower γ. Indeed, Eq. (2.4) shows that the central stellar relative potential is finite for $\gamma < 2$ and infinite for $\gamma \geq 2$. For $\gamma < 2$, the depth of the potential well, that is, $\Psi(0) = (2-\gamma)^{-1}$, increases with γ, whereas, for $\gamma \geq 2$, $\Psi(r)$ diverges faster at the centre for higher γ, being $\Psi(r) \propto \ln(1/r)$ for $\gamma = 2$, and $\Psi(r) \propto r^{2-\gamma}$ for $\gamma > 2$, as $r \to 0$. Therefore, the BH affects the DF of the models with shallower potential wells more significantly.

2.2 Isotropic Plummer Models with a Central Black Hole

According to the results explained in Section 2.1.2 and in Appendix A.2, we expect the isotropic Plummer sphere (Plummer 1911) to be inconsistent if it contains a central BH of any mass due to its flat central core. In this section, I verify this result, in the BH-dominated case, by explicitly evaluating the DF. The procedure adopted here to build Plummer models with central BHs is analogous to the one that will be followed for the King models (King 1966; Michie 1963) with central BHs in Section 2.5.

2.2.1 The Model

The Plummer sphere is a model of the family of spherically symmetric self-gravitating stellar polytropes (e.g., Ciotti 2021, Ch. 12). These models are characterised by an ergodic DF of the form

$$f(\mathcal{E}) = A\,(\mathcal{E} - \mathcal{E}_\mathrm{t})^{n-3/2}\,\theta\,(\mathcal{E} - \mathcal{E}_\mathrm{t})\,, \tag{2.9}$$

where A is a constant with dimensions of mass per unit volume per unit (velocity)^{2n}, $\mathcal{E}_\mathrm{t}$ is a truncation relative energy, $n > 1/2$ is a free parameter, and $\theta(x)$ is the Heaviside step function. One can then get the stellar density distribution as a function of the potential $\rho(\Psi)$ by integrating Eq. (2.9) over the velocity space. By solving Poisson's equation (Eq. 1.3) with the boundary conditions $\Psi(0) = \Psi_0 < \infty$ and $\mathrm{d}\Psi/\mathrm{d}r\,|_{r=0} = 0$,

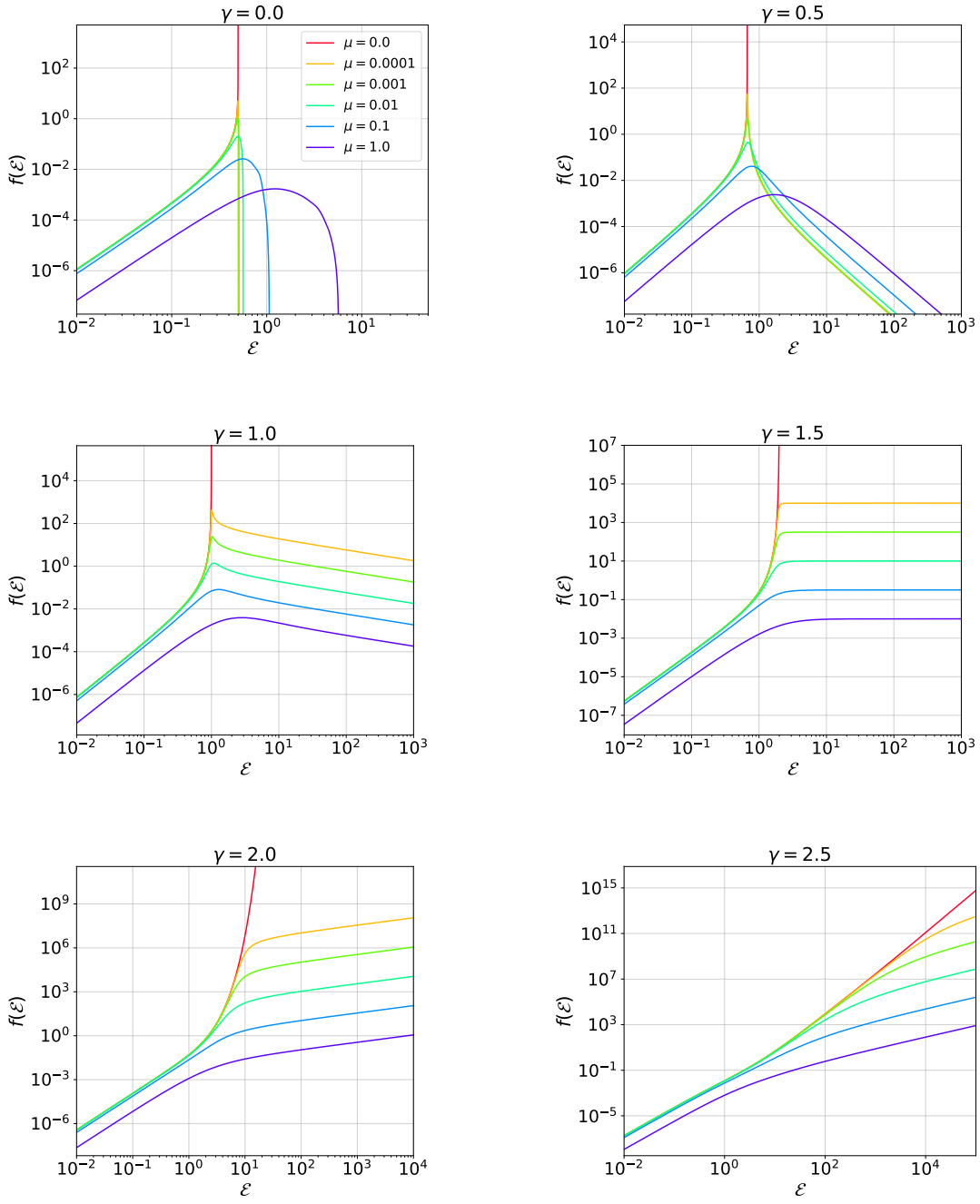

Figure 2.4. DFs of γ-models with $\gamma = 0,\ 1/2,\ 1,\ 3/2,\ 2,\ 5/2$ for BH-to-stellar mass ratios $\mu = 0,\ 10^{-4},\ 10^{-3},\ 10^{-2},\ 10^{-1},\ 1$. The legend is shown only in the first plot ($\gamma = 0$), but refers to all figures. In the $\gamma = 0$ plot, the curves that touch the x-axis reach negative values of $f(\mathcal{E})$. The DF is in units of $(MG^3a^3)^{-1/2}$, while the relative energy $\mathcal{E}$ is in units of GM/a, where M is the total stellar mass and a is the scale length of the models (Eq. 2.1).

one also gets the gravitational potential as a function of the spherical radius r, and consequently, the density profile $\rho(r)$.

In particular, the Plummer model is the stellar polytrope with $n = 5$, whose density distribution and relative stellar potential are, respectively,

$$\rho(r) = \frac{3M}{4\pi a^3} \frac{1}{\left[1 + (r/a)^2\right]^{5/2}} \tag{2.10}$$

and

$$\Psi(r) = \frac{GM}{a} \frac{1}{\sqrt{1 + (r/a)^2}}\,, \tag{2.11}$$

where M is the total stellar mass and $a \equiv \sqrt{3/(4\pi G B_5 \Psi_0^4)}$ is a scale length. For generic n, $B_n \equiv A(2\pi)^{3/2}\Gamma(n - 1/2)/\Gamma(n + 1)$, so $B_5 = 7\pi^2 A/(32\sqrt{2})$. The Plummer sphere is untruncated, i.e., $\mathcal{E}_\mathrm{t} = 0$, and with finite total mass; the density profile is flat at the centre and drops as r^{-5} at infinity.

Now, we want to study systems with the density profile as in Eq. (2.10) and with a central BH. Therefore, the DF of Eq. (2.9) is no longer valid for the stellar systems because the total potential differs from the one in Eq. (2.11). Still, we assume an ergodic DF, so that it can be recovered through Eq. (1.16) to provide the *same* density profile (Eq. 2.10) in the *new* total potential. It is convenient to use dimensionless quantities (see Section 2.1.1), so Eqs. (2.10) and (2.11) become

$$\rho(r) = \frac{3}{4\pi} \frac{1}{(1 + r^2)^{5/2}} \tag{2.12}$$

and

$$\Psi(r) = \frac{1}{\sqrt{1 + r^2}}\,. \tag{2.13}$$

By integrating Eq. (2.12), we obtain a cumulative stellar mass profile

$$M(r) = \frac{r^3}{(1 + r^2)^{3/2}}\,. \tag{2.14}$$

If we include a central BH of mass $M_\bullet = \mu M$ in the system, the total relative potential and the total cumulative mass profile are

$$\Psi_\mathrm{T}(r) = \frac{1}{\sqrt{1 + r^2}} + \frac{\mu}{r}\,, \quad M_\mathrm{T}(r) = \frac{r^3}{(1 + r^2)^{3/2}} + \mu\,. \tag{2.15}$$

2.2.2 Consistency Conditions

An inspection of Eq. (2.12) shows immediately that the NC for the consistency provided by Eq. (1.20) is satisfied for isotropic Plummer spheres embedded in whatever total potential. Conversely, the SSC is satisfied only for $\mu = 0$, as can be seen by substituting Eqs. (2.12) and (2.15) into Eq. (1.22), and posing $r_\mathrm{a} \to \infty$. As discussed in Section 1.2.4, this implies that the WSC is not satisfied for $\mu > 0$ as well.

In fact, according to Theorem A.2, we could immediately rule out the consistency of a Plummer sphere with a central BH because this model has $\rho(r) \sim \rho_0 - Ar^2$, as $r \to 0$, with $A > 0$ (i.e., it has a *regular* density profile; see Appendix A.2). Notwithstanding, below I show the explicit formula for the BH-dominated DF, to illustrate a particular example in which the theorem works, and for which an analytic expression of the DF exists.

2.2.3 The Distribution Function

Black Hole-Dominated Systems

Considering BH-dominated systems, the total relative potential reduces to

$$\Psi_\mathrm{T}(r) = \frac{\mu}{r}\,. \tag{2.16}$$

Thus, one can easily write the density as a function of Ψ_T as

$$\rho(\Psi_\mathrm{T}) = \frac{3}{4\pi}\left[1 + \left(\frac{\mu}{\Psi_\mathrm{T}}\right)^2\right]^{-5/2}\,. \tag{2.17}$$

Substituting into Eq. (1.16), it is then possible to obtain the following DF:

$$\begin{aligned} f(\mathcal{E}) = \frac{8\sqrt{2}\,\mathcal{E}^{7/2}}{1001\pi^3\mu^7}\Big[&429\mu^2\,{}_3F_2\left(\tfrac{5}{2}, 3, \tfrac{7}{2}; \tfrac{11}{4}, \tfrac{13}{4}; -\tfrac{\mathcal{E}^2}{\mu^2}\right) \\ &- 560\mathcal{E}^2\,{}_3F_2\left(\tfrac{7}{2}, 4, \tfrac{9}{2}; \tfrac{15}{4}, \tfrac{17}{4}; -\tfrac{\mathcal{E}^2}{\mu^2}\right)\Big]\,, \end{aligned} \tag{2.18}$$

where ${}_pF_q(a_1, ..., a_q; b_1, ..., b_q; z)$ are the generalised hypergeometric functions. The formula has been derived using *Wolfram Mathematica*.[5]

I computed $f(\mathcal{E})$ in Eq. (2.18) over a range of relative energies, for a selection of values of $\mu \in [10, 10^6]$, finding that the DF is always negative above some value $\mathcal{E}_0$ of the relative energy. Fig. 2.5 shows, as an example, the DF for a BH-dominated Plummer

[5]Wolfram Research, Inc., *Mathematica*, Version 14.2, Champaign, IL (2025)

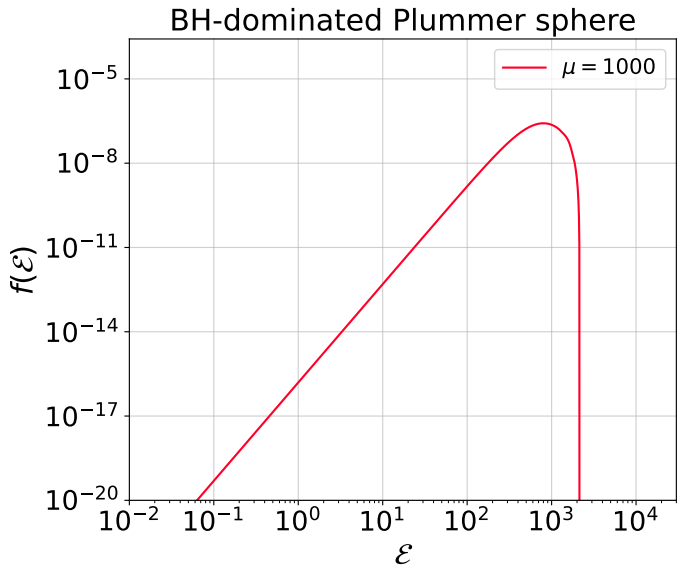

Figure 2.5. DF of the BH-dominated Plummer sphere with BH-to-stellar mass ratio $\mu = 10^3$ as a function of the relative energy $\mathcal{E}$. The DF is provided by the analytic expression in Eq. (2.18). In this plot, $f(\mathcal{E})$ is in units of $(MG^3a^3)^{-1/2}$, while $\mathcal{E}$ is in units of GM/a, where M is the total stellar mass and a is the scale length of the model (Eq. 2.10).

model with $\mu = 10^3$, for which $\mathcal{E}_0 \approx 2 \times 10^3$ (in units of GM/a). We can conclude that the DF in Eq. (2.18) is not positive definite, so BH-dominated Plummer models are inconsistent.

2.3 Isotropic Einasto Models with a Central Black Hole

The Einasto (1965) models are a family of models that have been extensively used to describe simulated DM halos (e.g., Wang et al. 2020). Understanding whether these models are physically acceptable in the presence of a central BH could be important to constrain the poorly-known central density profiles of DM halos in galaxies and galaxy clusters. However, my results are limited to spherical, one-component systems with isotropic velocity dispersion of the DM particles. More realistic models should be needed to account for deviations from sphericity and isotropy (e.g., see Baes 2022 for a study of self-gravitating, spherical Einasto models with OM orbital structure), and for the inclusion of the baryonic component, which is expected to be dominant at intermediate radii, outside the BH's influence radius (e.g., see Cappellari et al. 2013 for the case of early-type galaxies).

One-component systems like those discussed here can still be relevant for DM-

dominated systems such as dwarf spheroidal galaxies (e.g., Battaglia & Nipoti 2022).

2.3.1 Models and Consistency

The density profile of the Einasto models is

$$\rho(r) = \rho_0 \exp\left\{-d\left(\frac{r}{r_\mathrm{h}}\right)^{1/n}\right\}. \tag{2.19}$$

The free parameters are the central density ρ_0, the scale radius r_h and the Einasto index $n > 0$. The dimensionless constant $d > 0$ is set by imposing that r_h is the half-mass radius, i.e., $M(r_\mathrm{h}) \equiv 0.5\,M$, so that it must satisfy the equation $\Gamma(3n, d) = \frac{1}{2}\Gamma(3n)$. Here, $\Gamma(x, y)$ is the upper incomplete gamma function and $\Gamma(x)$ is the complete gamma function. I plot this density profile, for some values of the Einasto index, in Fig. 2.6.

As $r \to 0$, since $n > 0$, the argument of the exponential function goes to zero. Thus, we can write

$$\rho(r) \sim \rho_0 \left[1 - d\left(\frac{r}{r_\mathrm{h}}\right)^{1/n}\right], \quad r \to 0. \tag{2.20}$$

The leading term is a constant, so the Einasto models with isotropic dynamical structure cannot host a central BH, according to Theorem A.1 (Eq. A.26). This can also be seen from Eq. (A.16) provided by An & Evans (2006). Indeed, the logarithmic density slope $\gamma(r) \equiv -\,\mathrm{d}\ln\rho/\mathrm{d}\ln r$ vanishes at the centre of any system with finite central density, so the necessary condition for consistency $\lim_{r\to 0}\gamma(r) \geq 1/2$ is not satisfied.

Nonetheless, note that the models with high Einasto index (e.g., $n = 4$ and $n = 10$ in Fig. 2.6) do not flatten even down to $r = 10^{-2}\,r_\mathrm{h}$, so such Einasto models could be acceptable down to very small radii, even in the presence of a BH. Hence, the Einasto models cannot describe spherical, isotropic DM halos with central BHs down to the very centre, but the size of the region where this description is no longer valid must be determined case by case, and will likely be smaller for higher n, for a fixed BH's mass. In other words, the DF of an Einasto model with high n and a central BH of low-enough mass may become negative only in the phase-space region corresponding to very high relative energies. This corresponds to a *spatial* region very close to the centre, which might be of no practical relevance. For example, it may be smaller than the resolution of the simulation, or it may not contain a significant number of DM particles.

I do not investigate further this aspect here, since it goes beyond the scope of this work. However, I provide a more quantitative discussion of this topic in Sections 2.5.3, 3.2.4 and 3.2.5 for models that are more appropriate to describe GCs. The arguments provided in those sections can be easily extended to the models described here.

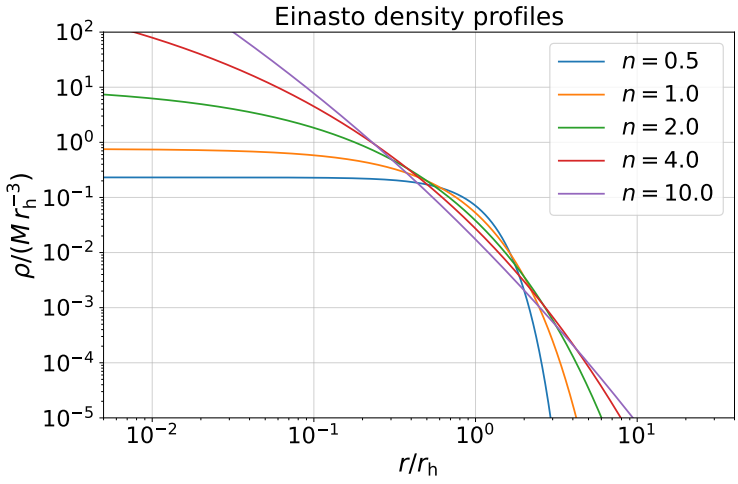

Figure 2.6. Einasto density profiles for a selection of values of the Einasto index n (Eq. 2.19). The density is in units of $Mr_{\rm h}^{-3}$, while the radius is in units of $r_{\rm h}$, where M is the total stellar mass and $r_{\rm h}$ is the half-mass radius.

2.4 Isotropic Deprojected Sérsic Models with a Central Black Hole

2.4.1 The Models

The Sérsic (1968) profiles are a family of projected mass density profiles widely used for early-type galaxies (e.g., Caon et al. 1993). These models have also been used to describe GCs (e.g., Barmby et al. 2007), although this is not customary.

Here, we consider spherically symmetric systems, which produce circular isophotes. The projected mass density following the Sérsic law, in this case, reads

$$\Sigma(R) = \Sigma_0 \exp\left\{-b\left(\frac{R}{R_{\rm e}}\right)^{1/n}\right\}, \tag{2.21}$$

where R is the radius on the projection plane, Σ_0 is the central projected mass density, n is the Sérsic index, and b is a positive dimensionless constant, dependent on n, defined such that $R_{\rm e}$ is the effective radius, i.e., the projected radius containing half of the total projected mass. This condition implies that b must satisfy the relation $\Gamma(2n) = 2\Gamma(2n, b)$, where $\Gamma(x)$ and $\Gamma(x, y)$ are the complete and the upper incomplete gamma functions, respectively.

The deprojected mass density profile (shown in Fig. 2.7) can be obtained through

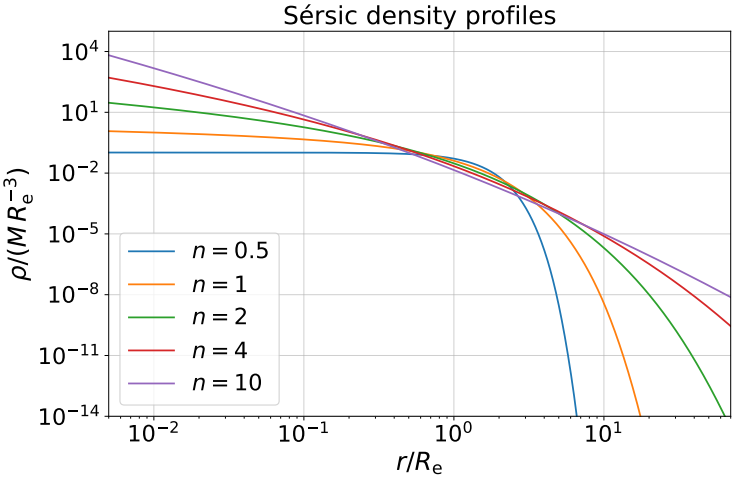

Figure 2.7. Radial deprojected mass density profiles of Sérsic models with Sérsic index $n = 0.5$, 1, 2, 4, 10. The density is in units of MR_e^{-3}, while the radius is in units of R_e, where M is the total stellar mass and R_e is the effective radius.

an Abel deprojection integral (e.g., Ciotti 2021) as

$$\rho(r) = -\frac{1}{\pi}\int_r^\infty \frac{\mathrm{d}\Sigma(R)}{\mathrm{d}R}\frac{\mathrm{d}R}{\sqrt{R^2-r^2}}, \tag{2.22}$$

under the assumption that the system is *transparent*, i.e., that there is no overlapping of stars along the line of sight, which is justified for typical GCs and galaxies. If $\Sigma(R)$ is given by the Sérsic law, $\rho(r)$ cannot be expressed in terms of elementary functions. However, in order to apply Theorem A.1 to these models, an analytic expression for the asymptotic behaviour of $\rho(r)$ as $r \to 0$ is sufficient. This is provided by Ciotti (1991), who found that, as $r \to 0$,

$$\rho(r) \sim \frac{\Sigma_0}{R_e} \times \begin{cases} \frac{b^n\Gamma(1-n)}{\pi}\mathrm{e}^{-bs^{1/n}}, & 0 < n < 1, \\ \frac{b}{\pi}\left(\ln\frac{2}{bs} - \gamma_\mathrm{E}\right), & n = 1, \\ \mathrm{B}\left(\frac{1}{2}, \frac{n-1}{2n}\right)\frac{b}{2\pi n}\frac{\mathrm{e}^{-bs^{1/n}}}{s^{1-1/n}}, & n > 1, \end{cases} \tag{2.23}$$

where $s = r/R_e$, $B(x, y)$ is the Euler Beta function, and $\gamma_\mathrm{E} \simeq 0.577$ is the Euler-Mascheroni constant.

2.4.2 Consistency with a Central Black Hole

Case $0 < n < 1$

The two lowest-order terms in the asymptotic expansion of Eq. (2.23) give $\rho(r) \propto \mathrm{e}^{-bs^{1/n}} \sim 1 - bs^{1/n}$. Therefore, models with $0 < n < 1$ belong to the family of profiles that go as $r^{-\alpha}$, with $\alpha = 0$, as $r \to 0$, so they cannot host a central BH, if the DF is ergodic (see Theorem A.1 and Eq. A.16).

Case $n = 1$

In this case, we cannot apply Theorem A.1, since the asymptotic behaviour of ρ is of the form $\ln(1/r)$. The central asymptotic expansion of the density profile can be written as

$$\rho(r) \sim A \ln \frac{B}{r} = A \left(\ln \frac{1}{r} + \ln B \right) \sim A \ln \frac{1}{r}, \tag{2.24}$$

where $A \equiv \Sigma_0 b/(\pi R_\mathrm{e})$ and $B \equiv 2/\left(b\mathrm{e}^{\gamma}\right)$. We can then exploit Theorem A.3, which proves the fact that spherical, isotropic systems with a density profile following Eq. (2.24) as $r \to 0$ are inconsistent, if they host a central BH.

Case $n > 1$

We can consider the lowest order in the asymptotic expansion of Eq. (2.23), which gives $\rho(r) \propto s^{1/n-1}$. From Theorem A.1, we can conclude that systems with $1 < n < 2$ are inconsistent if they host a central BH, since $1 - 1/n < 1/2$, so their profile is flatter than $r^{-1/2}$ at the centre. Nonetheless, we have no proof that the models with $n \geq 2$ are consistent nor that they are inconsistent, in the presence of a central BH. Hence, we need a more detailed analysis to establish whether they are acceptable models or not.

I show the numerically evaluated DFs in Fig. 2.8, for a selection of values of $n \geq 2$ and for $\mu = 0,\ 10^{-4},\ 10^{-3},\ 10^{-2},\ 10^{-1},\ 1$. In the computations, I used the same normalisation as for the other models, effectively placing $G = M = a = 1$, where now $a = R_\mathrm{e}$ (see Section 2.1.1). I recall that the unit of mass is the total stellar mass M, the unit of length is R_e, and the unit of velocity is $\sqrt{GM/R_\mathrm{e}}$. Therefore, $f(\mathcal{E})$ is normalised by $(MG^3R_\mathrm{e}^3)^{-1/2}$, and the relative energy $\mathcal{E}$ is normalised by GM/R_e.

I found that no model with $n \geq 2$ has a somewhere negative DF for such values of μ, in the explored energy range. A peculiar fact is that, in the $n = 2$ models, all the DFs with $\mu > 0$, converge to the same curve at high $\mathcal{E}$, suggesting that the normalisation of their asymptotic expansion for $\mathcal{E} \to \infty$ is independent of μ. This is not true, in general (e.g., see Eq. A.25).

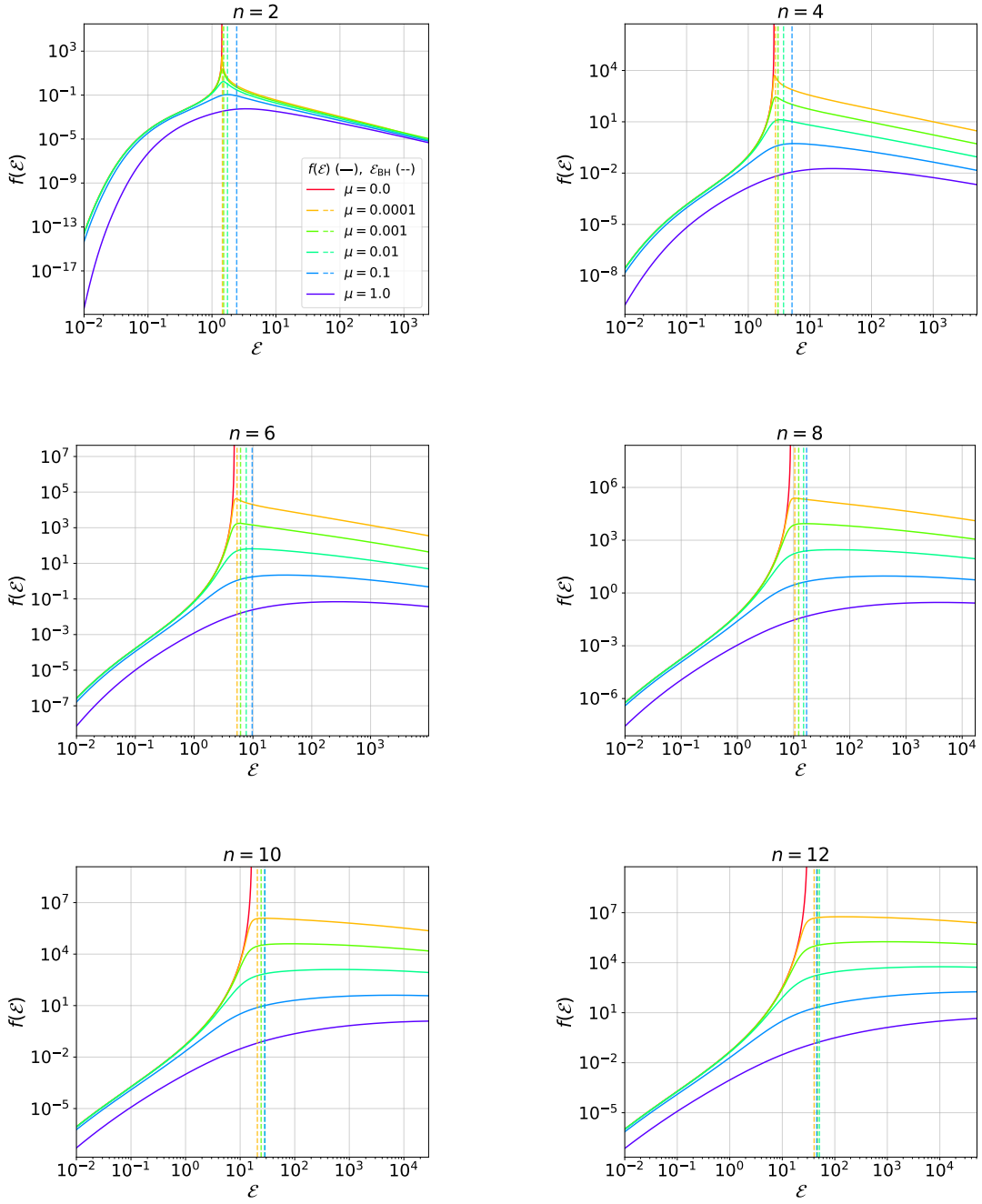

Figure 2.8. DFs of Sérsic models with $n = 2$, 4, 6, 8, 10, 12 for BH-to-stellar mass ratios $\mu = 0$, 10^{-4}, 10^{-3}, 10^{-2}, 10^{-1}, 1. The vertical lines indicate the relative energies $\mathcal{E}_{\rm BH} \equiv \Psi_{\rm T}(r_{\rm BH})$, where $r_{\rm BH}$ is the radius enclosing 10% of the BH's mass in stars (Eq. 2.25). I computed $\mathcal{E}_{\rm BH}$ only for $0 < \mu < 1$: if $\mu = 0$, $r_{\rm BH}$ is null, while if $\mu \geq 1$, it is meaningless, as the BH's influence is relevant at all radii. I use the same colour for the DFs and the $\mathcal{E}_{\rm BH}$ lines with the same μ. The legend is shown only in the first plot ($n = 2$), but refers to all figures. The DF is in units of $(MG^3R_{\rm e}^3)^{-1/2}$, while the relative energy $\mathcal{E}$ is in units of $GM/R_{\rm e}$, where M is the total stellar mass and $R_{\rm e}$ is the effective radius.

Since the magnitude of the (dimensionless) gravitational force is $[\mu + M(r)]/r^2$, when $\mu = 1 = M(\infty)$, the BH's gravitational attraction is larger than the stellar one at any radius. As a consequence, the DF, for $\mu = 1$, never overlaps with the self-consistent one. Instead, for $0 < \mu < 1$, this occurs, so it makes sense to define the critical energies $\mathcal{E}_{\rm BH}(\mu) \equiv \Psi_{\rm T}(r_{\rm BH}; \mu)$, to predict the relative energy at which the BH becomes dominant. Here, $r_{\rm BH}$ is the BH radius of influence, which I defined as the radius enclosing a stellar mass equal to 10% of the BH's mass, as done by Miocchi (2007):

$$M(r_{\rm BH}) = 0.1 M_\bullet. \tag{2.25}$$

This definition of the BH's influence radius ensures that the motion of stars within $r_{\rm BH}$ is dominated by the BH's attraction, as 9/10 of the gravitational force's intensity felt by stars at $r_{\rm BH}$ comes from the BH. As explained in Section 2.1.3 (see the subsection 'The Distribution Function'), all stars with relative energy $\mathcal{E} \geq \mathcal{E}_{\rm BH}$ are at radii smaller than or equal to $r_{\rm BH}$. This is why $\mathcal{E}_{\rm BH}$ roughly predicts the relative energy at which the DF changes slope with respect to the self-gravitating case due to the BH's influence, as can be seen in Fig. 2.8. Note that $\mathcal{E}_{\rm BH}$ is slightly larger than the energy at which the DFs with $\mu > 0$ depart from the self-consistent ones, because $\mathcal{E}_{\rm BH}$ determines the energy at which the BH is dominant, not the one at which it begins to be relevant.

2.5 Isotropic King Models with a Central Black Hole

The *lowered isothermal models* form a class of models, obtained by diminishing the DF of the so-called *isothermal sphere*, designed to describe systems with finite total mass that resemble the isothermal sphere at small radii (Binney & Tremaine 2008). This class of models is motivated by the fact that two-body interactions, in GCs, drive the velocity distribution of stars towards a Maxwell-Boltzmann distribution (corresponding to thermal equilibrium), especially in the core, where the two-body relaxation time is shorter.

Among these models, the family of King (1966) models[6] has proven quite successful in describing the radial density profiles of GCs (e.g., Barmby et al. 2007; Miocchi et al. 2013), but not always in reproducing their kinematic properties (e.g., Zocchi et al. 2012). Therefore, the following results might be observationally relevant, though some refinements are in order.

In this section, I analyse the consistency of 'modified' King models with a central BH. Similarly to what I did in Section 2.2, below I will use the self-consistent DF to

[6]These models were originally introduced by Michie (1963), but King (1966) made them well known.

obtain the King density profiles. Then, I will compute, through Eddington's formula, the DFs able to reproduce such density profiles when also a central BH is contributing to the total potential, and I will assess their non-negativity.

2.5.1 The Models

As mentioned above, the DF of King models is obtained starting from that of the isothermal sphere (e.g., Ciotti 2021):

$$f_{\rm iso}(\mathcal{E}) = \frac{\rho_1}{(2\pi\sigma^2)^{3/2}} \mathrm{e}^{\mathcal{E}/\sigma^2}, \tag{2.26}$$

where ρ_1 is a density scale and σ is the velocity dispersion along any direction, which is independent of radius. This model has infinite total mass, since $M(r) \propto r$ as $r \to \infty$. This problem can be avoided by lowering its DF at low relative energies. Recalling that $\mathcal{E} = \Psi_{\rm T}(r) - v^2/2$, and that $\Psi_{\rm T}(r)$ decreases with r, this means lowering the spatial density in the outer regions. Mimicking the effects of escapers below the truncation relative energy $\mathcal{E}_{\rm t}$, King models are obtained by subtracting to $f_{\rm iso}(\mathcal{E})$ its value at $\mathcal{E}_{\rm t}$ and setting $f_{\rm K} = 0$ at $\mathcal{E} \geq \mathcal{E}_{\rm t}$:

$$f_{\rm K}(\mathcal{E}) = \frac{\rho_1}{(2\pi\sigma^2)^{3/2}} \left(\mathrm{e}^{\mathcal{E}/\sigma^2} - \mathrm{e}^{\mathcal{E}_{\rm t}/\sigma^2}\right) \theta(\mathcal{E} - \mathcal{E}_{\rm t}), \tag{2.27}$$

where the Heaviside step function $\theta(x)$ ensures the non-negativity. Note that now σ is not the velocity dispersion of the stars, but just a model's parameter with dimensions of a velocity. Models truncated in relative energy are spatially truncated as well, with $\rho(r) = 0$ beyond a truncation radius $r_{\rm t}$ given by $\Psi_{\rm T}(r_{\rm t}) \equiv \mathcal{E}_{\rm t}$ (in this case, $\Psi_{\rm T} = \Psi$). King models have thus finite total mass, and their spatial truncation is physically motivated by the tidal influence of the host galaxy on its star clusters (King 1966).

To determine the density profiles, $f_{\rm K}(\mathcal{E})$ is integrated over the velocity space, giving $\rho(\Psi)$. Then, Poisson's equation (Eq. 1.3) is solved, with boundary conditions

$$\begin{cases} \Psi(0) = \sigma^2 W_0, \\ \left.\dfrac{\mathrm{d}\Psi}{\mathrm{d}r}\right|_{r=0} = 0, \end{cases} \tag{2.28}$$

to get $\Psi(r)$ and, consequently, $\rho(r)$. In Eq. (2.28), W_0 is the dimensionless central (relative) potential, which is the free parameter that sets the shape of King models.[7]

[7] In the following, for brevity, I omit the fact that W_0 is a *relative* potential. Moreover, despite it being 'dimensionless', it is *not* normalised according to the convention adopted here. Indeed, $W_0 = \Psi(0)/\sigma^2$, while our normalised relative stellar potential is $\tilde{\Psi}(r) = \Psi(r) r_{\rm K}/(GM)$, so $W_0 = \tilde{\Psi}(0) GM/(r_{\rm K}\sigma^2)$.

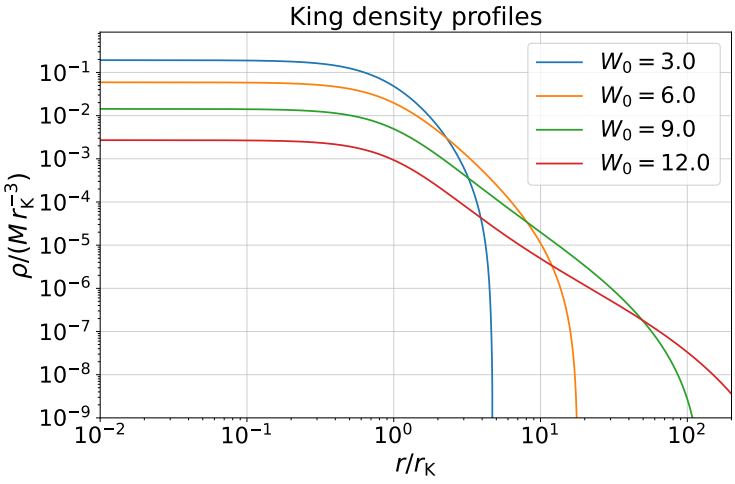

Figure 2.9. Density profiles of King models for some values of the dimensionless central potential W_0 (Eq. 2.28). The density is in units of Mr_K^{-3} and the radius is in units of r_K, where M is the total stellar mass and r_K is the King radius in Eq. (2.29).

There are two other independent free parameters of the models, which can be freely chosen among the total stellar mass M, the central density ρ_0, the density scale ρ_1, σ^2 and the so-called King radius

$$r_K = \sqrt{\frac{9\sigma^2}{4\pi G\rho_0}}. \tag{2.29}$$

Given two of these five parameters, for a fixed W_0, the remaining three are univocally determined.

We can work with dimensionless models, as usual, in which the mass unit is M, the length unit is r_K, and the velocity unit is $\sqrt{GM/r_K}$. We will thus consider a family of two-parameter (W_0 and μ) models easily scalable to systems of any physical size and total mass (see Section 2.1.1).

The King density profiles have no analytic expression, and some of them are shown in Fig. 2.9. The truncation radius (in units of r_K) is an increasing function of W_0, so models with higher W_0 are more concentrated, as they have more extended faint wings (Fig. 2.10). This reflects in an increasing ratio between the radius enclosing half the total stellar mass, namely, the half-mass radius r_h, and the King radius r_K as a function of W_0 (Fig. 2.10). All King profiles are flat for $r \ll r_K$, suggesting that they are incompatible with a central BH.

To verify this, let us compute their DFs in the presence of a BH, starting from the density profiles obtained in the way I have just described, adding to the total potential the BH's contribution $\Psi_\bullet = \mu/r$, and using Eddington's formula (Eq. 1.16). I shall refer

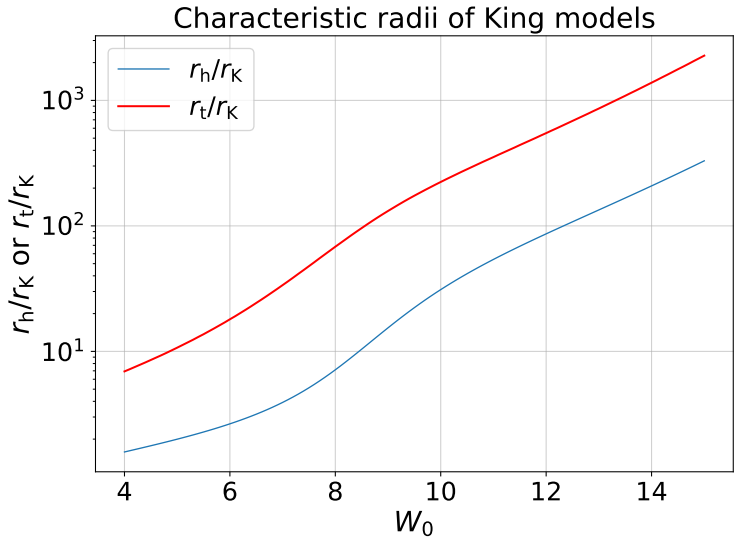

Figure 2.10. Half-mass radius r_h and truncation radius r_t as a function of the dimensionless central potential W_0 (Eq. 2.28) of the corresponding self-gravitating King models. The radii are in units of King radii r_K (Eq. 2.29).

to the models constructed in this way as *King models with BH*.

2.5.2 The Distribution Function

Since the density profiles of King models lack an analytic expression, I could not exploit any consistency condition among those cited in the previous sections. The numerical evaluation of the DFs with AGAMA still provides the information we need.[8] I show, in Fig. 2.11, the DFs for $\mu = 0,\ 10^{-3},\ 10^{-2},\ 10^{-1},\ 1$, and for even values of W_0 between 4 and 14.

The self-consistent DFs (red lines) are 'interrupted' at the relative energy $\mathcal{E}_{max} \equiv \Psi(0) = \sigma^2 W_0$ because the maximum relative energy of the stars coincides with the (finite) depth of the total potential well. For all values of W_0 and for all $\mu > 0$, f vanishes at two values of $\mathcal{E}$: the truncation relative energy $\mathcal{E}_t = \Psi_T(r_t)$ and a higher relative energy which I call $\mathcal{E}_0$. Note that, for $\mu < 1$, $\mathcal{E}_t$ is very similar to that of the self-consistent King models because at such low relative energies Ψ_T is dominated by Ψ, but this does not occur when the total stellar mass equals the BH's mass ($\mu = 1$), as the BH's attraction is relevant everywhere. Below $\mathcal{E}_t$, the DF is identically null, while,

[8] Conversely to what was done in the previous sections, here I do not show the DFs in the case $\mu = 10^{-4}$, for which I did not find a reliable numerical result.

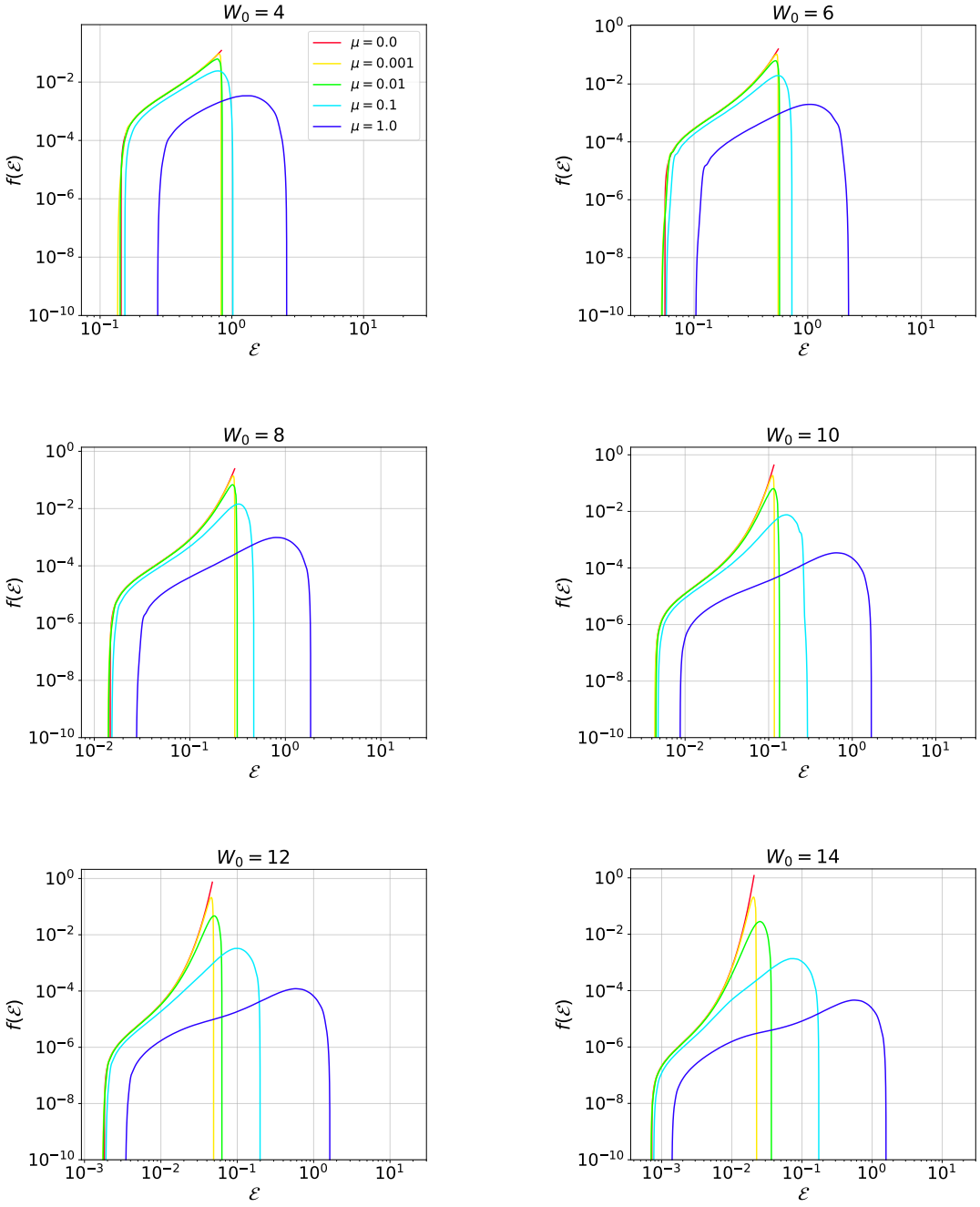

Figure 2.11. DFs of King models with $W_0 = 4$, 6, 8, 10, 12, 14 for BH-to-stellar mass ratios $\mu = 0$, 10^{-3}, 10^{-2}, 10^{-1}, 1. The legend is shown only in the first plot ($W_0 = 2$), but refers to all figures. When the DF crosses the $\mathcal{E}$-axis at high relative energies, it eventually becomes negative, while at low relative energies it just vanishes, as is normal for spatially truncated systems. The DF is in units of $(MG^3 r_\mathrm{K}^3)^{-1/2}$, while $\mathcal{E}$ is in units of GM/r_K, where M is the total stellar mass and r_K is the King radius (Eq. 2.29).

for $\mathcal{E} > \mathcal{E}_0$, $f(\mathcal{E}) < 0$. Hence, $\mathcal{E}_0$ can be defined as

$$\mathcal{E}_0 \equiv \inf \{\mathcal{E} \in [0, \Psi_{\rm T}(0)] \mid f(\mathcal{E}) < 0\} \,. \tag{2.30}$$

Therefore, all isotropic models with King density profiles are inconsistent when they host a central BH.

2.5.3 Observational Relevance

The aforementioned result is strictly true, from a mathematical point of view, but is it physically meaningful, too? In other words, does the consistency break in a phase-space region that we are able to probe and where our mathematical description of the stellar system is still valid? These questions are important for all the models encountered so far. Still, I chose to answer them in detail only for the specific case of King models, since they are those of greatest observational relevance for our scientific purposes, as King density profiles closely resemble those of several observed GCs (e.g., Barmby et al. 2007, Miocchi et al. 2013). The following conclusions can be easily extended to other models, repeating similar considerations.

Inconsistency Radius and Black Hole's Influence Radius

To understand whether our results are observationally testable, we need, first of all, to establish a connection between the relative energy of a star and its spatial position. As anticipated in Section 2.1.3, if a star has relative energy $\mathcal{E}$, it must be located at a radius r such that $\Psi_{\rm T}(r) = \mathcal{E} + v^2/2 \geq \mathcal{E}$. Since $\Psi_{\rm T}$ is always a decreasing function of r, this means that a star with relative energy $\mathcal{E}$ is always found within the spherical surface where $\Psi_{\rm T} = \mathcal{E}$. I call $r_{\mathcal{E}}$ the radius of this surface. Therefore, for a given BH-to-stellar mass ratio μ, all the stars with 'problematic' relative energies ($\mathcal{E} > \mathcal{E}_0$) are at radii smaller than $r_0 \equiv r_{\mathcal{E}_0}$. I shall call r_0 the *inconsistency radius*. Note, however, that stars with velocities $v \geq \sqrt{2(\Psi_{\rm T}(r) - \mathcal{E}_0)}$ have relative energies $\mathcal{E} \leq \mathcal{E}_0$ even if $r < r_0$. Hence, to prove the absence of a BH of mass $M_\bullet$ in a GC with isotropic stellar velocity dispersion whose density profile is well fitted by a King model, one would need to observationally probe *at least* the corresponding r_0, but more realistically even smaller radii.

To get a sense of the scales we are talking about, I show in Fig. 2.12a the inconsistency radius, in units of King radii, as a function of W_0, for BH-to-stellar mass ratios $\mu = 10^{-3},\ 10^{-2},\ 10^{-1}$. For fixed W_0 and $r_{\rm K}$, r_0 is an increasing function of μ, although for high W_0 the gap between the different curves decreases. Furthermore, this gap is

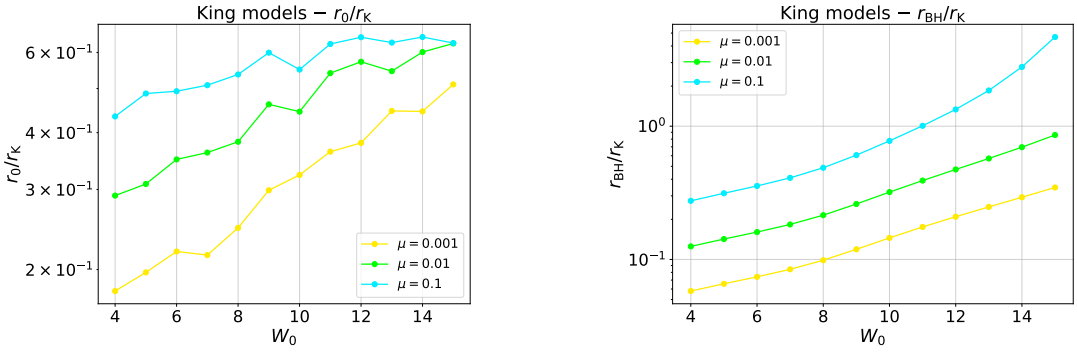

(a) **(b)**

Figure 2.12. (a) Inconsistency radius r_0 and (b) BH's influence radius $r_{\rm BH}$ as a function of W_0 for King models with BH. The parameter W_0 sets the shape of the King profiles (Eq. 2.28). Both radii are in units of King radii $r_{\rm K}$ (Eq. 2.29). In (a), r_0 is the radius at which $\Psi_{\rm T}(r_0) = \mathcal{E}_0$, which is the relative energy above which $f < 0$ (Eq. 2.30). In (b), $r_{\rm BH}$ is the radius enclosing 10% of the BH's mass in stars (Eq. 2.25). The different lines refer to the models with the BH-to-stellar mass ratios $\mu = 0.001,\ 0.01$ and 0.1

only of a factor $\lesssim 1.5$ between adjacent curves, although they are separated by a decade in μ. Thus, r_0 changes slowly with μ. Leaving aside some numerical fluctuations, $r_0/r_{\rm K}$ increases with W_0, for fixed μ. This is because more concentrated models (higher W_0) have lower central densities, in units of $Mr_{\rm K}^{-3}$ (Fig. 2.9), so the 'inconsistency' region is larger, for fixed μ and $r_{\rm K}$, because the BH dominates further out from the centre. In other words, in a family of King models with the same stellar mass and King radius, for a fixed BH's mass, r_0 increases as a function of W_0. Note, however, that the increase is by a factor of about 2, at most, between $W_0 = 4$ and $W_0 = 15$.

In Fig. 2.12b, I also show the BH's influence radius defined in Eq. (2.25), again normalised by the King radius, for the same values of μ as those used for r_0. Similarly to r_0, it increases as a function of μ, for fixed W_0 and $r_{\rm K}$, and as a function of W_0, for fixed μ and $r_{\rm K}$, but it does so in a more regular way. While the slopes of the $\mu = 10^{-3}$ and $\mu = 10^{-2}$ lines are roughly the same, the $\mu = 0.1$ line steepens when $r_{\rm BH} \approx r_{\rm K}$ (for $W_0 \approx 10$) because, near $r_{\rm K}$, ρ starts to decrease significantly (see Fig. 2.9). As a result, $M(r)$ increases more slowly with r than it does within the King radius, and a larger gap in $r_{\rm BH}$ between two subsequent values of $W_0 \gtrsim 10$ is required to obtain the same enclosed stellar mass, namely, $M(r_{\rm BH}) = 0.1\mu$.

Probing the Black Hole's Influence Radius

For a clearer comparison, I show, in Fig. 2.13, $r_0/r_{\rm BH}$ versus W_0, for $\mu = 10^{-3}$, 10^{-2}, 10^{-1}. As can be seen, r_0 is mostly larger than $r_{\rm BH}$, except for very high values of μ and

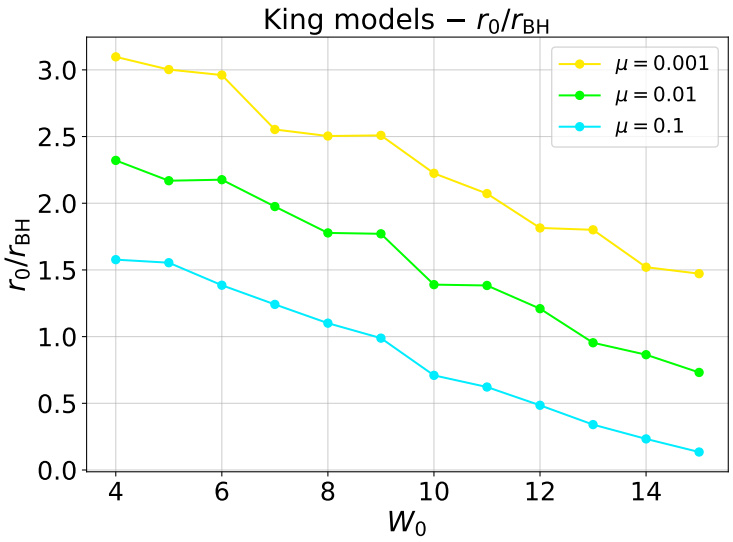

Figure 2.13. Ratio between the inconsistency radius r_0 and the BH's influence radius $r_{\rm BH}$ as a function of W_0 for King models with BH. The parameter W_0 sets the shape of the King profiles (Eq. 2.28); r_0 is the radius at which $\Psi_{\rm T}(r_0) = \mathcal{E}_0$, which is the relative energy above which $f < 0$ (Eq. 2.30); $r_{\rm BH}$ is the radius enclosing 10% of the BH's mass in stars (Eq. 2.25). The different lines refer to models with the BH-to-stellar mass ratios $\mu = 0.001,\ 0.01$ and 0.1.

W_0. This means that, in most cases, stars that would have $\mathcal{E} > \mathcal{E}_0$, in the presence of a BH of mass $M_\bullet = \mu M_{\rm GC}$, may begin to appear outside the region where the BH's gravitational attraction would be dominant. Note, however, that the gap between r_0 and $r_{\rm BH}$ is at most a factor of about 3, for $\mu = 10^{-3}$ and $W_0 = 4$, and it decreases as μ and W_0 increase. Considering the contamination of stars with $\mathcal{E} \leq \mathcal{E}_0$ within r_0, we can presume that $r_{\rm BH}$ (except when $r_0 \lesssim r_{\rm BH}$) is roughly the minimum radius that one should probe to gain a significant population of stars which would have $\mathcal{E} > \mathcal{E}_0$, if the BH-to-stellar mass ratio was the given μ. Below, I discuss the detectability of stars within $r_{\rm BH}$, although in Section 3.2 we will see that, to prove the absence of a central BH in a GC based on inconsistency arguments, even smaller radii should be probed, as an inner rise in the density profile may keep the DF non-negative. Still, the following discussion will be useful for understanding the validity of our results from an observational perspective, and we shall come back to it several times throughout Chapter 3.

For observational purposes, the yellow lines ($\mu = 10^{-3}$) in Figs. 2.12 and 2.13 are probably the most interesting, since an extrapolation of the Magorrian et al. (1998) relation down to GCs' masses predicts $M_\bullet \approx 10^{-3} M_{\rm GC}$. Fig. 2.12b shows that the ratio between the BH's influence radius and the King radius is of order 10^{-1}, so, for a typical

$r_{\rm K} \approx 1$ pc, we have $r_{\rm BH} \approx 0.1$ pc. At a distance of 10 kpc, typical for Galactic GCs, $r_{\rm BH}$ subtends an angle $\theta_{\rm BH} \approx 2''$. This is a rather small angular scale, but instruments like the HST or the recently launched JWST have the sub-arcsecond resolution needed to probe it, so they could be used for the closest and/or largest clusters, at least. Future observations with very-high-resolution telescopes such as the ELT will be even more successful in observing the central regions of nearby GCs.

Still, we need to answer an additional question: is there a sufficient number of stars within $r_{\rm BH}$ to make our DF-based description of GCs still valid? To answer, we can compute the mass of a King model enclosed within $r_{\rm BH}$. By definition, this is $0.1M_\bullet = 0.1\mu M_{\rm GC}$. Assuming $\mu \approx 10^{-3}$ and $M_{\rm GC} \approx 10^6$ $\mathrm{M}_\odot$ (for a quite massive cluster), one gets $M(r_{\rm BH}) \approx 100$ $\mathrm{M}_\odot$. For an average stellar mass $m \approx 1$ $\mathrm{M}_\odot$, we expect roughly 100 stars[9] to be within the BH's influence radius of such a GC, suggesting that the DF is valid.

This loose estimate is not to be taken as a reliable calculation of the number of stars that could be *detected* within $r_{\rm BH}$, which is highly uncertain. For instance, this number depends on the fraction of mass contained in 'dark' stellar remnants and faint stars, on the level of crowding in the field of view, etc. Still, dynamical studies exploiting some tens of stars detected within the innermost $1'' - 2''$ have already been performed (although they were often debated) for the closest and most massive clusters (e.g., Lanzoni et al. 2013, Mann et al. 2019, Della Croce et al. 2024), so we expect that the situation will improve in the future.

In Fig. 2.14, I show the mass enclosed within the inconsistency radius, $M_0 \equiv M(r_0)$, normalised by the total stellar mass, as a function of W_0 and for several values of μ. Again, there are some fluctuations in M_0, attributable to those in r_0 (Fig. 2.12a). As obvious from the fact that $r_0 \gtrsim r_{\rm BH}$, $M_0 \gtrsim M(r_{\rm BH}) = 0.1\mu$. The interesting fact is that M_0 can be even an order of magnitude larger than $M(r_{\rm BH})$, for low W_0 models, despite that r_0 is only a factor of a few larger than $r_{\rm BH}$. Indeed, e.g., for $\mu = 10^{-3}$, $M_0 \approx 10^{-3} M_{\rm GC}$, if $W_0 \lesssim 10$, while $M(r_{\rm BH}) = 10^{-4} M_{\rm GC}$. This is readily explained by the fact that, since $\rho(r)$ is approximately constant within r_0, as long as $r_0 \lesssim r_{\rm K}$, $M(r) \propto r^3$, roughly. Thus, if $r_0/r_{\rm BH} \approx 2 - 3$, then $M_0/M(r_{\rm BH}) \approx 8 - 27$. This suggests that a significant number of stars with $\mathcal{E} > \mathcal{E}_0$ might be detected even between r_0 and $r_{\rm BH}$.

[9] It is important to recall that we use the term 'star' to denote any point particle belonging to the system, but these could be even stellar remnants such as stellar-mass BHs or neutron stars. Hence, only an uncertain fraction of these ≈ 100 particles will be actual stars.

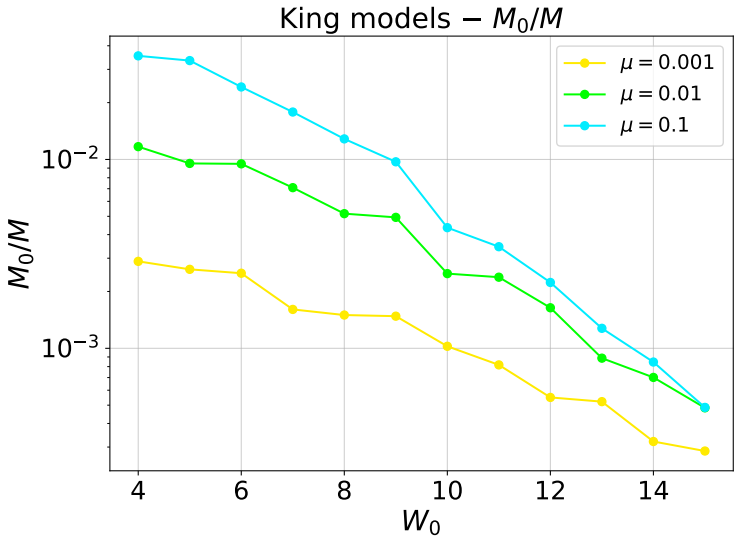

Figure 2.14. Stellar mass M_0 enclosed within the inconsistency radius r_0 as a function of W_0 for King models with BH. The parameter W_0 sets the shape of the King profiles, while r_0 is such that $\Psi_{\rm T}(r_0) = \mathcal{E}_0$, which is the relative energy above which the DF is negative. The different lines refer to models with the BH-to-stellar mass ratios $\mu = 0.001,\ 0.01$ and 0.1.

Chapter 3

Extent of the Central Cusp and Consistency

The theorems in Appendix A.2 establish that a large class of spherical density profiles is incompatible with the presence of a central point mass (i.e., a BH) sourcing an external gravitational field, when the stellar kinematic structure is isotropic. This class contains models with a density profile that is flat or rising more slowly than $r^{-1/2}$ towards the centre. The result of An & Evans (2006) confirms that *all* models with such density profiles and a central point mass are inconsistent (Eq. A.16). In the previous chapter, we verified this in many examples. However, all models encountered with a central density cusp at least as steep as $r^{-1/2}$ turned out to have a positive definite ergodic DFs, although this is not guaranteed a priori. A question may then arise: is the presence of a central density cusp proportional to $r^{-1/2}$ or steeper a *sufficient* condition for the consistency of spherical, isotropic systems with a central BH?

In this chapter, I answer this question by analysing the consistency of models where the density profile has three regimes: a central 'cusp' for $r \lesssim r_{\rm cusp}$, an almost flat 'core' for $r_{\rm cusp} \lesssim r \lesssim r_{\rm core}$, and an outer 'envelope' of lower stellar density. In particular, in Section 3.1, I construct a family of models where the inner cusp is the one predicted by Bahcall & Wolf (1976) for relaxed systems in the vicinity of a central BH, while the outer profile follows that of a King model. In Section 3.2, I show that the consistency of such models depends on the mass of the central BH and on the size of the central cusp. Furthermore, for a given BH-to-stellar mass ratio, I evaluate the size of the minimum cusp required for consistency, and of the cusp of the models where this arises at the BH's influence radius. I find that the latter is systematically larger than the former, and I discuss the observational relevance of both.

3.1 Bahcall-Wolf-King Models

We saw, in the last section of Chapter 2, that isotropic models with a King density profile and a central BH are inconsistent. This is important because King models have proven successful in reproducing the observed surface brightness profiles of many GCs (Barmby et al. 2007; Miocchi et al. 2013). However, in Section 2.5.3, we discussed how this is not sufficient to rule out the presence of a central IMBH, unless the observational data sample its relatively small sphere of influence, whose radius was estimated as $r_{\rm BH}$ (Eq. 2.25). For instance, a central rise in the density profile, not detected by the observations, may 'save' the consistency of the models with a central BH of sufficiently low mass. Such a feature has been predicted by a number of theoretical studies (e.g., Peebles 1972; Bahcall & Wolf 1976; Cipollina & Bertin 1994). A cusp in the observed surface brightness profile has even been used to infer the presence of an IMBH in some GCs, although these claimed detections are subject to many uncertainties and thus under debate (e.g., Lanzoni et al. 2007; Miocchi 2007).

3.1.1 Definition of the Models

A steep central density profile has been predicted to form in stellar systems hosting a central BH by several studies. One of the most important was the one of Bahcall & Wolf (1976), who found that a stellar system with a central BH should have a central density profile well approximated by a $r^{-7/4}$ power law within the BH's sphere of influence. The formation of a similar density cusp has been later confirmed by more sophisticated studies, including N-body simulations (e.g., Baumgardt et al. 2004a).

This finding was exploited by Miocchi (2007), who defined a self-consistent model for GCs with a central BH by taking King's DF in Eq. (2.27), for $\mathcal{E} \leq \Psi_{\rm T}(r_{\rm BH})$, and $f \propto \mathcal{E}^{1/4}$, for $\mathcal{E} > \Psi_{\rm T}(r_{\rm BH})$, which is the approximate DF found by Bahcall & Wolf (1976). He estimated the BH's influence radius $r_{\rm BH}$ as the radius enclosing 10% of the BH's mass in stars, which is the same definition we adopted (Eq. 2.25). In this way, he obtained a density profile resembling the $r^{-7/4}$ cusp for $r \lesssim r_{\rm BH}$ and King's density profiles for $r \gtrsim r_{\rm BH}$.

Here, we will construct models that are similar to those of Miocchi (2007), but with a complementary approach. Let us start by defining their stellar density profile (see Eq. 82 of Bahcall & Wolf 1976):

$$\rho(r) = \rho_{\rm K}(r) \left[1 + \left(\frac{r}{r_{\rm cusp}} \right)^{-7/4} \right], \tag{3.1}$$

where $\rho_{\rm K}$ is the density profile of King models (see Fig. 2.9) and $r_{\rm cusp}$ is a scale length which we shall call the *cusp radius*. For $r \ll r_{\rm cusp}$, $\rho \sim \rho_{\rm K}(r/r_{\rm cusp})^{-7/4}$. Since $\rho_{\rm K}$ is almost flat within its King radius $r_{\rm K}$ (Eq. 2.29), by choosing $r_{\rm cusp} \ll r_{\rm K}$, within $r_{\rm cusp}$ we have the desired power-law behaviour. For $r \gg r_{\rm cusp}$, the $\rho_{\rm K}$ term becomes dominant, so ρ is roughly constant for $r_{\rm cusp} \ll r \ll r_{\rm K}$, and then decreases out to the truncation radius $r_{\rm t}$. The shape of $\rho_{\rm K}$ is determined by the parameter W_0, which is the dimensionless central potential of the self-consistent King model producing the density profile $\rho_{\rm K}$. In this case, W_0 loses its original physical meaning and is just a dimensionless parameter of the models. Since $r_{\rm t}/r_{\rm K}$ is an increasing function of W_0 (see Section 2.5.1 and Fig. 2.10), the outer density decrease of the profiles in Eq. (3.1) is shallower for higher W_0. This family of density profiles reproduces all the features required: an inner Bahcall-Wolf cusp, a flat profile out to a 'core' radius[1] $r_{\rm K}$, and an outer 'envelope' of lower density out to the truncation radius $r_{\rm t}$, as can be seen from Fig. 3.1. The profile in Eq. (3.1) clearly reduces to a King density profile in the limit as $r_{\rm cusp} \to 0$. I will call Bahcall-Wolf-King (BWK) models the collisionless equilibrium models with density profiles as in Eq. (3.1), a central BH and an ergodic DF.

The BWK density profiles depend on four parameters: $\rho_{\rm K}$ needs W_0, $r_{\rm K}$ and its total mass $M_{\rm K}$, to be determined (Section 2.5.1); $r_{\rm cusp}$ defines the transition radius between the 'King regime' and the 'Bahcall-Wolf regime'. As we will see in Section 3.1.2, $M_{\rm K}$ is uniquely determined by the total stellar mass M and $r_{\rm cusp}/r_{\rm K}$, so $M_{\rm K}$ and M are interchangeable as free parameters. In the following, we will work with dimensionless quantities, with the unit of length being $r_{\rm K}$, the unit of mass being M, and the unit of velocity being $\sqrt{GM/r_{\rm K}}$ (see Section 2.1.1). We then reduce to a two-parameter family of density profiles defined by W_0 and $r_{\rm cusp}$ (in units of $r_{\rm K}$).

To complete our models, we assume an ergodic DF $f(\mathcal{E})$, so that it can be recovered through Eddington's formula (Eq. 1.16) and the velocity distribution is isotropic. The total relative potential is $\Psi_{\rm T} = \Psi + \Psi_\bullet$, where Ψ is the stellar relative potential related to ρ via Poisson's equation (Eq. 1.3; recall that $\Psi = -\Phi$) and $\Psi_\bullet = \mu/r$ is the (dimensionless) potential produced by a central BH of mass $M_\bullet = \mu M$. The family of dimensionless BWK models is then characterised by the three free parameters W_0, $r_{\rm cusp}$ (in units of $r_{\rm K}$) and μ.[2]

[1] The usual definition of the core radius $r_{\rm c}$, in GCs, is actually the radius at which the surface brightness is half the central value. Although $r_{\rm c}$ and $r_{\rm K}$ are rather similar for King models (e.g., Peterson & King 1975), in the following, I shall circumvent referring to $r_{\rm K}$ as the core radius to avoid confusion.

[2] From now on, I will refer to such models as BWK models, without specifying that they are dimensionless, if not otherwise stated.

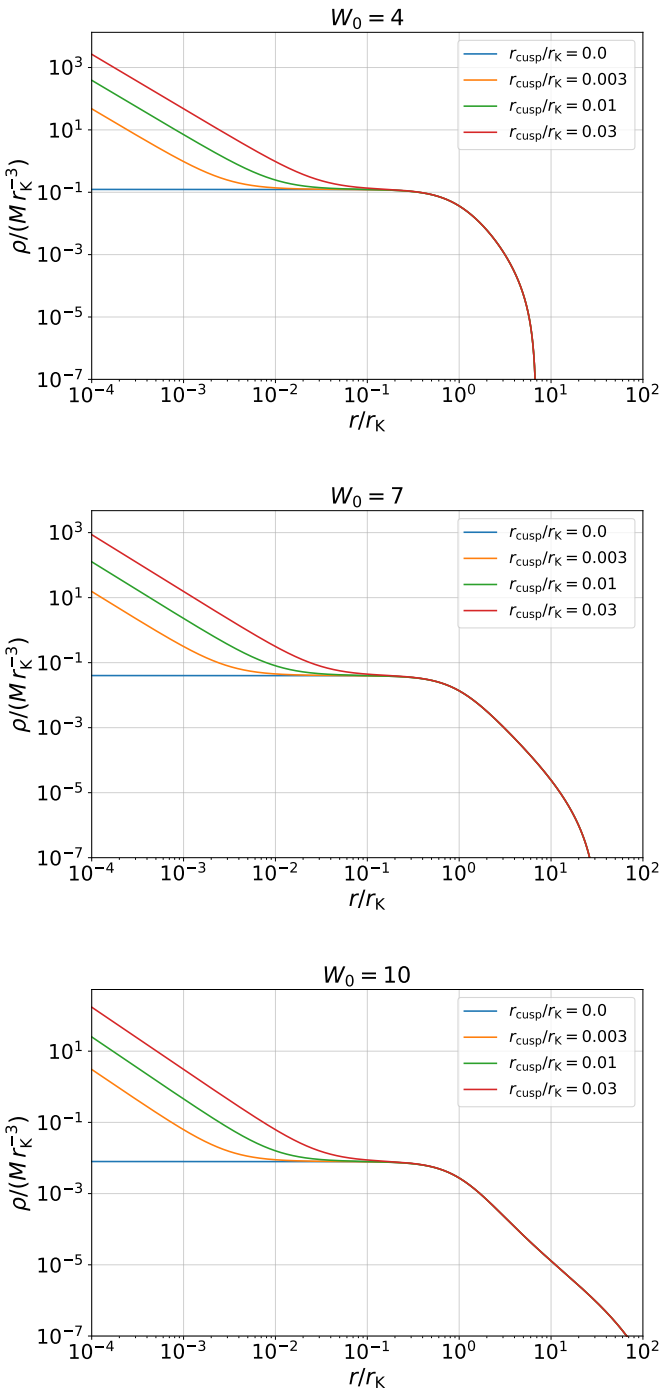

Figure 3.1. Bahcall-Wolf-King density profiles with $W_0 = 4,\ 7$ and 10 (Eq. 3.1). The parameter W_0 sets the shape of the outer profile. In each figure, I show the profiles for $r_{\rm cusp}/r_{\rm K} = 0.003,\ 0.01$ and 0.03, where $r_{\rm K}$ is the King radius (Eq. 2.29). The $r_{\rm cusp}/r_{\rm K} = 0$ profiles are the standard King profiles with dimensionless central potential W_0 (Section 2.5.1). The density is in units of $M r_{\rm K}^{-3}$, where M is the total stellar mass.

3.1.2 Construction of the Models

Let us go through the procedure for the construction of a BWK model with given W_0, $\xi_{\rm cusp} \equiv r_{\rm cusp}/r_{\rm K}$ and BH-to-stellar mass ratio μ. We want to create a model with a given total stellar mass M. This quantity can be obtained by integrating Eq. (3.1) over all space. Hence,

$$M = 4\pi \int_0^\infty \rho_{\rm K}(r) r^2 {\rm d}r + 4\pi \int_0^\infty \rho_{\rm K}(r) \left(\frac{r}{r_{\rm cusp}}\right)^{-7/4} r^2 {\rm d}r. \tag{3.2}$$

Call $M_{\rm K}$ the first term on the right-hand side (RHS) and $M_{\rm cusp}$ the second. Defining $x \equiv M_{\rm cusp}/M_{\rm K}$, we can write $M_{\rm K} = M/(1+x)$. Recall that to compute a King profile, one needs to specify two parameters, besides W_0, which we choose to be its total mass $M_{\rm K}$ and King radius $r_{\rm K}$. To define the adequate $\rho_{\rm K}$ so that the RHS of Eq. (3.2) evaluates to M, we need to find x.

For the given W_0, using the DF in Eq. (2.27), one can compute the density profile $\rho_{\rm K,0}$ for a King model with arbitrary mass $M_{\rm K,0}$ and King radius $r_{\rm K,0}$. Then, for the given $\xi_{\rm cusp}$, we can compute the ratio

$$\begin{aligned} y \equiv \frac{M_{\rm cusp,0}}{M_{\rm K,0}} &= 4\pi \int_0^\infty \frac{\rho_{\rm K,0}(r)}{M_{\rm K,0}} \left(\frac{r}{\xi_{\rm cusp}\, r_{\rm K,0}}\right)^{-7/4} r^2 {\rm d}r \\ &= 4\pi \int_0^\infty \frac{\rho_{\rm K,0}(\xi r_{\rm K,0})}{M_{\rm K,0}\, r_{\rm K,0}^{-3}} \left(\frac{\xi}{\xi_{\rm cusp}}\right)^{-7/4} \xi^2 {\rm d}\xi, \end{aligned} \tag{3.3}$$

where $\xi \equiv r/r_{\rm K,0}$. This is independent of $M_{\rm K,0}$ and $r_{\rm K,0}$ because $\rho_{\rm K,0}/(M_{\rm K,0}\, r_{\rm K,0}^{-3})$ is the density profile of a King model of unitary total mass and King radius for all $M_{\rm K,0}$ and $r_{\rm K,0}$.

Therefore, for the assumed W_0 and $\xi_{\rm cusp}$, $y \equiv M_{\rm cusp,0}/M_{\rm K,0}$ can be computed for arbitrary $M_{\rm K,0}$ and $r_{\rm K,0}$, and $x = y$. To produce the model with the wanted M, we can then compute $M_{\rm K} = M/(1+y)$. By specifying also $r_{\rm K}$, we can then determine $r_{\rm cusp} = \xi_{\rm cusp}\, r_{\rm K}$ and $\rho_{\rm K}$, which is computed as the King profile with the given W_0, total mass $M_{\rm K}$ and King radius $r_{\rm K}$. Substituting $\rho_{\rm K}$ and $r_{\rm cusp}$ into Eq. (3.1), one gets the BWK density profile with the desired parameters W_0 and $\xi_{\rm cusp}$, and the desired total stellar mass M and King radius $r_{\rm K}$.

In our dimensionless units, $\tilde{M}_{\rm K} \equiv M_{\rm K}/M = 1/(1+x)$ and $\tilde{r}_{\rm K} = 1$. Hence, $\rho_{\rm K}$ can be computed as the King density profile with the assumed W_0, mass $\tilde{M}_{\rm K}$ and King radius $\tilde{r}_{\rm K}$. Substituting $\rho_{\rm K}$ and $r_{\rm cusp} = \xi_{\rm cusp}$ into Eq. (3.1), one obtains the BWK density profile, in units of $M r_{\rm K}^{-3}$, for the given W_0 and $\xi_{\rm cusp}$, expressed as a function of

the radius r in units of $r_{\rm K}$. At this point, $\Psi(r)$ can be calculated by solving Poisson's equation, so that $\Psi_{\rm T}(r) = \Psi(r) + \mu/r$ is known for the chosen μ, and Eddington's formula can be used to find $f(\mathcal{E})$.

I executed this entire procedure with the AGAMA software. I used it for constructing the density profiles, which required the evaluation of Eq. (3.3) and of $\rho_{\rm K}(r)$, and for computing $\Psi(r)$ and $f(\mathcal{E})$.

3.2 Consistency of the Bahcall-Wolf-King Models

In the present section, I analyse which, among the models described above, can be physically acceptable, by assessing the sign of their DFs. In practice, they are modifications of the isotropic King models with central BHs presented in Section 2.5, which we found to be inconsistent whenever the mass $M_\bullet$ of the BH is non-vanishing. This is likely ascribed to their centrally flat profile, as in Appendix A.2 I show that a large class of spherical systems which host a central point mass and have density profiles flatter than $r^{-1/2}$ at the centre have a negative ergodic DF at high relative energies (see also An & Evans 2006). For this reason, one may expect that the BWK models can be consistent even when $M_\bullet > 0$, thanks to their central power-law cusp. As we will shortly see, this is true, but not all models of the family are consistent for a given BH-to-stellar mass ratio μ.

3.2.1 The Distribution Function

The main feature affecting the consistency of a BWK model with a given μ is the extent of the central cusp. Intuitively, we may expect that the stars inside the region of influence of the BH must be distributed in such a way that the density profile is steep. When a significant number of stars producing a flat ρ is located inside this region, namely, when the cusp's extent is small enough, the DF becomes negative at the relative energies of such stars. In the following, I illustrate this concept on more quantitative grounds. To maintain the focus on the key aspect of the chapter, that is, how the size of the cusp and μ affect the consistency, I restrict the analysis to BWK models with $W_0 = 7$, corresponding roughly to the median value for the Galactic GCs fitted with a King profile.[3] The remaining free parameters of the models are $r_{\rm cusp}$ (in units of $r_{\rm K}$) and μ.

[3]Value obtained by taking the median concentrations $c \equiv \log(r_{\rm t}/r_{\rm K})$ of the globular clusters in the Harris (1996) catalogue and finding the unique values of W_0 producing the given concentrations. Core-collapsed clusters were excluded from the sample.

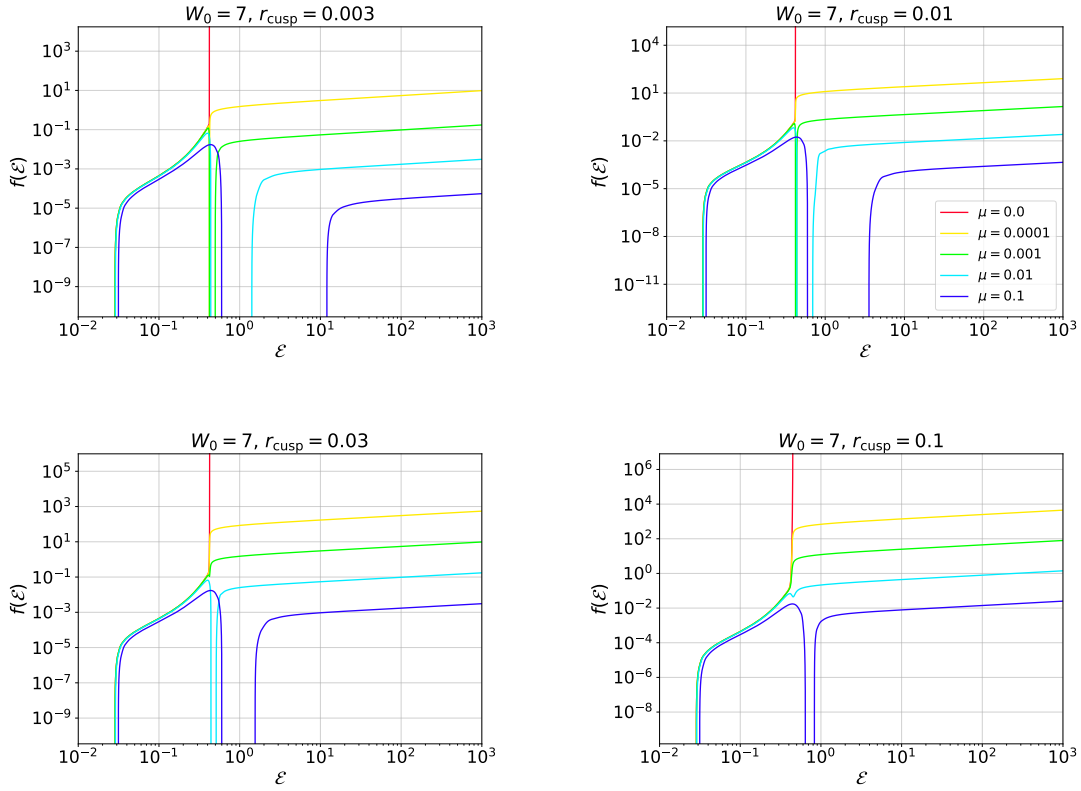

Figure 3.2. DFs of Bahcall-Wolf-King models with $W_0 = 7$ and $r_{\rm cusp} = 0.003,\ 0.01,\ 0.03$ and 0.1 versus the relative energy $\mathcal{E}$. Each plot shows the DFs for the BH-to-stellar mass ratios $\mu = 0,\ 10^{-4},\ 10^{-3},\ 10^{-2}$, and 10^{-1}. The legend is shown only in the figure for $r_{\rm cusp} = 0.01$, but refers to all of them. All the curves cross the $\mathcal{E}$-axis once at the truncation relative energy $\mathcal{E}_{\rm t}$, below which $f(\mathcal{E}) = 0$. Curves crossing the $\mathcal{E}$-axis more than once reach negative values. The DF is in units of $(MG^3 r_{\rm K}^3)^{-1/2}$, $\mathcal{E}$ is in units of $GM/r_{\rm K}$ and $r_{\rm cusp}$ is in units of $r_{\rm K}$. M is the total stellar mass and $r_{\rm K}$ is the King radius (Eq. 2.29).

Below, I report the quantities in dimensionless units, according to the convention introduced at the end of Section 3.1.1. As a useful reminder, I report here the unit of length is $r_{\rm K}$, the unit of relative energy is $GM/r_{\rm K}$, and the unit of phase-space mass density is $(M\,G^3\,r_{\rm K}^3)^{-1/2}$.

In Fig. 3.2, we can see how the cusp's extent affects the consistency of the BWK models with $W_0 = 7$, looking at the DFs computed for several values of the cusp radius and of the BH-to-stellar mass ratio. It is important to recall that these models are spatially truncated beyond $r_{\rm t}$, so the DF vanishes at $\mathcal{E}_{\rm t} = \Psi_{\rm T}(r_{\rm t})$. For $\mathcal{E} \leq \mathcal{E}_{\rm t}$, $f(\mathcal{E})$ is identically null. The curves that cross the $\mathcal{E}$-axis more than once in Fig. 3.2 vanish even at $\mathcal{E} > \mathcal{E}_{\rm t}$, and they are *negative* in the region where they are outside the boundaries of the plot. All the self-gravitating models ($\mu = 0$) have a positive definite DF. On the contrary, for the cusp radius $r_{\rm cusp} = 0.003$, the DF is negative at some relative energies

for all the considered non-vanishing BH-to-stellar mass ratios, i.e., $\mu = 10^{-4}$, 10^{-3}, 10^{-2} and 10^{-1}. Increasing $r_{\rm cusp}$ to 0.01, the $\mu = 10^{-4}$ DF becomes positive definite. For $r_{\rm cusp} = 0.03$, even the $\mu = 10^{-3}$ model attains consistency, while for $r_{\rm cusp} = 0.1$, the only inconsistent model remains that with $\mu = 0.1$. This clearly suggests that there is a minimum $r_{\rm cusp}$ for the consistency of a BWK model with given μ, and that this value is an increasing function of μ.

3.2.2 Extent of the Bahcall-Wolf Cusp

We then need a way to define the extent of the density cusp. The most straightforward one is by means of $r_{\rm cusp}$. However, we have seen that inconsistency occurs when the logarithmic density slope

$$\gamma(r) \equiv -\frac{\mathrm{d}\ln\rho}{\mathrm{d}\ln r} \tag{3.4}$$

is below the threshold of 1/2 at the centre. Hence, I defined the radius

$$r_{1/2} \equiv \min\{r \in \mathbb{R}^+ \mid \gamma(r) = 1/2\} \tag{3.5}$$

as a possible alternative estimate for the cusp's size. Some examples of the logarithmic density slope profile for BWK models with $W_0 = 7$ are shown in Fig. 3.3. It is evident that the equation $\gamma(r) = 1/2$ has two roots for most values of $r_{\rm cusp}$: one at $r_{1/2}$, where the $r^{-7/4}$ power law transitions to the flat King core, and one where the core steepens at the outskirts, close to $r_{\rm K}$. I show in Fig. 3.4 how the ratio $r_{1/2}/r_{\rm cusp}$ changes as a function of $r_{\rm cusp}$, for $W_0 = 7$. This ratio is fairly constant around 1.7 for $r_{\rm cusp} \lesssim 0.01$, while it increases up to about 2.4 at $r_{\rm cusp} \simeq 0.1$. This is because, for $0.01 \lesssim r_{\rm cusp} \lesssim 0.1$, $\rho_{\rm K}$ starts to be slightly steep close to the cusp radius, so the cuspy behaviour 'survives' up to a larger fraction of $r_{\rm cusp}$. We note that for higher values of $r_{\rm cusp}$ the equation $\gamma(r) = 1/2$ has no roots, so $r_{1/2}$ cannot be defined. Thus, for $r_{\rm cusp} \gtrsim 0.1$, the flat core is erased by the Bahcall-Wolf cusp.

3.2.3 Critical Bahcall-Wolf-King Models

Within this framework, I determined which $W_0 = 7$ BWK models have a positive definite DF over a grid of parameters $r_{\rm cusp}$ and μ. I numerically calculated the dimensionless DF f as a function of the dimensionless relative energy $\mathcal{E}$ (i.e., the relative energy in units of $GM/r_{\rm K}$) over the interval $\mathcal{E} \in [\mathcal{E}_{\rm t}, 10^8]$ for 13 logarithmically spaced values of μ between 10^{-4} and 0.1, and for $r_{\rm cusp} \in [10^{-5}, 1]$, in units of $r_{\rm K}$, choosing a logarithmic spacing $\Delta \log r_{\rm cusp} = 0.01$, corresponding to $(r_{{\rm cusp},i+1} - r_{{\rm cusp},i})/r_{{\rm cusp},i} \simeq 2.3\%$. For each μ, I found the minimum cusp radius $\bar{r}_{\rm cusp}(\mu)$ that makes the model consistent, which I

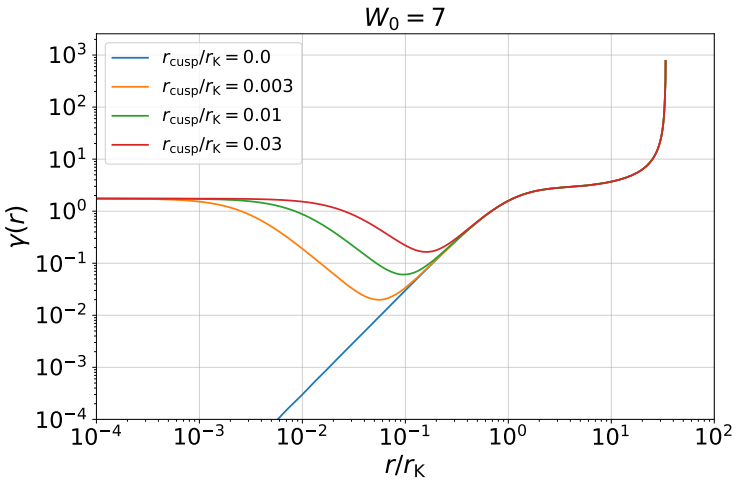

Figure 3.3. Logarithmic density slope $\gamma = -\,\mathrm{d}\ln\rho/\mathrm{d}\ln r$ as a function of radius (in units of $r_{\rm K}$) for Bahcall-Wolf-King models with $W_0 = 7$ and $r_{\rm cusp}/r_{\rm K} = 0.003,\ 0.01$ and 0.03, where $r_{\rm K}$ is the King radius (Eq. 2.29). The curve with $r_{\rm cusp}/r_{\rm K} = 0$ corresponds to the King model with $W_0 = 7$.

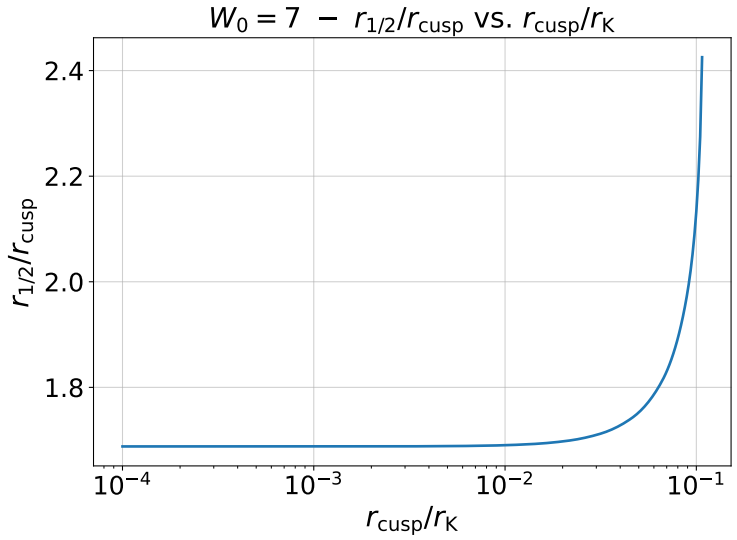

Figure 3.4. Ratio between $r_{1/2}$ (Eq. 3.5) and $r_{\rm cusp}$ (Eq. 3.1) for Bahcall-Wolf-King models with $W_0 = 7$. At odds with the y-axis, the x-axis is on a logarithmic scale. The radius $r_{\rm cusp}$ is normalised by the King radius defined in Eq. (2.29).

shall call the *critical cusp radius*. I call this model the *critical model*, for the given μ, and I indicate with an overbar the quantities related to it. For each critical model, I also computed $\bar{r}_{1/2} \equiv r_{1/2}(\bar{r}_{\rm cusp})$ and $\bar{r}_{\rm BH}$. The latter is the radius at which $M(\bar{r}_{\rm BH}) = 0.1\mu$, with $M(r)$ being the cumulative mass profile of the critical model, namely, the BWK model with $W_0 = 7$ and $r_{\rm cusp} = \bar{r}_{\rm cusp}(\mu)$.

To make a comparison with the models studied in Section 2.5, I evaluated some quantities for the corresponding King models with BH, namely, the BWK models with the same W_0 and μ as the critical models, but $r_{\rm cusp} \to 0$. These quantities are the BH's influence radius $r_{\rm BH,K}(\mu)$ (Eq. 2.25) and the inconsistency radius r_0, which I recall being the radius at which $\Psi_{\rm T}(r_0) = \mathcal{E}_0$, with

$$\mathcal{E}_0 \equiv \inf \{\mathcal{E} \in [0, \Psi_{\rm T}(0)] \mid f(\mathcal{E}) < 0\} \,. \tag{3.6}$$

Note that, in Eq. (3.6), f is the DF of the King model with BH, not of the critical BWK model. Also, note that $r_{\rm BH,K} \neq \bar{r}_{\rm BH}$ for the same μ, although they are defined in the same way, because $M(r)$ changes in the two cases.

For all the radii listed above, I also computed the stellar mass they enclose and the maximum relative energy of stars at such radii, i.e., $\mathcal{E}_l \equiv \Psi_{\rm T}(r_l)$, with $l =$ 'cusp', '1/2', 'BH', and so on.[4] I show all these parameters in Tables 3.1 and 3.2. I recall here that the quantities in the tables, as well as in the following discussion, are dimensionless, with all the lengths normalised by $r_{\rm K}$, all the masses normalised by the total stellar mass M, and all the relative energies normalised by $GM/r_{\rm K}$.

Fig. 3.5 shows the trend of $\bar{r}_{\rm cusp}$ with the BH-to-stellar mass ratio μ. This critical cusp radius, as is intuitive, increases with μ. For $10^{-4} \leq \mu \leq 10^{-1}$, $\bar{r}_{\rm cusp}$ covers the range 5.1×10^{-3} to 1.2×10^{-1}. I note that for the largest two values of μ considered ($\mu = 0.056,\ 0.1$), $\bar{r}_{1/2}$ is not defined, since $\bar{r}_{\rm cusp}$ is so large that $\gamma(r) > 1/2$ for all r (Table 3.1). Our models thus suggest that IMBHs with mass ratios $M_\bullet/M_{\rm GC} \approx 0.05-0.1$, well above the Magorrian et al. (1998) relation for galaxies, should steepen the density profile of a GC for the whole extent of the core. For more plausible BH-to-stellar mass ratios, $\bar{r}_{1/2}$ exists, and we can consider it as the minimum cusp's extent for consistency. Indeed, since it is larger than $\bar{r}_{\rm cusp}$ (Fig. 3.4), we regard it as a reasonable estimate for the maximum radius where the density profile of the critical BWK models is significantly steep.

We can now compare the properties of these critical BWK models (i.e., the consistent BWK models with the smallest cusp for the given μ) with those of the King models with

[4] Recall that stars with $\mathcal{E} \geq \mathcal{E}_l$ are necessarily within a distance r_l to the centre because $\Psi_{\rm T}(r) = \mathcal{E} + v^2/2 \geq \mathcal{E} \geq \mathcal{E}_l = \Psi_{\rm T}(r_l)$ implies $r < r_l$, since $\Psi_{\rm T}(r)$ is a decreasing function of radius.

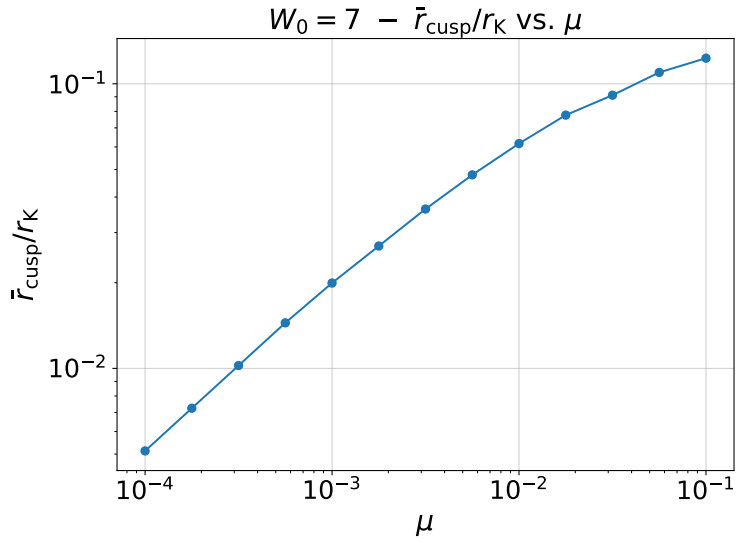

Figure 3.5. Minimum cusp radius (Eq. 3.1) for the consistency of $W_0 = 7$ Bahcall-Wolf-King models as a function of the BH-to-stellar mass ratio μ. The radius $\bar{r}_{\rm cusp}$ is in units of King radii (Eq. 2.29).

BH studied in Section 2.5. I argued, in Section 2.5.3, that the minimum radius to be observationally probed to hope ruling out the presence of a BH of given mass, assuming a spherical isotropic system, should be its influence radius $r_{\rm BH,K}$, which I defined as the radius enclosing 10% of the BH's mass in stars. However, Fig. 3.6 shows that a cusp may save the consistency of the model even if its extent is a fraction of $r_{\rm BH,K}$. Therefore, observations detecting stars within $r_{\rm BH,K}(\mu)$, but not within $\bar{r}_{1/2}(\mu)$, cannot rule out the presence of a BH of mass $M_\bullet = \mu M_{\rm GC}$ based on our models, because an inner 'hidden' cusp could prevent the models from being inconsistent. For BWK models with $W_0 = 7$, $\bar{r}_{1/2}$ ranges from about $0.2\,r_{\rm BH,K}$, for $\mu = 10^{-4}$, to about $0.6\,r_{\rm BH,K}$, for $\mu = 10^{-2}$. For $\mu \approx 10^{-3}$, which is the value suggested by Magorrian's relation, $\bar{r}_{1/2} \approx 0.4\,r_{\rm BH,K}$. Note that $\bar{r}_{1/2}$ is smaller than the inconsistency radius r_0 as well, since $r_{\rm BH,K} < r_0$ in most King models with BH, including those with $W_0 = 7$ and $\mu \lesssim 0.1$ (Fig. 2.13).

3.2.4 Observational Relevance of the Critical Cusp

Another aspect to investigate is whether such a small density cusp could be statistically significant or not. The fraction of the total stellar mass enclosed within $\bar{r}_{1/2}$ is shown as a function of μ in Fig. 3.7 (see also Table 3.1). Our models predict that a fraction of the order of 10^{-5} of the total stellar mass should be contained within the inner cusp, if $\mu \approx 10^{-3}$. For a quite massive GC of mass $M_{\rm GC} \approx 10^6$ $\mathrm{M}_\odot$, this means that only roughly 10 $\mathrm{M}_\odot$ are within $\bar{r}_{1/2}$. It seems then unlikely that this radius can contain

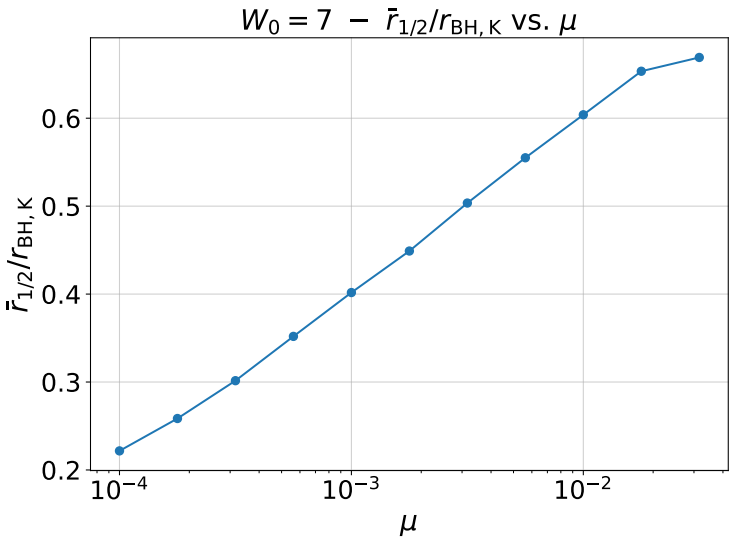

Figure 3.6. Ratio between $\bar{r}_{1/2}$, i.e., the minimum $r_{1/2}$ for the consistency of Bahcall-Wolf-King models, and $r_{\mathrm{BH,K}}$, i.e., the BH's influence radius in the King models, as a function of the BH-to-stellar mass ratio μ. The quantities are computed for Bahcall-Wolf-King models with $W_0 = 7$ and King models with $W_0 = 7$. The radius $r_{1/2}$ is the minimum radius of a given Bahcall-Wolf-King model at which $\mathrm{d}\ln\rho/\mathrm{d}\ln r = -1/2$ (Eq. 3.5), while $r_{\mathrm{BH,K}}$ contains a stellar mass equal to 10% of the BH's mass (Eq. 2.25).

enough stars to produce a significant cusp. This means that ruling out the presence of a central BH of mass $M_\bullet \approx 10^{-3} M_{\mathrm{GC}}$ using these models would be almost impossible in typical GCs, because the DF cannot reliably describe the distribution of stars (and remnants) where the minimum cusp needed for the consistency would arise. Therefore, it would be extremely difficult to distinguish between a King profile, incompatible with a central BH, and the corresponding critical BWK profile with minimal cusp, which would prevent the inconsistency of the model.

The situation is even worse, of course, for $\mu \lesssim 10^{-3}$. However, more massive BHs, producing a BH-to-stellar mass ratio of about 5×10^{-3}, are predicted to have $M(\bar{r}_{1/2}) \approx 1.6 \times 10^{-4} M_{\mathrm{GC}} \approx 160\ \mathrm{M}_\odot$, if $M_{\mathrm{GC}} \approx 10^6\ \mathrm{M}_\odot$. This indicates that such massive IMBHs should produce a statistically significant critical cusp, whose extent should be $\bar{r}_{1/2} \approx 0.08\, r_{\mathrm{K}}$. For $r_{\mathrm{K}} \approx 1$ pc, at a distance of 10 kpc, $\bar{r}_{1/2}$ subtends an angle of about $1.6''$. As discussed in Section 2.5.3, we have some hope of detecting a significant number of stars within this angular scale around the centre of the Galactic GCs using the best current and future facilities. Therefore, if our assumptions matched the observed properties of a cluster and if there were no sign of a density cusp, constraining the presence of BHs of mass $M_\bullet \gtrsim 5 \times 10^{-3} M_{\mathrm{GC}}$ at the centre of that cluster could be

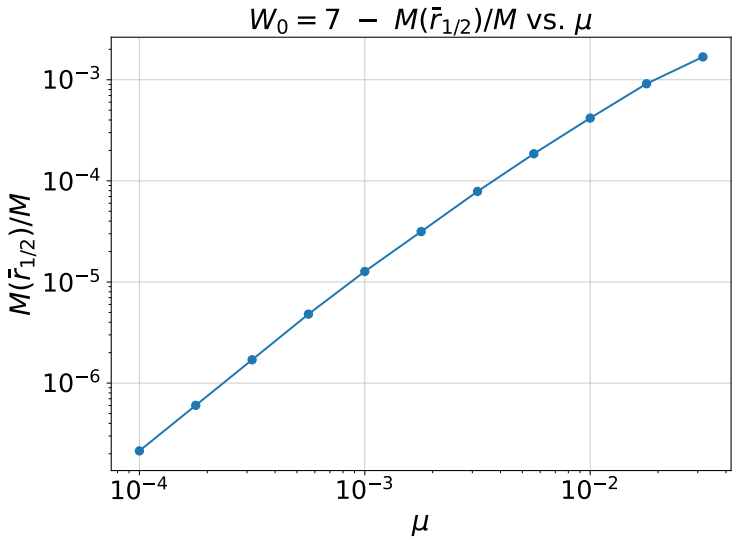

Figure 3.7. Stellar mass enclosed within $\bar{r}_{1/2}$ for Bahcall-Wolf-King models with $W_0 = 7$ as a function of the BH-to-stellar mass ratio μ. The radius $\bar{r}_{1/2}$ is the minimum radius at which $\mathrm{d}\ln\rho/\mathrm{d}\ln r = -1/2$, computed for the model with the smallest r_{cusp} (Eq. 3.1) required for the consistency. Here, $M(\bar{r}_{1/2})$ is normalised by the total stellar mass.

possible using these BWK models.

3.2.5 Detectability of a Physically Plausible Cusp

Of course, a central BH could produce a cusp more extended than $\bar{r}_{1/2}$, and the model would still be consistent. For instance, Miocchi (2007) suggests that r_{BH}, as defined in Eq. (2.25), should be the appropriate transition radius between the Bahcall-Wolf cusp and the King profile. He argues that this might be the correct compromise between the BH dominating inside it, so that the power-law profile is established, and the stellar distribution being isothermal outside it. However, it is important to note that other definitions have been proposed for the BH's radius of influence, at which the cusp should rise (e.g., Merritt 2013, Sec. 2.2), and that, for a given model, these may differ from the value obtained using the prescription of Miocchi (2007). The results presented below using $r_{\mathrm{BH}} = r_{\mathrm{cusp}}$ are thus to be taken as order-of-magnitude estimates, as the actual value of r_{cusp} produced by a given BH could be somewhat different.

For our illustrative purposes, let us assume that the picture of Miocchi (2007) is correct. Since they place the transition between the Bahcall-Wolf DF and King's DF at $\mathcal{E}_{\mathrm{BH}} \equiv \Psi_{\mathrm{T}}(r_{\mathrm{BH}})$, we can identify their profiles as BWK profiles where $r_{\mathrm{BH}}(\mu; r_{\mathrm{cusp}}) = r_{\mathrm{cusp}}$. I recall that r_{BH} is the radius at which $M(r_{\mathrm{BH}}) = 0.1\,\mu$, so it depends on r_{cusp}

because $M(r)$ depends on the shape of the density profile. More and more mass is concentrated in the central regions as $r_{\rm cusp}$ increases, implying that $r_{\rm BH}(\mu; r_{\rm cusp})$ is a decreasing function of $r_{\rm cusp}$ (see Fig. 3.8). Therefore, the function $D(\mu; r_{\rm cusp}) \equiv r_{\rm BH}(\mu; r_{\rm cusp}) - r_{\rm cusp}$ decreases with $r_{\rm cusp}$. Also, for all $\mu > 0$, this function is positive as $r_{\rm cusp} \to 0$, because it tends to $r_{\rm BH}(\mu; 0) > 0$, and negative for some sufficiently large $r_{\rm cusp}$, because, as $r_{\rm cusp} \to \infty$, $r_{\rm BH}(\mu; r_{\rm cusp})$ decreases. Hence, $D(\mu; r_{\rm cusp})$ has one and only one root, for a given $\mu \in]0, 10[$,[5] which I call $r_{\rm BH,M}(\mu)$ (e.g., see the filled circles in Fig. 3.8).

Fig. 3.9 shows that the minimum cusp radius $\bar{r}_{\rm cusp}$ required for the consistency of our models ranges between $0.2\, r_{\rm BH,M}$ and $0.5\, r_{\rm BH,M}$. Hence, if the assumption of Miocchi (2007) were correct, the cusp produced by a central BH would be systematically larger than the minimum cusp for consistency. Recalling that $\bar{r}_{1/2} \approx 2\, \bar{r}_{\rm cusp}$ (Fig. 3.4), we can write $0.4 \lesssim \bar{r}_{1/2}/r_{\rm BH,M} \lesssim 1$, for μ between 10^{-4} and 10^{-2}. Over the same range, we have seen that $\bar{r}_{1/2}/r_{\rm BH,K}$ increases from about 0.2 to about 0.6. Hence, $r_{\rm BH,M} \approx 0.5\, r_{\rm BH,K}$ over this range of BH-to-stellar mass ratios, as can be deduced also from Fig. 3.8. Since $r_{\rm BH,M}$ coincides with $r_{\rm cusp}$, in the BWK models with Miocchi's cusp we have $r_{1/2} \approx 2 r_{\rm BH,M} \approx r_{\rm BH,K}$. In other words, the extent of the Miocchi's cusp produced by a given BH in a BWK profile is roughly coincident with the size of the sphere of influence of that BH in a stellar system following a King density profile with the same W_0 as that of the BWK profile. Therefore, for the observational relevance of such a cusp, I refer the reader to Section 2.5.3, where I qualitatively discussed the detectability of stars within $r_{\rm BH,K}$ for typical GCs with King density profiles. Here, it suffices to recall that we found that $r_{\rm BH,K}$ subtends an angle of the order of $2''$ at a distance of 10 kpc, if $\mu \approx 10^{-3}$, and that we expect it to contain about 100 $\mathrm{M}_\odot$,[6] assuming $M_{\rm GC} \approx 10^6$ $\mathrm{M}_\odot$.

Note that the absence of a similar cusp in the density profiles of putative systems that match our assumptions should be regarded as a *hint* of the absence of a central BH of given mass, rather than a definitive proof. A crucial aspect, in this regard, is that we assume one-component systems, thus neglecting any effect of mass segregation. As the more massive 'dark' remnants are more likely to sink to the central regions, it has been argued that, though a power-law cusp might form in the total *mass* density profile, this might not reflect in the *luminosity* density profile, due to an increase of the

[5] The upper limit is because the equation $M(r_{\rm BH}) = 0.1\mu$ has no solution if $M(r_{\rm BH}) > M(\infty) = 1$, that is, $\mu > 10$, where I used the fact that $M(r)$ is normalised by the total stellar mass M. If $M(r_{\rm BH}) = 1$, $r_{\rm BH}$ is infinite, so I exclude $\mu = 10$ as well.

[6] This value should be slightly larger for a BWK model, since the same radius encloses a larger fraction of the total stellar mass with respect to the King model with the same W_0, because of the central cusp. This small difference should not alter much my order-of-magnitude estimates.

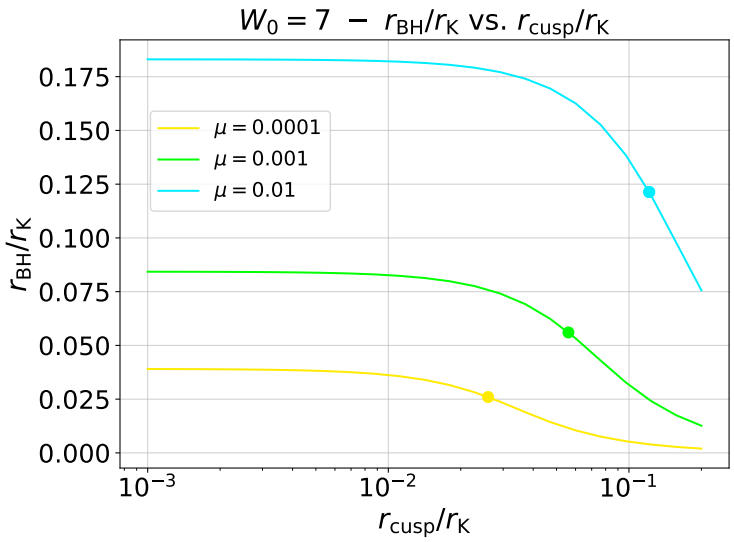

Figure 3.8. BH's influence radius r_{BH} (Eq. 2.25) as a function of r_{cusp} (Eq. 3.1) for Bahcall-Wolf-King models with $W_0 = 7$ and BH-to-stellar mass ratios $\mu = 10^{-4},\ 10^{-3},\ 10^{-2}$. The two radii are in units of King radii (Eq. 2.29). The filled circles are placed where $r_{BH} = r_{cusp}$.

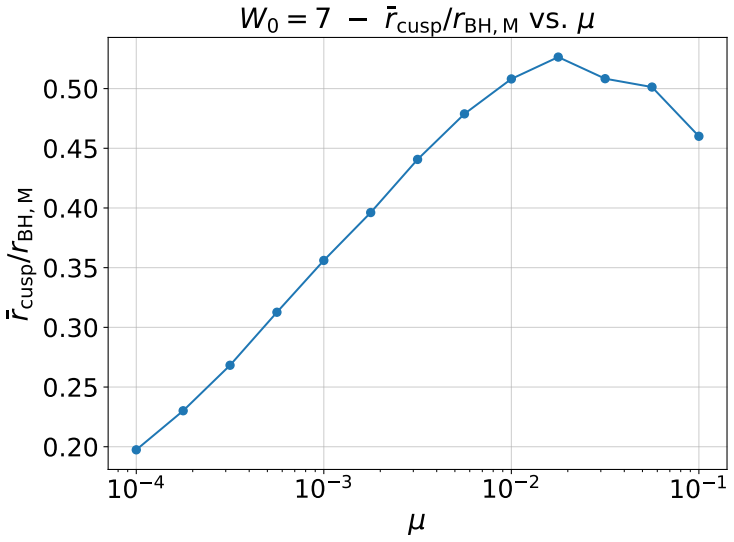

Figure 3.9. Ratio between $\bar{r}_{cusp}$ and $r_{BH,M}$ for Bahcall-Wolf-King models with $W_0 = 7$ as a function of the BH-to-stellar mass ratio μ. The radius r_{cusp} is the transition radius between the central Bahcall-Wolf cusp and the King core (Eq. 3.1), while $r_{BH,M}$ is the value of r_{cusp} such that it encloses 10% of the BH's mass in stars (Eq. 2.25). The overbar indicates that $\bar{r}_{cusp}$ is computed for the consistent model with the smallest central density cusp for the given μ.

mass-to-light ratio of the stellar population towards the centre (e.g., Baumgardt et al. 2004b).

Here, I showed how the presence of an inner density cusp is necessary for spherical, isotropic systems with a flat core to host a central BH. Still, it is important to mention that the detection of a similar feature in the observed density profile cannot be trivially interpreted as a signature of a central massive BH, as other possible explanations are equally plausible (e.g., Vesperini & Trenti 2010).

Table 3.1. Parameters of the Bahcall-Wolf-King models with $W_0 = 7$ and minimum cusp to prevent inconsistency (Part 1). All radii with an overbar are computed from the density profiles in Eq. (3.1) with $r_{\rm cusp} = \bar{r}_{\rm cusp}(\mu)$, which is the minimum cusp radius to prevent inconsistency for the BH-to-stellar mass ratio μ.
μ: BH-to-stellar mass ratio; $\bar{r}_{\rm cusp}$ minimum cusp radius to prevent inconsistency for the given μ; $M(\bar{r}_{\rm cusp})$: stellar mass enclosed within $\bar{r}_{\rm cusp}$; $\mathcal{E}_{\rm cusp}$: relative energy of stars whose maximum possible distance from the centre is $\bar{r}_{\rm cusp}$; $\bar{r}_{1/2}$ smallest $r_{1/2}$ (Eq. 3.5) for consistency; $M(\bar{r}_{1/2})$: stellar mass enclosed within $\bar{r}_{1/2}$; $\mathcal{E}_{1/2}$: relative energy of stars whose maximum possible distance from the centre is $\bar{r}_{1/2}$; $\bar{r}_{\rm BH}$: BH's influence radius (Eq. 2.25).

μ	$\bar{r}_{\rm cusp}$	$M(\bar{r}_{\rm cusp})$	$\mathcal{E}_{\rm cusp}$	$\bar{r}_{1/2}$	$M(\bar{r}_{1/2})$	$\mathcal{E}_{1/2}$	$\bar{r}_{\rm BH}$
1.00×10^{-4}	5.13×10^{-3}	7.70×10^{-8}	4.41×10^{-1}	8.66×10^{-3}	2.14×10^{-7}	4.33×10^{-1}	3.82×10^{-2}
1.78×10^{-4}	7.24×10^{-3}	2.17×10^{-7}	4.46×10^{-1}	1.22×10^{-2}	6.03×10^{-7}	4.36×10^{-1}	4.59×10^{-2}
3.16×10^{-4}	1.02×10^{-2}	6.12×10^{-7}	4.53×10^{-1}	1.73×10^{-2}	1.70×10^{-6}	4.40×10^{-1}	5.51×10^{-2}
5.62×10^{-4}	1.45×10^{-2}	1.72×10^{-6}	4.61×10^{-1}	2.45×10^{-2}	4.81×10^{-6}	4.45×10^{-1}	6.60×10^{-2}
1.00×10^{-3}	2.00×10^{-2}	4.53×10^{-6}	4.73×10^{-1}	3.39×10^{-2}	1.27×10^{-5}	4.52×10^{-1}	7.90×10^{-2}
1.78×10^{-3}	2.69×10^{-2}	1.11×10^{-5}	4.89×10^{-1}	4.59×10^{-2}	3.15×10^{-5}	4.62×10^{-1}	9.45×10^{-2}
3.16×10^{-3}	3.63×10^{-2}	2.73×10^{-5}	5.12×10^{-1}	6.25×10^{-2}	7.86×10^{-5}	4.75×10^{-1}	1.13×10^{-1}
5.62×10^{-3}	4.79×10^{-2}	6.24×10^{-5}	5.44×10^{-1}	8.36×10^{-2}	1.86×10^{-4}	4.92×10^{-1}	1.35×10^{-1}
1.00×10^{-2}	6.17×10^{-2}	1.33×10^{-4}	5.90×10^{-1}	1.11×10^{-1}	4.18×10^{-4}	5.17×10^{-1}	1.62×10^{-1}
1.78×10^{-2}	7.76×10^{-2}	2.65×10^{-4}	6.60×10^{-1}	1.46×10^{-1}	9.13×10^{-4}	5.50×10^{-1}	1.95×10^{-1}
3.16×10^{-2}	9.12×10^{-2}	4.28×10^{-4}	7.80×10^{-1}	1.82×10^{-1}	1.68×10^{-3}	6.03×10^{-1}	2.40×10^{-1}
5.62×10^{-2}	1.10×10^{-1}	7.40×10^{-4}	9.50×10^{-1}	NA	NA	NA	2.94×10^{-1}
1.00×10^{-1}	1.23×10^{-1}	1.04×10^{-3}	1.25	NA	NA	NA	3.67×10^{-1}

Table 3.2. Parameters of the Bahcall-Wolf-King models with $W_0 = 7$ and minimum cusp to prevent inconsistency (Part 1). All radii with an overbar are computed from the density profiles in Eq. (3.1) with $r_{\rm cusp} = \bar{r}_{\rm cusp}(\mu)$, which is the minimum cusp radius to prevent inconsistency for the BH-to-stellar mass ratio μ. The others are computed from the King models with BH and $W_0 = 7$ (Section 2.5).
$M(\bar{r}_{\rm BH})$: stellar mass enclosed within $\bar{r}_{\rm BH}$; $\mathcal{E}_{\rm BH}$: relative energy of stars whose maximum possible distance from the centre is $\bar{r}_{\rm BH}$; r_0: radius containing all stars with $\mathcal{E} > \mathcal{E}_0$ (Eq. 3.6); $M(r_0)$: stellar mass enclosed within r_0; $\mathcal{E}_0$: relative energy beyond which the DF of the $W_0 = 7$ King model with BH is negative; $r_{\rm BH,K}$: BH's influence radius for the $W_0 = 7$ King model; $M(r_{\rm BH,K})$: stellar mass enclosed within $r_{\rm BH,K}$; $\mathcal{E}_{\rm BH,K}$: relative energy of stars whose maximum possible distance from the centre is $r_{\rm BH,K}$.

$M(\bar{r}_{\rm BH})$	$\mathcal{E}_{\rm BH}$	r_0	$M(r_0)$	$\mathcal{E}_0$	$r_{\rm BH,K}$	$M(r_{\rm BH,K})$	$\mathcal{E}_{\rm BH,K}$
1.00×10^{-5}	4.24×10^{-1}	1.37×10^{-1}	4.22×10^{-4}	4.21×10^{-1}	3.91×10^{-2}	1.00×10^{-5}	4.24×10^{-1}
1.78×10^{-5}	4.25×10^{-1}	1.58×10^{-1}	6.53×10^{-4}	4.21×10^{-1}	4.73×10^{-2}	1.78×10^{-5}	4.25×10^{-1}
3.16×10^{-5}	4.27×10^{-1}	1.59×10^{-1}	6.54×10^{-4}	4.21×10^{-1}	5.74×10^{-2}	3.16×10^{-5}	4.27×10^{-1}
5.62×10^{-5}	4.30×10^{-1}	1.87×10^{-1}	1.06×10^{-3}	4.22×10^{-1}	6.95×10^{-2}	5.62×10^{-5}	4.29×10^{-1}
1.00×10^{-4}	4.35×10^{-1}	2.14×10^{-1}	1.59×10^{-3}	4.22×10^{-1}	8.43×10^{-2}	1.00×10^{-4}	4.33×10^{-1}
1.78×10^{-4}	4.41×10^{-1}	2.44×10^{-1}	2.31×10^{-3}	4.24×10^{-1}	1.02×10^{-1}	1.78×10^{-4}	4.38×10^{-1}
3.16×10^{-4}	4.51×10^{-1}	2.77×10^{-1}	3.32×10^{-3}	4.27×10^{-1}	1.24×10^{-1}	3.16×10^{-4}	4.46×10^{-1}
5.62×10^{-4}	4.65×10^{-1}	3.19×10^{-1}	5.01×10^{-3}	4.31×10^{-1}	1.51×10^{-1}	5.62×10^{-4}	4.57×10^{-1}
1.00×10^{-3}	4.87×10^{-1}	3.61×10^{-1}	7.04×10^{-3}	4.39×10^{-1}	1.83×10^{-1}	1.00×10^{-3}	4.73×10^{-1}
1.78×10^{-3}	5.17×10^{-1}	3.87×10^{-1}	8.56×10^{-3}	4.56×10^{-1}	2.23×10^{-1}	1.78×10^{-3}	4.97×10^{-1}
3.16×10^{-3}	5.58×10^{-1}	4.68×10^{-1}	1.43×10^{-2}	4.72×10^{-1}	2.72×10^{-1}	3.16×10^{-3}	5.32×10^{-1}
5.62×10^{-3}	6.17×10^{-1}	5.02×10^{-1}	1.72×10^{-2}	5.15×10^{-1}	3.33×10^{-1}	5.62×10^{-3}	5.82×10^{-1}
1.00×10^{-2}	6.96×10^{-1}	5.07×10^{-1}	1.77×10^{-2}	5.99×10^{-1}	4.10×10^{-1}	1.00×10^{-2}	6.53×10^{-1}

Chapter 4

Discussion and Conclusions

In this final chapter, I summarise the results obtained in the present work and place them in the astrophysical context. In doing so, I discuss how these findings might pave the way for future studies of more complex and realistic models, as well as their limitations.

In Section 4.1, I focus mainly on this latter aspect, highlighting in which directions this work may be extended. In Section 4.2, I review what has been done in Chapters 2 and 3. Finally, in Section 4.3, I recapitulate the main results of the thesis and conclude.

4.1 Discussion and Future Prospects

In this thesis, I investigated the non-negativity of the distribution function (DF) – i.e., the consistency – of several families of spherical models with isotropic kinematic structure. In particular, I focused on one-component systems embedded in the gravitational field produced by a point mass placed at their centre. These models are intended to represent globular clusters (GCs) hosting a central black hole (BH) of intermediate mass ($100\ \mathrm{M}_\odot \lesssim M_\bullet \lesssim 10^5\ \mathrm{M}_\odot$), but my results are fully general and hold for any physical system matching my assumptions (see Sections 1.2 and 1.3), such as a dark matter-dominated dwarf spheroidal galaxy (e.g., Battaglia & Nipoti 2022) with a central BH.

4.1.1 Stability

Testing the consistency of models for collisionless stellar systems is of paramount importance because, if this condition is not satisfied, a model must be rejected as unphysical even if it provides a satisfactory description of the data. However, the

non-negativity of the DF is a much weaker requirement than the model's stability, and an unstable model, even if consistent, cannot describe a long-lasting equilibrium configuration.

A complete stability analysis is beyond the scope of this work. However, it is worth mentioning a theorem stating that a spherical stellar system with an ergodic DF $f(\mathcal{E})$ is stable if $\mathrm{d}f/\mathrm{d}\mathcal{E} > 0$ for every accessible relative energy $\mathcal{E}$ (e.g., Binney & Tremaine 2008, Section 5.5.1). Among the consistent models encountered, those satisfying this condition are certainly stable; nothing regarding stability can be concluded for the others. As a general trend, the central BH tends to decrease the slope of the DF at high relative energies, thus making this sufficient condition for stability less likely to be satisfied. For example, the DFs of all the self-gravitating γ-models are everywhere increasing functions of $\mathcal{E}$ (Fig. 2.4), while those with a central BH and $\gamma < 3/2$ do not satisfy this condition because their DF goes as $\mathcal{E}^{\gamma-3/2}$ at high relative energies (Eq. 2.7).

4.1.2 Multi-Component Systems

More specifically, the present work dealt with the relation between the stellar density profile and the consistency of isotropic systems with a central BH, which was possible thanks to Eddington's formula (Eq. 1.16), through which the ergodic DF can be recovered for any given density-total potential pair. In Sections 2.5.3, 3.2.4 and 3.2.5, I also investigated under what circumstances it could be possible to observationally constrain the phase-space density of stars from the observed density profile in the region where the BH's influence is dominant. These discussions are somewhat oversimplified because the real observable is the surface brightness profile $I(R)$ of the system in the plane of the sky. Two additional steps are thus needed to connect observational data to the intrinsic stellar mass density:

1. the determination of the stellar mass-to-light ratio $\Upsilon(r)$ to recover the projected mass density $\Sigma(R)$ of the observed system;

2. the projection of the theoretical density profiles $\rho(r; \{\lambda_i\})$, depending on some free parameters λ_i, to be compared with $\Sigma(R)$ to infer the best-fit parameters.

I expect that these complications should not alter much the qualitative arguments made in Sections 2.5.3, 3.2.4 and 3.2.5 regarding the observational relevance of my results, especially in the case of a spatially uniform mass-to-light ratio. Still, I note that this approximation may not be satisfactory for mass-segregated systems, as is likely the case for many GCs (e.g., Baumgardt 2017; Aros et al. 2020). Mass segregation could

limit the room for a central rise in $I(R)$, even if $\rho(r)$ is cusped, as briefly mentioned in Section 3.2.5 (see also Baumgardt et al. 2004b).

Some DF-based models with multiple mass components have been built to account for mass segregation in GCs (e.g., Michie 1963; Miocchi 2007; Gieles & Zocchi 2015). This can be done even in the ρ-to-f approach adopted in the present study. Ciotti & Pellegrini (1992) showed that the consistency of a multi-component model stems from the consistency of each k-th mass component with spatial density distribution ρ_k. Taking into account that, in this case, the total potential is the sum of the potentials produced by each component and of the external potential, the corresponding ergodic DFs $f_k(\mathcal{E})$ can be obtained from Eddington's formula (Eq. 1.16), and the consistency conditions in Eqs. (1.20)–(1.22) can be exploited (posing $r_a \to \infty$ and substituting ϱ with ρ_k), as well as the necessary condition in Eq. (A.16). Even the theorems in Appendix A.2 remain valid for each individual component, since close enough to the centre, the potential due to the BH is always dominant.

A similar analysis can be carried out even with more general parametrisations of the orbital anisotropy than the isotropic case, as long as a way to recover the DF of each component exists (Section 4.1.4; see also Ciotti & Pellegrini 1992; Ciotti 1996, 1999; Ciotti & Morganti 2009; Ciotti & Ziaee Lorzad 2018 for some examples of consistency analyses of two-component Osipkov-Merritt systems).

4.1.3 The Velocity Dispersion Profile

Throughout this thesis, I have not addressed the properties of the kinematic distribution of stars, except for the assumption of an isotropic velocity dispersion tensor. However, this is also an important topic in the quest for intermediate-mass BHs in GCs. For the present case, it suffices to note that if one of the models encountered, say e.g., a Bahcall-Wolf-King (BWK) model (Section 3.1), were to be used to constrain the presence of a central BH in a stellar system, not only must the model reproduce well the observed density profile, but also the velocity dispersion profile.

4.1.4 Anisotropic Systems

One of the main limitations of the present study is the assumption of an isotropic kinematic structure. Although this is a good zeroth-order approximation for GCs, accurate observations often show some level of orbital anisotropy. This plays a fundamental role in the detection of IMBHs through dynamical studies. For instance, a radially anisotropic velocity distribution produces a rise in the central *projected* velocity dispersion, mimicking the effect of a central BH (e.g., Zocchi et al. 2016a, 2017). The

effect can be significant even if the anisotropy becomes relevant only at large (three-dimensional) distances from the cluster's centre. An anisotropic velocity dispersion is also predicted by several theoretical investigations to arise naturally in GCs (e.g., Zocchi et al. 2016b, and references therein). If a massive BH is present at the centre of a star cluster, Frank & Rees (1976) and Lightman & Shapiro (1977) suggest that stars on more eccentric orbits are more likely to be disrupted by the BH. If this is the case, the velocity distribution might be tangentially biased near the centre. For all these reasons, extending our analysis to spherical, anisotropic systems would be of great interest.

Some trends have already been outlined in the literature concerning the consistency of spherical systems with anisotropic kinematic structure. In particular, several studies have been carried out for systems with Osipkov-Merritt (OM; Section 1.2.4) anisotropy, i.e., with an anisotropy radius r_a separating a region of nearly isotropic orbital structure, for $r \ll r_\mathrm{a}$, from a region characterised by radial anisotropy, for $r \gtrsim r_\mathrm{a}$. A smaller value of r_a corresponds to a larger amount of radial anisotropy. As a general trend for systems with two components – a 'reference' component and a 'halo' component – it has been noted that one component admits a *lower* degree of radial anisotropy as the other one becomes more concentrated (e.g., Ciotti 1996, 1999; Ciotti & Morganti 2009; Ciotti & Ziaee Lorzad 2018). For instance, Ciotti (1996) found that the greatest lower limit on r_a for the consistency of a Hernquist component (i.e., a component with the density profile of a γ-model with $\gamma = 1$) in a Hernquist halo is found when the scale radius of the halo shrinks to zero, that is, when its potential becomes that of a central point mass. In other words, when the halo is replaced by a central BH, the reference component supports the lowest amount of radial orbital anisotropy. Note that this also implies that even if a system with central BH is consistent when isotropic, this is not guaranteed with an OM anisotropy, although the orbital structure is asymptotically isotropic at the centre, where the BH exerts its major influence. In addition, components with flatter central (Ciotti 1999) or outer (Ciotti & Morganti 2009) density profiles can generally support less radial anisotropy, for fixed properties of the halo (or BH). It then seems unlikely that isotropic models that are inconsistent with a central BH can attain consistency if they are given an OM kinematic structure. Quite the opposite, the expectation is that steeper central density profiles, or more extended cusps, than in the isotropic case may be required for consistency, if a central BH is present.

Further evidence that radial anisotropy is 'damaging' to phase-space consistency comes from the existence of some theorems relating the logarithmic density slope $\gamma(r)$ (Eq. 3.4) to the anisotropy parameter $\beta(r)$ defined in Eq. (1.17) (e.g., An & Evans 2006; Ciotti & Morganti 2010a,b,c; Van Hese et al. 2011). Recall that $\beta > 0$ indicates

radial anisotropy, while $\beta < 0$ for tangential anisotropy. These theorems prove that, in many cases, for a given γ, there is a maximum value of β allowed for consistency, i.e., a maximum amount of radial anisotropy. For instance, the 'cusp slope-central anisotropy' theorem stated by An & Evans (2006) shows that the inequality

$$\gamma_0 \equiv \lim_{r\to 0} \gamma(r) \geq \beta_0 + \frac{1}{2}, \tag{4.1}$$

where $\beta_0 \equiv \lim_{r\to 0} \beta(r)$, is a necessary condition for the consistency of an arbitrary spherical model with a central BH. In other words, Eq. (4.1) is satisfied by any *consistent* system where the central potential is Keplerian. It is evident that, in the isotropic case, the condition is $\gamma_0 \geq 1/2$, in agreement with what we found in Appendix A.2 for a large class of density profiles (see also Tremaine et al. 1994). A smaller range of central logarithmic density slopes is admitted for models with increasing central radial anisotropy. On the contrary, the condition becomes less and less restrictive as β_0 becomes more and more negative. We then expect that tangential anisotropy could 'help' the models' consistency.

My study can be extended to spherical, anisotropic systems by exploiting families of models with known inversion formulae and/or consistency conditions. The most straightforward continuation of this thesis would be to consider systems with density profiles such as those studied here and add an OM anisotropic velocity distribution. All the techniques used in this thesis are easily extendable to these models, as briefly discussed in Section 1.2.4. However, there are several other families of spherical models which allow the construction of more general anisotropy profiles, even including tangential anisotropy, for which an inversion formula is known, so that the phase-space consistency can be studied starting from a given density-total potential pair (e.g., Cuddeford 1991; Cuddeford & Louis 1995; Baes & van Hese 2007; Ciotti & Morganti 2010a).

4.1.5 Rotating Systems

Another key assumption adopted throughout the thesis is that the stellar systems do not rotate. Giving up this assumption brings several difficulties because inversion techniques for rotating (non-spherical, in general) systems are far more complex than those for spherical, non-rotating systems. Most of them are limited to two-integral axisymmetric systems, where the DF depends on the relative energy $\mathcal{E}$ and on the component of the angular momentum L_z parallel to the symmetry axis (e.g., Fricke 1952; Lynden-Bell 1962b; Hunter & Qian 1993; Qian et al. 1995; see also Dejonghe 1986 for a review, and Binney & Tremaine 2008). However, some amount of ordered rotation and of flattening

is being observed in an increasing number of Galactic GCs (e.g., White & Shawl 1987; Bianchini et al. 2013; Kamann et al. 2018; Bianchini et al. 2018), which motivates the effort for understanding the interplay between the presence of a central BH and the density profile even in rotating systems.

A remarkable example of this kind of study is provided by Qian et al. (1995), who, using the technique developed by Hunter & Qian (1993), assess the consistency of some two-integral, axisymmetric, ellipsoidal models, with an application to the modelling of the dwarf elliptical galaxy M32 with a central supermassive BH. They carried out the analysis for scale-free density profiles proportional to $(R^2 + z^2/q^2)^{-\gamma/2}$, where R is the cylindrical radius, z is the vertical coordinate on the symmetry axis, and q is the axial ratio ($q < 1$ for oblates and $q > 1$ for prolates). The inclusion of an external potential due to a central BH led to the result that models with $\gamma < 1/2$ are inconsistent for all axial ratios. This suggests that even flattened, rotating systems with central power-law cusps cannot host a central BH if the cusp has a logarithmic slope lower than $1/2$, as found for spherical, isotropic systems (Theorem A.1; see also Tremaine et al. 1994; An & Evans 2006).

This interesting work gives some hope that a generalisation of the present study to two-integral, axisymmetric systems for GCs with central intermediate-mass BHs might be possible.

4.2 Summary

This thesis addresses the problem of the existence of intermediate-mass BHs in GCs from a theoretical perspective. I studied the relation between the stellar density profile and the mass of the central BH for the phase-space consistency (i.e., the non-negativity of the DF) of one-component, spherical, non-rotating systems with isotropic velocity distribution. These assumptions lead to a DF $f(\mathcal{E})$, depending only on the relative energy, which is uniquely determined for a given density-total potential pair through Eddington's formula (Eq. 1.16). This allowed us to determine the consistency of several models by exploiting some necessary and sufficient conditions, and by explicitly computing the DF.

If it turns out to be inconsistent, whatever model must be rejected as unphysical, even if it describes the observational data well. Hence, understanding which stellar density profiles are incompatible with the presence of a central BH of a given mass could be useful to place upper limits on the masses of putative intermediate-mass BHs in GCs based on their observed density profiles. The fact that, despite intensive searches,

there is still no confirmed evidence for GCs hosting these BHs motivates this work (Greene et al. 2020; Häberle et al. 2024; Bañares-Hernández et al. 2025). Although my assumptions are quite restrictive, the models studied here can represent a discrete zeroth-order approximation of some globular clusters and form a basis for future studies of more complex and realistic systems.

γ-Models

In Chapter 2, I assessed the consistency of models constructed from several known families of density profiles, taking into account the contribution of a central point mass (i.e., the BH) to the total gravitational potential. In Section 2.1, I thoroughly studied the consistency of the isotropic γ-models, where γ is a free parameter determining the central logarithmic slope of their density profiles. First, I considered systems with a dominant BH, whose mass is much larger than the total stellar mass of the system. This is a simple case where the effects of a central BH should be most evident. The strong sufficient condition (Eq. 1.22) found by Ciotti & Pellegrini (1992) and the necessary condition $\gamma \geq 1/2$ found by Tremaine et al. (1994; see also Appendix A.1) constrain the consistency of BH-dominated γ-models over almost the entire parameter space, without the need of explicitly recovering the DF. They allowed us to conclude that all the models with $\gamma < 1/2$ are inconsistent, while those with $\gamma \geq 36/65 \simeq 0.554$ have an everywhere non-negative DF. I then exploited Eddington's formula (Eq. 1.16) to establish that the BH-dominated models with $1/2 \leq \gamma < 36/65$ are consistent as well by numerically evaluating their DFs. The analysis was repeated for γ-models with BHs of finite mass, finding that models with $\gamma \geq 1/2$ are consistent and models with $\gamma < 1/2$ are not, independently of the BH's mass.

Central Cusp's Slope and Consistency

As briefly mentioned, Tremaine et al. (1994) found that γ-models with $\gamma < 1/2$ and a central BH of arbitrary mass are inconsistent. They argue that $\gamma_0 \equiv -\,\mathrm{d}\ln\rho/\mathrm{d}\ln r\,|_{r=0} \geq 1/2$ should be a necessary condition for the consistency of *any* spherical, isotropic model with central BH. In Appendix A.2, I indeed prove that the DF becomes negative at high relative energies for: (i) models with a central power-law cusp flatter than $r^{-1/2}$ (Theorem A.1), (ii) models with a central logarithmic divergence (Theorem A.3), and (iii) models with regular density profiles (i.e., with finite density and null first derivative at the centre; Theorem A.2). However, these are alternative proofs of special cases of a more general theorem proved by An & Evans (2006), showing that $\gamma_0 \geq 1/2$ is necessarily true for *all* consistent, spherical, isotropic systems with a central BH.

Plummer Models

As a further example supporting this finding, in Section 2.2 I show the analytic ergodic DF of BH-dominated systems with a Plummer density profile, which falls within the class of regular profiles. As expected, the resulting DF becomes negative at high relative energies. Since the original Plummer models are self-gravitating and built from an assumed DF, in practice, I took the 'original' density profiles – self-consistently generated by the 'original' DF –, and I recovered a new DF that allows the system to maintain the same density distribution when a BH is located at the centre.

Einasto Models

Section 2.3 is devoted to the study of isotropic Einasto models with central BHs. Although the Einasto profiles are of little use in the context of GCs' modelling, the models introduced in that section may serve for describing dark matter-dominated dwarf spheroidal galaxies (e.g., Battaglia & Nipoti 2022) with central BHs, as the Einasto profiles are often used to describe simulated dark matter halos (e.g., Wang et al. 2020). It is straightforward to see that the Einasto profiles have a finite central density, so isotropic Einasto models cannot host a central BH.

However, I noted that the profiles with a high Einasto index remain steep down to rather small radii. Therefore, in the presence of BHs of sufficiently low mass, the spatial region corresponding to $f(\mathcal{E}) < 0$ might be so small to be of no practical relevance. For instance, it may be smaller than the resolution element of the simulation, or it may contain a non-significant number of dark matter particles. A more quantitative discussion of this aspect is left to future work.

Sérsic Models

In Section 2.4, I investigated the consistency of models with Sérsic density profiles and a central BH. I exploited the asymptotic expansions provided by Ciotti (1991) to rule out the models with a Sérsic index $n < 2$, since they have a central logarithmic slope $\gamma_0 < 1/2$. I numerically computed the DFs of the models with $n \geq 2$ and central BHs of finite mass, discovering that all these models are consistent. I also defined a critical relative energy $\mathcal{E}_{\rm BH} \equiv \Psi_{\rm T}(r_{\rm BH})$, where $r_{\rm BH}$ is the radius containing 10% of the BH's mass in stars. Thus, within $r_{\rm BH}$ the BH dominates the motion of stars, and I referred to it as the BH's influence radius. I found that indeed $\mathcal{E}_{\rm BH}$ approximately predicts the relative energy beyond which the behaviour of the DF is dominated by the BH's influence (Fig. 2.8), as expected from the fact that stars with $\mathcal{E} \geq \mathcal{E}_{\rm BH}$ are confined

within the sphere of radius $r_{\rm BH}$.

King Models

These results are crucial to understand the general properties of spherical, isotropic ρ-to-f models with central BHs, but the density profiles of the models described above are not customarily used for GCs. Instead, this is the case of the profiles of King models (e.g., Barmby et al. 2007; Miocchi et al. 2013). Therefore, in Section 2.5, I introduced King models with central BHs, with the same procedure followed for the Plummer models. Not unexpectedly, as their central profile is flat, they are all inconsistent. For any given BH-to-stellar mass ratio, I then defined the inconsistency radius r_0 as the radius containing stars whose relative energy $\mathcal{E}$ would be such that $f(\mathcal{E}) < 0$, if the BH were present. I found that $r_{\rm BH} \lesssim r_0$ in most cases, and that it should be possible to probe the region within $r_{\rm BH}$ with the current and future observational facilities, its angular size being of about $2''$ at a distance of 10 kpc for a typical GC and a BH-to-stellar mass ratio $\mu \approx 10^{-3}$. I predicted that roughly 100 $\mathrm{M}_\odot$ should be contained within $r_{\rm BH}$ for a 10^6 $\mathrm{M}_\odot$ GC with a 10^3 $\mathrm{M}_\odot$ central BH.

Bahcall-Wolf-King Models

In the light of these results, one might be tempted to think that, if the observed density profile follows a King profile all the way into $r_{\rm BH}$, it could be observationally possible to rule out the existence of a central intermediate-mass BH of mass $M_\bullet \gtrsim 10^{-3}\, M_{\rm GC}$, for phase-space consistency reasons, at least in the closest and most massive GCs. However, in Chapter 3, I showed that the situation is more complicated, as a central density cusp may 'save' the models' consistency even if it is less extended than $r_{\rm BH}$. To this end, I constructed models with density profiles characterised by a $r^{-7/4}$ power law within a cusp radius $r_{\rm cusp}$ and a King profile outwards, which I called Bahcall-Wolf-King (BWK) models (from Bahcall & Wolf 1976 and King 1966). For simplicity, I restricted the analysis to BWK models where the King part of the profile has a dimensionless central potential $W_0 = 7$.

For several BH-to-stellar mass ratios, I numerically computed the ergodic DFs of these BWK models for increasing cusp radii, and found those with the smallest cusp to prevent inconsistency. I estimated the minimum cusp's size as the (minimum) radius $\bar{r}_{1/2}$ at which $\mathrm{d}\ln\rho/\mathrm{d}\ln r = -1/2$, which turned out to be less than 60% of $r_{\rm BH}$ as computed for the King profile with the same W_0. This makes it very difficult to reliably infer the absence of a 10^3 $\mathrm{M}_\odot$ BH in a 10^6 $\mathrm{M}_\odot$ GC, as only about 10 $\mathrm{M}_\odot$ in stars (and remnants) should be contained within $\bar{r}_{1/2}$. For slightly more massive BHs of 5×10^3 $\mathrm{M}_\odot$,

the minimum cusp is predicted to contain about 160 $M_\odot$, thus leaving some hope to constrain the presence of such BHs in massive GCs based on consistency arguments.

I noted that the cusp produced by the influence of a BH could be, in general, larger than the minimum required for consistency. Supposing that $r_{\rm BH} = r_{\rm cusp}$, as suggested by Miocchi (2007), I estimated that the size of the cusp of the $W_0 = 7$ BWK models satisfying this condition is roughly equal to that of $r_{\rm BH}$ computed for $W_0 = 7$ King models. This suggests that the cusp of these BWK models could be detected even for 10^3 $M_\odot$ BHs in massive ($M_{\rm GC} \gtrsim 10^6$ $M_\odot$) and near GCs.

As a byproduct, this analysis also showed that having a central logarithmic slope $\gamma_0 \geq 1/2$ in the density profile is *not* a sufficient condition for the consistency of a spherical, isotropic model with central BH, since the BWK models have $\gamma_0 = 7/4$ and they can still be inconsistent. This was not obvious, as all the γ- and Sérsic models with central BHs and $\gamma_0 \geq 1/2$ were found to have a positive definite DF, although this is not guaranteed a priori. One may then have been tempted to argue that this is a general fact. The BWK models with a cusp smaller than the minimum cusp for consistency provide a counterexample to this conjecture.

4.3 Conclusions

In the present work, the non-negativity of the DFs of several spherical, isotropic models was assessed in the case in which a central BH is contributing to the total potential.

I found, confirming previous evidence, that models with a density profile flatter than $r^{-1/2}$ at the centre do not leave room for phase-space consistency whenever the BH's mass is non-vanishing. Among these, we encountered the models with the following density profiles:

- γ-models' profiles with $\gamma < 1/2$;
- Plummer profiles;
- Einasto profiles;
- Sérsic profiles with Sérsic index $n < 2$;
- King profiles.

I confirmed that, in the presence of a central BH of any mass, all γ-models with $\gamma \geq 1/2$ are consistent (Tremaine et al. 1994), and found that this also holds for the models with a Sérsic profile with $n \geq 2$. All these models have a central profile steeper or proportional to $r^{-1/2}$.

As an example of models with a steep central cusp that nevertheless are inconsistent when a BH is present, I constructed and analysed models with a $r^{-7/4}$ inner cusp and an outer King-like profile with $W_0 = 7$, which belong to the family of what I called Bahcall-Wolf-King (BWK) models. The non-negativity of the DFs of these models depends on the size of the cusp and on the mass of the BH. All and only the models with a cusp larger than a minimum value, which depends on the BH-to-stellar mass ratio, are consistent.

I regarded the King models with BH and the BWK models as those of major observational relevance, as King profiles often fit the observed surface brightness profiles of GCs with good accuracy. I discussed whether these models could be used to observationally constrain the existence of intermediate-mass BHs inside GCs, when the inner cusp is not found, based on consistency arguments. I predict that this might be possible only in near and massive GCs for BHs more massive than about 0.5% of the host cluster's mass.

This thesis represents a first, preparatory investigation of the phase-space consistency of models for GCs with central intermediate-mass BHs, and of its possible observational implications. Models that recover the full phase-space distribution of the stellar populations can be used to provide independent upper limits on the BHs' masses at the centres of the GCs. Moreover, they can complement studies based on the Jeans equations. Since they involve only velocity moments of the DF, finding physically acceptable solutions to them is less restrictive than finding a positive definite DF.

Further studies are anyway needed to extend my results to more realistic models, including, e.g., orbital anisotropy or multiple stellar components, and to apply them to observational data.

Appendix A

Useful Proofs

A.1 High Relative Energy Limit for γ-Models with a Central Black Hole

In this section, I compute the asymptotic expansion of the DF of the isotropic γ-models with a central BH (see Section 2.1), in the limit of high relative energies, i.e., $\mathcal{E} \to \infty$. This limit highlights the effects of the presence of the central BH, since the relative energy grows to infinity only at the centre, where the BH dominates the potential well. This calculation will prove that γ-models with an isotropic dynamical structure and $\gamma < 1/2$ are inconsistent in the presence of a central BH of any mass. The following results were already obtained by Tremaine et al. (1994) and Baes et al. (2005), but here I show most of the calculations more explicitly using the normalisations introduced in Section 2.1.1.

To accomplish the task, we can exploit Eddington's formula in Eq. (1.16a) with $\mathcal{E}_\mathrm{t} = 0$. The first step is to evaluate the integral

$$J(\mathcal{E}) \equiv \int_0^{\mathcal{E}} \frac{\mathrm{d}\rho}{\mathrm{d}\Psi_\mathrm{T}} \frac{\mathrm{d}\Psi_\mathrm{T}}{\sqrt{\mathcal{E} - \Psi_\mathrm{T}}} \,. \tag{A.1}$$

It is convenient to change the variable of integration from Ψ_T to $u \equiv 1/r$. If we call $\varphi : u \mapsto \varphi(u) \equiv \Psi_\mathrm{T}(1/u)$ the map of change of variable, the integral becomes

$$J(\mathcal{E}) = \int_{\varphi^{-1}(0)}^{\varphi^{-1}(\mathcal{E})} \frac{\mathrm{d}\rho}{\mathrm{d}\Psi_\mathrm{T}}\bigg|_{\Psi_\mathrm{T}=\varphi(u)} \frac{\varphi'(u)\mathrm{d}u}{\sqrt{\mathcal{E} - \varphi(u)}} = \int_0^{u(\mathcal{E})} \frac{\mathrm{d}\rho(1/u)}{\mathrm{d}u} \frac{\mathrm{d}u}{\sqrt{\mathcal{E} - \Psi_\mathrm{T}(1/u)}} \,, \tag{A.2}$$

where I defined $u(\mathcal{E}) \equiv \varphi^{-1}(\mathcal{E})$, which is the reciprocal of the radius at which $\Psi_\mathrm{T} = \mathcal{E}$. The second identity comes from the fact that $\mathrm{d}\rho/\mathrm{d}\Psi_\mathrm{T} = (\mathrm{d}\rho/\mathrm{d}u)(\mathrm{d}\Psi_\mathrm{T}/\mathrm{d}u)^{-1} =$

$(\mathrm{d}\rho/\mathrm{d}u)[\varphi'(u)]^{-1}$.

Then, let us perform a second change of variable, defining $t \equiv \mu u/\mathcal{E}$, so that Eq. (A.2) becomes

$$\begin{aligned} J(\mathcal{E}) &= \int_0^{\frac{\mu u(\mathcal{E})}{\varepsilon}} \left.\frac{\mathrm{d}\rho(1/u)}{\mathrm{d}u}\right|_{u=\frac{\mathcal{E}t}{\mu}} \frac{(\mathcal{E}/\mu)\mathrm{d}t}{\sqrt{\mathcal{E}-\Psi_{\mathrm{T}}\left(\frac{\mu}{\mathcal{E}t}\right)}} \\ &= \frac{\sqrt{\mathcal{E}}}{\mu}\int_0^{\frac{\mu u(\mathcal{E})}{\varepsilon}} \left.\frac{\mathrm{d}\rho(1/u)}{\mathrm{d}u}\right|_{u=\frac{\mathcal{E}t}{\mu}} \frac{\mathrm{d}t}{\sqrt{1-\frac{1}{\mathcal{E}}\Psi_{\mathrm{T}}\left(\frac{\mu}{\mathcal{E}t}\right)}}\,. \end{aligned} \tag{A.3}$$

Using Eqs. (2.2) and (2.6), we can define

$$\begin{aligned} g(\mathcal{E},t) &\equiv \left(\frac{3-\gamma}{4\pi}\right)^{-1} \left.\frac{\mathrm{d}\rho(1/u)}{\mathrm{d}u}\right|_{u=\frac{\mathcal{E}t}{\mu}} \left[1-\frac{1}{\mathcal{E}}\Psi_{\mathrm{T}}\left(\frac{\mu}{\mathcal{E}t}\right)\right]^{-1/2} \\ &= \left(\frac{\mathcal{E}t}{\mu}\right)^3 \left(\gamma\frac{\mathcal{E}t}{\mu}+4\right)\left(1+\frac{\mathcal{E}t}{\mu}\right)^{\gamma-5} \left[1-\frac{1}{\mathcal{E}}\Psi\left(\frac{\mu}{\mathcal{E}t}\right)-t\right]^{-1/2}, \end{aligned} \tag{A.4}$$

where $\Psi(r)$ is given by Eq. (2.4). Defining $A(\mathcal{E}) \equiv \mu u(\mathcal{E})/\mathcal{E}$, we can rewrite Eq. (A.3) as

$$J(\mathcal{E}) = \frac{3-\gamma}{4\pi\mu}\sqrt{\mathcal{E}}\int_0^{A(\mathcal{E})} g(\mathcal{E},t)\mathrm{d}t\,. \tag{A.5}$$

In the limit as $\mathcal{E}\to\infty$, if $A(\mathcal{E})\to A_\infty$ and $g(\mathcal{E},t)\sim\tilde{g}(\mathcal{E},t)$, then

$$J(\mathcal{E}) \sim \frac{3-\gamma}{4\pi\mu}\sqrt{\mathcal{E}}\int_0^{A_\infty} \tilde{g}(\mathcal{E},t)\mathrm{d}t\,. \tag{A.6}$$

So we can exploit this equation to find the asymptotic expansion of the DF in the limit of high relative energy.

Since the relative potential of a continuous system cannot grow faster than r^{-1} at the centre, the BH's potential $\Psi_\bullet = \mu/r$ always becomes dominant as $r\to 0$. Thus, $\Psi_{\mathrm{T}}(1/u)\sim\mu u$ as $u\to\infty$, which implies $u(\mathcal{E})\sim\mathcal{E}/\mu$ as $\mathcal{E}\to\infty$, and so $A_\infty = 1$. For the same reason, we can write

$$\left[1-\frac{1}{\mathcal{E}}\Psi\left(\frac{\mu}{\mathcal{E}t}\right)-t\right]^{-1/2} \sim (1-t)^{-1/2}\,, \tag{A.7}$$

as $\mathcal{E}\to\infty$, because $\Psi[\mu/(\mathcal{E}t)]$ grows more slowly than $\mathcal{E}$ in this limit.

Now, we need to distinguish the cases $\gamma = 0$ and $\gamma = 1/2$ from the general one, because $\tilde{g}(\mathcal{E},t)$ will be different in the three cases.

Case $0 < \gamma < 3,\ \gamma \neq 1/2$

From Eqs. (A.4) and (A.7), the asymptotic expansion of $g(\mathcal{E}, t)$ is

$$\tilde{g}(\mathcal{E}, t) = \gamma \left(\frac{\mathcal{E}t}{\mu}\right)^{\gamma-1} (1-t)^{-1/2}, \tag{A.8}$$

so, substituting into Eq. (A.6), we get

$$J(\mathcal{E}) \sim \frac{(3-\gamma)\gamma}{4\pi\mu^\gamma}\mathcal{E}^{\gamma-1/2}\int_0^1 t^{\gamma-1}(1-t)^{-1/2}\mathrm{d}t = \frac{(3-\gamma)\gamma \mathrm{B}(\gamma, 1/2)}{4\pi\mu^\gamma}\mathcal{E}^{\gamma-1/2}\,, \tag{A.9}$$

where $\mathrm{B}(x, y)$ is the Euler Beta function. Using Eq. (1.16a) with $\mathcal{E}_\mathrm{t} = 0$, so that $f(\mathcal{E}) = h(\mathcal{E})\theta(\mathcal{E})$, we can write the asymptotic expansion of the DF as

$$f(\mathcal{E}) \sim \frac{(3-\gamma)\gamma \mathrm{B}(\gamma, 1/2)}{8\sqrt{2}\pi^3\mu^\gamma}\left(\gamma - \frac{1}{2}\right)\mathcal{E}^{\gamma-3/2}\,. \tag{A.10}$$

In the considered γ range, f becomes negative for $\gamma \in]0, 1/2[$. Therefore, isotropic γ-models with a central BH are inconsistent if $\gamma \in]0, 1/2[$.

Case $\gamma = 0$

In this case, the term $(\gamma\mathcal{E}t/\mu + 4)$ in Eq. (A.4) becomes just a constant, so the asymptotic expansion of $g(\mathcal{E}, t)$ becomes

$$\tilde{g}(\mathcal{E}, t) = 4\left(\frac{\mathcal{E}t}{\mu}\right)^{-2}(1-t)^{-1/2}\,. \tag{A.11}$$

Substituting this into Eq. (A.6), we get a divergent integral. However, if we take the limit as $\gamma \to 0$ of Eq. (A.10), we get

$$f(\mathcal{E}) \sim -\frac{3}{16\sqrt{2}\pi^3}\mathcal{E}^{-3/2}\,. \tag{A.12}$$

Therefore, the $\gamma = 0$ models with central BH are inconsistent, too.

Case $\gamma = 1/2$

If $\gamma = 1/2$, the leading term of the asymptotic expansion of $f(\mathcal{E})$ shown in Eq. (A.10) vanishes, so we need to keep higher-order terms. Here, I just report the result of Baes

et al. (2005) for this special case:

$$\frac{f(\mathcal{E})}{M_{\rm T}^{-1/2}(Ga)^{-3/2}} \sim \frac{\sqrt{8}}{\pi^3}\frac{1}{\sqrt{M_\bullet/M_{\rm T}}}\left(\frac{\mathcal{E}}{GM_{\rm T}/a}\right)^{-5/2}, \tag{A.13}$$

where I explicitly wrote their adopted normalisation. In Eq. (A.13), $M_\bullet$ is the BH's mass, $M_{\rm T} = M + M_\bullet$ is the total mass of the system, and a is the scale radius introduced in Eq. (2.1). Since the RHS of Eq. (A.13) is positive, we cannot rule out the consistency of γ-models with $\gamma = 1/2$ and a central BH from this analysis.

Note that the results derived in this section hold for any BH-to-stellar mass ratio μ, i.e., for BHs of arbitrary mass. Also, here we proved that isotropic γ-models with a central BH are inconsistent if $\gamma < 1/2$, but we cannot say anything about the consistency of the models with $\gamma \geq 1/2$, from this analysis.

A.2 Inner Density Slope of Spherical Isotropic Systems with a Central Black Hole

In this section, I provide the proofs of several theorems suggesting that spherical systems with an isotropic dynamical structure *can* sustain a central BH only if they have a central density cusp that goes as $r^{-1/2}$ or steeper. My results rule out some classes of models for inconsistency reasons, but they do not guarantee the consistency of the models that do not belong to such classes.

Note that a more general theorem already exists, stating that

$$\gamma_0 \equiv -\lim_{r\to 0}\frac{{\rm d}\ln\rho}{{\rm d}\ln r} \geq \lim_{r\to 0}\beta(r) + \frac{1}{2}, \tag{A.14}$$

where $\beta(r)$ is the anisotropy parameter defined in Eq. (1.17), is a necessary condition for the consistency of *all* spherical (anisotropic, in general) models with a central total potential dominated by a Keplerian potential. This result is a special case of the 'cusp slope-central anisotropy' theorem, proven by An & Evans (2006, but see also White 1981, de Bruijne et al. 1996) by assuming a DF of the form

$$f(\mathcal{E}, L) = L^{-2\alpha} f_1(\mathcal{E}), \tag{A.15}$$

for which $\beta(r) = \alpha$ for all r, and showing that any general DF, at the centre, is asymptotic to that in Eq. (A.15) with $\alpha = \lim_{r\to 0}\beta(r)$. For our isotropic models,

$\beta(r) = 0\ \forall r$, so the condition reduces to

$$\gamma_0 \geq 1/2. \tag{A.16}$$

In the following, I derive alternative proofs of this latter necessary condition by choosing a specific form for the asymptotic behaviour of the density profile at the centre, and by evaluating the sign of the associated ergodic DF in the limit as $\mathcal{E} \to \infty$, highlighting that the inconsistency due to a central BH occurs at high relative energies. I recall that this is the limit where the BH's effects arise because $\mathcal{E} = \Psi_{\rm T}(r) - v^2/2$ and $\Psi_{\rm T}(r)$ goes to infinity only at the centre. In Theorem A.1, I even provide a formula for the asymptotic expansion of $f(\mathcal{E})$ for generic spatially untruncated models with a central power-law cusp $r^{-\gamma}$, except for $\gamma = 1/2$.

The following theorem proves that spherical, isotropic, untruncated models with a central power-law density profile cannot host a central BH if the density profile rises more slowly than $r^{-1/2}$ at the centre (or decreases).

Theorem A.1. *Consider a spherical, ergodic, untruncated system hosting a central BH of arbitrary mass $\mu > 0$. If the density profile of the system is asymptotic to $Cr^{-\gamma}$, as $r \to 0$, with $C > 0$ and γ constants, then the system is inconsistent if $\gamma < 1/2$.*

Proof. The first step is to evaluate the integral in Eq. (1.16a) with $\mathcal{E}_{\rm t} = 0$

$$J(\mathcal{E}) \equiv \int_0^{\mathcal{E}} \frac{{\rm d}\rho}{{\rm d}\Psi_{\rm T}} \frac{{\rm d}\Psi_{\rm T}}{\sqrt{\mathcal{E} - \Psi_{\rm T}}}\,. \tag{A.17}$$

Repeating the exact same procedure as in Appendix A.1, we then get

$$J(\mathcal{E}) = \frac{\sqrt{\mathcal{E}}}{\mu} \int_0^{A(\mathcal{E})} g(\mathcal{E}, t){\rm d}t\,, \tag{A.18}$$

where $A(\mathcal{E})$ defined as in Appendix A.1, while $g(\mathcal{E}, t)$ is given by

$$g(\mathcal{E}, t) \equiv \left.\frac{{\rm d}\rho(1/u)}{{\rm d}u}\right|_{u=\frac{\mathcal{E}t}{\mu}} \left[1 - \frac{1}{\mathcal{E}}\Psi_{\rm T}\left(\frac{\mu}{\mathcal{E}t}\right)\right]^{-1/2}. \tag{A.19}$$

In the limit as $\mathcal{E} \to \infty$, if $A(\mathcal{E}) \to A_\infty$ and $g(\mathcal{E}, t) \sim \tilde{g}(\mathcal{E}, t)$, then

$$J(\mathcal{E}) \sim \frac{\sqrt{\mathcal{E}}}{\mu} \int_0^{A_\infty} \tilde{g}(\mathcal{E}, t){\rm d}t\,. \tag{A.20}$$

Following the considerations below Eq. (A.6), we can write $A_\infty = 1$ and

$$\left[1 - \frac{1}{\mathcal{E}}\Psi\left(\frac{\mu}{\mathcal{E}t}\right) - t\right]^{-1/2} \sim (1-t)^{-1/2}\,, \tag{A.21}$$

as $\mathcal{E} \to \infty$.

Now, we shall distinguish several cases, depending on the values of γ.

Case $\gamma < 0$

The NC for the consistency of OM-models in Eq. (1.20) is not satisfied because, for ergodic spherical systems, $r_\mathrm{a} \to \infty$, so $\varrho = \rho$, and the NC becomes

$$\frac{\mathrm{d}\rho}{\mathrm{d}r} \leq 0, \quad \forall r \in [0, \infty[. \tag{A.22}$$

If $\gamma < 0$, ρ is an increasing function of radius, close enough to the centre. Note that these models are always inconsistent, independently of the presence of a BH or any other external potential, because Eq. (A.22) depends only on the density profile of the considered system.

Case $0 < \gamma < 3$, $\gamma \neq 1/2$

From Eq. (A.19), the asymptotic expansion of $g(\mathcal{E}, t)$ is

$$\tilde{g}(\mathcal{E}, t) = \gamma C \left(\frac{\mathcal{E}t}{\mu}\right)^{\gamma-1} (1-t)^{-1/2}, \tag{A.23}$$

so, substituting into Eq. (A.20), we get

$$J(\mathcal{E}) \sim \frac{\gamma C}{\mu^\gamma}\mathcal{E}^{\gamma-1/2}\int_0^1 t^{\gamma-1}(1-t)^{-1/2}\mathrm{d}t = \frac{\gamma C \mathrm{B}(\gamma, 1/2)}{\mu^\gamma}\mathcal{E}^{\gamma-1/2}\,, \tag{A.24}$$

where $\mathrm{B}(x, y)$ is the Euler Beta function. Using Eq. (1.16a) with $\mathcal{E}_\mathrm{t} = 0$, so that $f(\mathcal{E}) = h(\mathcal{E})\theta(\mathcal{E})$, we can write the asymptotic expansion of the DF as

$$f(\mathcal{E}) \sim \frac{\gamma C \mathrm{B}(\gamma, 1/2)}{\sqrt{8}\pi^2\mu^\gamma}\left(\gamma - \frac{1}{2}\right)\mathcal{E}^{\gamma-3/2}\,. \tag{A.25}$$

It is clear that f becomes negative for $\gamma \in]0, 1/2[$, so such models are inconsistent, in the presence of a central BH.

Case $\gamma = 0$

In this case, the first term of the asymptotic expansion of $\tilde{g}(\mathcal{E}, t)$ vanishes, so we would need to keep a higher-order term in the asymptotic expansion. However, if we take the limit for $\gamma \to 0$ of Eq. (A.25), we get

$$f(\mathcal{E}) \sim -\frac{C}{4\sqrt{2}\pi^2}\mathcal{E}^{-3/2}\,. \tag{A.26}$$

Hence, untruncated systems with finite central density, namely, with $\rho(r) \sim C\,r^0 = C$, are inconsistent, too.

This proof may seem a bit unsatisfactory from a mathematical point of view. I provide a fairly more rigorous proof in Theorem A.2, for the special case of the so-called *regular profiles*, which can be easily extended to other kinds of density profiles with finite central density. Furthermore, one can show that $\mathrm{d}\ln\rho/\mathrm{d}\ln r = 0$ at the centre of all models with finite central density, so Eq. (A.16) proves the inconsistency of such models if they are isotropic and host a central BH.

Case $\gamma = 1/2$

In this case, the leading term of the asymptotic expansion in Eq. (A.25) vanishes. Therefore, the second term of the expansion of $\rho(r)$ for $r \to 0$ is needed to compute the asymptotic expansion of $f(\mathcal{E})$ as $\mathcal{E} \to \infty$. This term, in principle, might change case by case, so, without any further hypothesis on the asymptotic behaviour of $\rho(r)$, I was not able to establish the sign of $f(\mathcal{E})$ at high relative energies in a fully general way, when $\rho(r) \sim C\,r^{-1/2}$.

However, the fact that isotropic γ-models with a central BH and $\gamma = 1/2$ are consistent (see Figures 2.2 and 2.4 and Eq. A.13) shows that, in general, an isotropic system with $\rho(r) \sim C\,r^{-1/2}$ is not necessarily inconsistent if it hosts a BH at its centre, since γ-models with $\gamma = 1/2$ have this asymptotic behaviour.

□

Remark A.2.1. Note that the theorem holds even if $\mathcal{E}_\mathrm{t} \equiv \Psi_\mathrm{T}(r_\mathrm{t}) \geq 0$, that is, for truncated systems having $\rho(r) = 0$ for $r > r_\mathrm{t}$. In this case, the only relevant modification is that the lower limit of the integral in Eq. (A.24) is $A(\mathcal{E}_\mathrm{t}) = \mu/(\mathcal{E}_\mathrm{t} r_\mathrm{t})$ instead of zero. This does not affect the sign of the asymptotic expansion of the DF because the integral remains positive, but the expressions given in Eqs. (A.25) and (A.26) are no longer valid.

I now provide a proof of the fact that regular density profiles cannot host a central

BH, if their dynamical structure is isotropic. Regular density profiles are those for which $\rho(r) \sim \rho_0 - Ar^2$, as $r \to 0$, with $A \equiv -\,\mathrm{d}^2\rho/\mathrm{d}r^2\big|_{r=0} > 0$. This family of density profiles include important models such as the Plummer sphere (Section 2.2, and references therein) and the perfect sphere (spherical limit of the perfect ellipsoid; Eq. 36 of de Zeeuw & Lynden-Bell 1985).

Theorem A.2. *Ergodic spherical models with regular density profiles are inconsistent in the presence of a central BH.*

Proof. The proof relies again on the derivation of the asymptotic behaviour of $f(\mathcal{E})$ in the limit as $\mathcal{E} \to \infty$. First, let us call $J(\mathcal{E})$ the integral in Eq. (1.16a):

$$J(\mathcal{E}) \equiv \int_{\mathcal{E}_\mathrm{t}}^{\mathcal{E}} \frac{\mathrm{d}\rho}{\mathrm{d}\Psi_\mathrm{T}} \frac{\mathrm{d}\Psi_\mathrm{T}}{\sqrt{\mathcal{E}-\Psi_\mathrm{T}}}. \tag{A.27}$$

It is convenient to split it as $J(\mathcal{E}) = J_1(\mathcal{E}) + J_2(\mathcal{E})$, where

$$J_1(\mathcal{E}) \equiv \int_{\mathcal{E}_\mathrm{t}}^{a} \frac{\mathrm{d}\rho}{\mathrm{d}\Psi_\mathrm{T}} \frac{\mathrm{d}\Psi_\mathrm{T}}{\sqrt{\mathcal{E}-\Psi_\mathrm{T}}}, \tag{A.28}$$

$$J_2(\mathcal{E}) \equiv \int_{a}^{\mathcal{E}} \frac{\mathrm{d}\rho}{\mathrm{d}\Psi_\mathrm{T}} \frac{\mathrm{d}\Psi_\mathrm{T}}{\sqrt{\mathcal{E}-\Psi_\mathrm{T}}}, \tag{A.29}$$

with $a \in]\mathcal{E}_\mathrm{t}, \mathcal{E}[$. Now, we will examine the two terms separately. All the asymptotic expansions below are meant to be in the limit as $\mathcal{E} \to \infty$.

The term J_1 depends on $\mathcal{E}$ only in the integrand, so when applying the derivative, we get

$$\begin{aligned} \frac{\mathrm{d}J_1}{\mathrm{d}\mathcal{E}} &= -\frac{1}{2}\int_{\mathcal{E}_\mathrm{t}}^{a} \frac{\mathrm{d}\rho}{\mathrm{d}\Psi_\mathrm{T}} \frac{\mathrm{d}\Psi_\mathrm{T}}{(\mathcal{E}-\Psi_\mathrm{T})^{3/2}} = -\frac{1}{2}\mathcal{E}^{-3/2}\int_{\mathcal{E}_\mathrm{t}}^{a} \frac{\mathrm{d}\rho}{\mathrm{d}\Psi_\mathrm{T}} \frac{\mathrm{d}\Psi_\mathrm{T}}{(1-\Psi_\mathrm{T}/\mathcal{E})^{3/2}} \\ &\sim -\frac{1}{2}\mathcal{E}^{-3/2}\int_{\mathcal{E}_\mathrm{t}}^{a} \frac{\mathrm{d}\rho}{\mathrm{d}\Psi_\mathrm{T}}\mathrm{d}\Psi_\mathrm{T} = -\left.\frac{\rho(\Psi_\mathrm{T})}{2\mathcal{E}^{3/2}}\right|_{\Psi_\mathrm{T}=a} < 0, \end{aligned} \tag{A.30}$$

where I used the fact that $\rho(\Psi_\mathrm{T}) \to 0$, as $\Psi_\mathrm{T} \to \mathcal{E}_\mathrm{t}$, which is true for all $\mathcal{E}_\mathrm{t} > 0$ by definition, and for all physically meaningful (untruncated) models with $\mathcal{E}_\mathrm{t} = 0$ (recall that, in the adopted convention, $\Psi_\mathrm{T} \to 0$ at $r \to \infty$).

For the J_2 term, it is convenient to change the integration variable to $t = \Psi_\mathrm{T}/\mathcal{E}$:

$$J_2(\mathcal{E}) = \sqrt{\mathcal{E}}\int_{a/\mathcal{E}}^{1} \left.\frac{\mathrm{d}\rho}{\mathrm{d}\Psi_\mathrm{T}}\right|_{\Psi_\mathrm{T}=\mathcal{E}t} \frac{\mathrm{d}t}{(1-t)^{1/2}}. \tag{A.31}$$

Note that a is fixed, but we can choose it arbitrarily large because $\mathcal{E} \to \infty$. Therefore, the argument of $\mathrm{d}\rho/\mathrm{d}\Psi_\mathrm{T}$ in the integral of Eq. (A.31), which ranges between a and $\mathcal{E}$,

is always very large, and we can substitute the integrand with its asymptotic expansion for $\Psi_{\rm T} \to \infty$.

A regular density profile is defined to have $\rho(r) \sim \rho_0 - Ar^2$ at the centre, where ρ_0 is the central density and $A \equiv -\,\mathrm{d}^2\rho/\mathrm{d}r^2|_{r=0} > 0$. Given that μ is the BH's mass, $\Psi_{\rm T} \sim \mu/r$, as $r \to 0$. We can then conclude that $\rho(\Psi_{\rm T}) \sim \rho_0 - A\,(\mu/\Psi_{\rm T})^2$, as $\Psi_{\rm T} \to \infty$. Therefore, $\mathrm{d}\rho/\mathrm{d}\Psi_{\rm T} \sim 2A\mu^2\Psi_{\rm T}^{-3}$, as $\Psi_{\rm T} \to \infty$. Hence, in the limit as $\mathcal{E} \to \infty$, we can write

$$\begin{aligned} J_2(\mathcal{E}) \sim & \frac{2A\mu^2}{\mathcal{E}^{5/2}} \int_{a/\mathcal{E}}^{1} \frac{\mathrm{d}t}{t^3\sqrt{1-t}} \\ = & \frac{A\mu^2}{4a^2\mathcal{E}^{5/2}} \left\{ 6a\sqrt{\mathcal{E}(\mathcal{E}-a)} + 4\sqrt{\mathcal{E}^3(\mathcal{E}-a)} \right. \\ & \left. + 3a^2 \left[\ln\mathcal{E} + 2\ln\left(1+\sqrt{1-\frac{a}{\mathcal{E}}}\right) - \ln a \right] \right\}. \end{aligned} \tag{A.32}$$

Considering only the leading term of the expansion, one gets

$$J_2(\mathcal{E}) \sim \frac{A\mu^2}{a^2\sqrt{\mathcal{E}}}. \tag{A.33}$$

Therefore, using Eq. (A.30) and differentiating Eq. (A.33) with respect to $\mathcal{E}$, we can write

$$\begin{aligned} \frac{\mathrm{d}J}{\mathrm{d}\mathcal{E}} \sim & -\left.\frac{\rho(\Psi_{\rm T})}{2\mathcal{E}^{3/2}}\right|_{\Psi_{\rm T}=a} - \frac{A\mu^2}{2a^2\mathcal{E}^{3/2}} \\ = & -\frac{1}{2}\mathcal{E}^{-3/2}\left[\rho(\Psi_{\rm T})|_{\Psi_{\rm T}=a} + \frac{A\mu^2}{a^2}\right] < 0. \end{aligned} \tag{A.34}$$

This proves Theorem A.2 because it entails that the DF, given by $f(\mathcal{E}) = (\sqrt{8}\pi^2)^{-1}\,(\mathrm{d}J/\mathrm{d}\mathcal{E})\,\theta(\mathcal{E}-\mathcal{E}_{\rm t})$, is not positive definite.

□

Remark A.2.2. A similar procedure can be carried out to assess the sign of $f(\mathcal{E})$ at high relative energies for other kinds of asymptotically constant density profiles. The main difference will be in the integral to compute in Eq. (A.32).

A similar result holds for another kind of density profiles: those with a logarithmic divergence in the centre. Although this may seem a rather peculiar example, note that this is the case of, e.g., the Sérsic profile with Sérsic index $n = 1$ (see Eq. 2.23).

Theorem A.3. *Consider an ergodic spherical system hosting a central BH of arbitrary mass $\mu > 0$. If the density profile of the system is asymptotic to $A\ln(1/r)$, as $r \to 0$, with A being a positive constant, then the system is inconsistent.*

Proof. Following the same procedure as the one for Theorem A.1, one would get that,

for untruncated systems, $J(\mathcal{E}) \propto \int_0^1 t^{-1}(1-t)^{-1/2}\mathrm{d}t$, as $\mathcal{E} \to \infty$, which is a divergent integral. Hence, a different approach is needed, analogous to that described in the proof of Theorem A.2.

Let us split Eq. (A.27) as $J(\mathcal{E}) = J_1(\mathcal{E}) + J_2(\mathcal{E})$, with J_1 and J_2 defined as in Eqs. (A.28) and (A.29). The derivative of the J_1 term is then given by Eq. (A.30), while J_2 can be written as in Eq. (A.31). Since $\rho(r) \sim A\ln(1/r)$, as $r \to 0$, then $\rho(\Psi_\mathrm{T}) \sim A\ln(\Psi_\mathrm{T}/\mu)$, as $\Psi_\mathrm{T} \to \infty$. As in the proof of Theorem A.2, we assume a is arbitrarily large, but fixed. Thus, we can write

$$\begin{aligned} J_2(\mathcal{E}) &\sim \frac{A}{\sqrt{\mathcal{E}}}\int_{a/\mathcal{E}}^1 \frac{\mathrm{d}t}{t\sqrt{1-t}} \\ &= \frac{A}{\sqrt{\mathcal{E}}}\left[\ln\mathcal{E} + 2\ln\left(1+\sqrt{1-\frac{a}{\mathcal{E}}}\right) - \ln a\right] \\ &\sim A\mathcal{E}^{-1/2}\ln\mathcal{E}. \end{aligned} \tag{A.35}$$

Therefore, differentiating the final expression of Eq. (A.35) and summing with $\mathrm{d}J_1/\mathrm{d}\mathcal{E}$ in Eq. (A.30), one gets

$$\frac{\mathrm{d}J}{\mathrm{d}\mathcal{E}} \sim -\frac{\rho(\Psi_\mathrm{T})}{2\mathcal{E}^{3/2}}\bigg|_{\Psi_\mathrm{T}=a} + \frac{A}{\mathcal{E}^{3/2}} - A\frac{\ln\mathcal{E}}{2\mathcal{E}^{3/2}} \sim -A\frac{\ln\mathcal{E}}{2\mathcal{E}^{3/2}} < 0. \tag{A.36}$$

Since $f(\mathcal{E}) = (\sqrt{8}\pi^2)^{-1}\,(\mathrm{d}J/\mathrm{d}\mathcal{E})\,\theta(\mathcal{E}-\mathcal{E}_\mathrm{t})$, this proves Theorem A.3.

□

A.3 Weak Sufficient Condition for the Consistency of Osipkov-Merritt Models with Central Black Hole

As proven by Ciotti & Pellegrini (1992) (see also Ciotti 2021, Ch. 14), the k-th consistent component of a spatially untruncated, multi-component system with OM anisotropy (see Section 1.2.4) must satisfy the necessary condition (NC)

$$\frac{\mathrm{d}\varrho_k}{\mathrm{d}r} \leq 0\,, \quad \forall r \in [0,\infty[\,, \tag{A.37}$$

where $\varrho_k \equiv \rho_k[1+(r/r_{\mathrm{a}k})^2]$ is the augmented density, ρ_k is the density profile of the k-th component and $r_{\mathrm{a}k}$ is the corresponding anisotropy radius. Note that the NC depends exclusively on ρ_k and $r_{\mathrm{a}k}$, so its validity is unaffected by the other components or by any external potential. A sufficient condition for the consistency of this k-th component,

provided that it satisfies the NC is

$$\frac{\mathrm{d}}{\mathrm{d}r}\left[\frac{\mathrm{d}\varrho_k}{\mathrm{d}r}\frac{r^2}{M_\mathrm{T}(r)}\right] \geq 0, \quad \forall r \in [0,\infty[\,, \tag{A.38}$$

where $M_\mathrm{T}(r) = M_\mathrm{ext}(r) + \sum_k M_k(r)$ is the total cumulative mass profile. Eq. (A.38) is called the weak sufficient condition (WSC).

In this section, I provide a generalisation of a theorem stated by Ciotti & Ziaee Lorzad (2018), saying that if a component of an OM model (1) is consistent in the self-gravitating case and (2) satisfies the WSC in the BH-dominated case (limit for infinite mass of a central BH), then it is consistent for all finite BH's masses. Below, I prove that if a multi-component OM model with a central BH has a component satisfying the WSC in the BH-dominated case (and the NC), then the WSC is satisfied for *all* finite (and null) BH's masses by that component, and vice versa.

Theorem A.4. *If a mass component belongs to a spatially untruncated, multi-component OM model with a central BH of mass μ and satisfies the NC, then it satisfies the WSC when $\mu \to \infty$ (BH-dominated case) if and only if it satisfies the WSC for all $\mu \in [0,\infty[$.*[1]

Proof. Suppose that the system is made by n components with mass density profiles $\rho_i(r)$ and cumulative mass profiles $M_i(r)$ (Eq. 1.15). Call $M(r) = \sum_{i=1}^n M_i(r)$ the cumulative stellar mass profile and suppose μ is finite, i.e., $\mu \in [0,\infty[$. Then, for the k-th component, let us define

$$a(r) \equiv \frac{\mathrm{d}\varrho_k}{\mathrm{d}r} r^2, \quad b(r,\mu) \equiv \frac{1}{M_\mathrm{T}(r,\mu)} = \frac{1}{M(r)+\mu}\,, \tag{A.39}$$

with $k \in \{1,\ldots,n\}$. The WSC for the k-th component now reads

$$\frac{\partial}{\partial r}\left[a(r)b(r,\mu)\right] \geq 0, \quad \forall r \in [0,\infty[. \tag{A.40}$$

In the following, I will omit the interval in which r is contained, which is always $[0,\infty[$ because we consider spatially untruncated systems.

From the NC (Eq. A.37), we know that $a(r) \leq 0$ for all r. Moreover, it is obvious from its definition that $b(r) > 0$ for all r. Now, let us suppose that the WSC holds for all $\mu \in [0,\infty[$. This is equivalent to writing

$$\frac{\partial}{\partial r}\left[a(r)b(r,\mu)\right] \geq 0, \quad \forall r,\, \forall \mu \iff a'(r) \geq -\frac{a(r)}{b(r,\mu)}\frac{\partial b(r,\mu)}{\partial r}, \quad \forall r,\, \forall \mu\,, \tag{A.41}$$

[1] This includes the self-gravitating case when setting $\mu = 0$.

where the second inequality has been obtained using Leibniz's product rule. Such inequality is satisfied for all μ if and only if its left-hand side (LHS) is larger than or equal to the maximum value of its RHS with respect to μ, since the former is independent of μ. Hence, the statement in Eq. (A.41) is equivalent to

$$a'(r) \geq -a(r) \sup_{\mu\in[0,\infty[} \left[\frac{1}{b(r,\mu)}\frac{\partial b(r,\mu)}{\partial r}\right], \quad \forall r\,, \tag{A.42}$$

where $-a(r)$ exits the sup operator because it is nonnegative and it does not depend on μ. From Eq. (A.39), it is easy to compute that

$$\frac{1}{b(r,\mu)}\frac{\partial b(r,\mu)}{\partial r} = -\frac{4\pi\rho(r)r^2}{M(r)+\mu}, \tag{A.43}$$

where $\rho = \sum_{i=1}^{n}\rho_i$. The RHS of Eq. (A.43) is always non-positive, so also the sup of $(b^{-1})(\partial b/\partial r)$ is smaller than or equal to zero. Since $(b^{-1})(\partial b/\partial r) \to 0$, as $\mu \to \infty$, then

$$\sup_{\mu\in[0,\infty[}\left[(b^{-1})(\partial b/\partial r)\right] = \lim_{\mu\to\infty}\left[(b^{-1})(\partial b/\partial r)\right] = 0. \tag{A.44}$$

Therefore, the WSC is satisfied for all $\mu \in [0,\infty[$ if and only if

$$a'(r) \geq 0, \quad \forall r\,. \tag{A.45}$$

In fact, this is equivalent to the WSC in the BH-dominated case because, since at any radius $\mu \gg M(r)$, Eq. (A.38) effectively becomes

$$\frac{\partial}{\partial r}\left[\frac{\mathrm{d}\varrho_k}{\mathrm{d}r}\frac{r^2}{\mu}\right] = \frac{1}{\mu}\frac{\mathrm{d}}{\mathrm{d}r}\left[\frac{\mathrm{d}\varrho_k}{\mathrm{d}r}r^2\right] \geq 0, \quad \forall r \iff a'(r) \geq 0, \quad \forall r\,. \tag{A.46}$$

To summarise, we can conclude that

$$\frac{\mathrm{d}}{\mathrm{d}r}\left[\frac{\mathrm{d}\varrho_k}{\mathrm{d}r}\frac{r^2}{M_{\mathrm{T}}(r)}\right] \geq 0, \quad \forall r\in[0,\infty[, \forall\mu\in[0,\infty[\iff \frac{\mathrm{d}}{\mathrm{d}r}\left[\frac{\mathrm{d}\varrho_k}{\mathrm{d}r}r^2\right] \geq 0, \quad \forall r\in[0,\infty[\,. \tag{A.47}$$

This proves Theorem A.4.

□

Remark A.3.1. The most important implication of this theorem is that if a component of an OM model satisfies the WSC in the BH-dominated case, then it is consistent when hosting a central BH of whatever finite mass, and when it is not hosting any BH at all.

Remark A.3.2. Theorem A.4 proves that the components of OM models which satisfy the WSC in the BH-dominated case satisfy it for all BH masses and in the self-gravitating case. Still, there could exist components that do not satisfy the WSC for $\mu \to \infty$, but do satisfy it for *some* (but not all!) $\mu \in [0, \infty[$.

To conclude, it is interesting to qualitatively explain why this result holds. For Eq. (A.38) to be satisfied, it means that

$$\frac{\mathrm{d}|a(r)|/\mathrm{d}r}{|a(r)|} \leq \frac{\mathrm{d}M_{\mathrm{T}}/\mathrm{d}r}{M_{\mathrm{T}}(r)}\,, \quad \forall r, \tag{A.48}$$

where $a(r)$ is given in Eq. (A.39), and I used the fact that $|a(r)| = -a(r)$, due to the NC. Also, we know that the RHS is non-negative. Therefore, Eq. (A.48) is satisfied when the relative increase of $|a(r)|$ is slower than or equal to that of $M_{\mathrm{T}}(r)$ at every radius, or when $|a(r)|$ decreases with radius (or stays constant). It follows that the condition is 'more difficultly' satisfied when the RHS is lower.

When considering a central BH of mass μ, $M_{\mathrm{T}}(r) = M(r) + \mu$, where $M(r)$ is the cumulative stellar mass profile and μ is the BH's mass. Clearly, the 'worst-case scenario' is when the RHS vanishes, i.e., when $\mu \to \infty$. Therefore, if the condition in Eq. (A.48) holds in this case, it follows that it holds in every other case.

Bibliography

Abbott, R., Abbott, T. D., Abraham, S., et al. 2020, The Astrophysical Journal Letters, 900, L13, doi: 10.3847/2041-8213/aba493

An, J. H., & Evans, N. W. 2006, The Astrophysical Journal, 642, 752, doi: 10.1086/501040

Aros, F. I., Sippel, A. C., Mastrobuono-Battisti, A., et al. 2020, Monthly Notices of the Royal Astronomical Society, 499, 4646, doi: 10.1093/mnras/staa2821

Bañares-Hernández, A., Calore, F., Martin Camalich, J., & Read, J. I. 2025, Astronomy and Astrophysics, 693, A104, doi: 10.1051/0004-6361/202451763

Baes, M. 2022, Astronomy and Astrophysics, 667, A47, doi: 10.1051/0004-6361/202244567

Baes, M., Dejonghe, H., & Buyle, P. 2005, Astronomy and Astrophysics, 432, 411, doi: 10.1051/0004-6361:20041907

Baes, M., & van Hese, E. 2007, Astronomy and Astrophysics, 471, 419, doi: 10.1051/0004-6361:20077672

Bahcall, J. N., & Wolf, R. A. 1976, The Astrophysical Journal, 209, 214, doi: 10.1086/154711

Barmby, P., McLaughlin, D. E., Harris, W. E., Harris, G. L. H., & Forbes, D. A. 2007, The Astronomical Journal, 133, 2764, doi: 10.1086/516777

Battaglia, G., & Nipoti, C. 2022, Nature Astronomy, 6, 659, doi: 10.1038/s41550-022-01638-7

Baumgardt, H. 2017, Monthly Notices of the Royal Astronomical Society, 464, 2174, doi: 10.1093/mnras/stw2488

Baumgardt, H., Makino, J., & Ebisuzaki, T. 2004a, The Astrophysical Journal, 613, 1133, doi: 10.1086/423298

—. 2004b, The Astrophysical Journal, 613, 1143, doi: 10.1086/423299

Baumgardt, H., Makino, J., & Hut, P. 2005, The Astrophysical Journal, 620, 238, doi: 10.1086/426893

Bianchini, P., van der Marel, R. P., del Pino, A., et al. 2018, Monthly Notices of the Royal Astronomical Society, 481, 2125, doi: 10.1093/mnras/sty2365

Bianchini, P., Varri, A. L., Bertin, G., & Zocchi, A. 2013, The Astrophysical Journal, 772, 67, doi: 10.1088/0004-637X/772/1/67

Binney, J., & Tremaine, S. 2008, Galactic Dynamics: Second Edition, second edition edn. (Princeton, NJ Oxford: Princeton University Press)

Caon, N., Capaccioli, M., & D'Onofrio, M. 1993, Monthly Notices of the Royal Astronomical Society, 265, 1013, doi: 10.1093/mnras/265.4.1013

Cappellari, M., Scott, N., Alatalo, K., et al. 2013, Monthly Notices of the Royal Astronomical Society, 432, 1709, doi: 10.1093/mnras/stt562

Ciotti, L. 1991, Astronomy and Astrophysics, 249, 99

—. 1996, The Astrophysical Journal, 471, 68, doi: 10.1086/177954

—. 1999, The Astrophysical Journal, 520, 574, doi: 10.1086/307478

—. 2021, Introduction to Stellar Dynamics (Cambridge: Cambridge University Press), doi: 10.1017/9780511736117

Ciotti, L., & Morganti, L. 2009, Monthly Notices of the Royal Astronomical Society, 393, 179, doi: 10.1111/j.1365-2966.2008.14187.x

—. 2010a, Monthly Notices of the Royal Astronomical Society, 401, 1091, doi: 10.1111/j.1365-2966.2009.15697.x

—. 2010b, Monthly Notices of the Royal Astronomical Society, 408, 1070, doi: 10.1111/j.1365-2966.2010.17184.x

Ciotti, L., & Morganti, L. 2010c, in Plasmas in the Laboratory and the Universe: Interactions, Patterns, and Turbulence, Vol. 1242 (eprint: arXiv:1001.3632: AIP), 300–305, doi: 10.1063/1.3460138

Ciotti, L., & Pellegrini, S. 1992, Monthly Notices of the Royal Astronomical Society, 255, 561, doi: 10.1093/mnras/255.4.561

Ciotti, L., & Ziaee Lorzad, A. 2018, Monthly Notices of the Royal Astronomical Society, 473, 5476, doi: 10.1093/mnras/stx2771

Cipollina, M., & Bertin, G. 1994, Astronomy and Astrophysics, 288, 43

Cuddeford, P. 1991, Monthly Notices of the Royal Astronomical Society, 253, 414, doi: 10.1093/mnras/253.3.414

Cuddeford, P., & Louis, P. 1995, Monthly Notices of the Royal Astronomical Society, 275, 1017, doi: 10.1093/mnras/275.4.1017

de Bruijne, J. H. J., van der Marel, R. P., & de Zeeuw, P. T. 1996, Monthly Notices of the Royal Astronomical Society, 282, 909, doi: 10.1093/mnras/282.3.909

de Zeeuw, P. T., & Lynden-Bell, D. 1985, Monthly Notices of the Royal Astronomical Society, 215, 713, doi: 10.1093/mnras/215.4.713

Dehnen, W. 1993, Monthly Notices of the Royal Astronomical Society, 265, 250, doi: 10.1093/mnras/265.1.250

Dejonghe, H. 1986, Physics Reports, 133, 217, doi: 10.1016/0370-1573(86)90098-0

Della Croce, A., Pascale, R., Giunchi, E., et al. 2024, Astronomy and Astrophysics, 682, A22, doi: 10.1051/0004-6361/202347569

Eddington, A. S. 1916, Monthly Notices of the Royal Astronomical Society, 76, 572, doi: 10.1093/mnras/76.7.572

Einasto, J. 1965, Trudy Astrofizicheskogo Instituta Alma-Ata, 5, 87

Frank, J., & Rees, M. J. 1976, Monthly Notices of the Royal Astronomical Society, 176, 633, doi: 10.1093/mnras/176.3.633

Freeman, K. C. 1993, in The Globular Cluster-Galaxy Connection, Vol. 48, 608

Fricke, W. 1952, Astronomische Nachrichten, 280, 193, doi: 10.1002/asna.19522800502

Genzel, R., Eisenhauer, F., & Gillessen, S. 2024, The Astronomy and Astrophysics Review, 32, 3, doi: 10.1007/s00159-024-00154-z

Giacconi, R., Gursky, H., Paolini, F. R., & Rossi, B. B. 1962, Physical Review Letters, 9, 439, doi: 10.1103/PhysRevLett.9.439

Gieles, M., & Zocchi, A. 2015, Monthly Notices of the Royal Astronomical Society, 454, 576, doi: 10.1093/mnras/stv1848

Giersz, M., Leigh, N., Hypki, A., Lützgendorf, N., & Askar, A. 2015, Monthly Notices of the Royal Astronomical Society, 454, 3150, doi: 10.1093/mnras/stv2162

Greene, J. E., Strader, J., & Ho, L. C. 2020, Annual Review of Astronomy and Astrophysics, 58, 257, doi: 10.1146/annurev-astro-032620-021835

Häberle, M., Neumayer, N., Seth, A., et al. 2024, Nature, 631, 285, doi: 10.1038/s41586-024-07511-z

Hamilton, C., Fouvry, J.-B., Binney, J., & Pichon, C. 2018, Monthly Notices of the Royal Astronomical Society, 481, 2041, doi: 10.1093/mnras/sty2295

Harris, W. E. 1996, The Astronomical Journal, 112, 1487, doi: 10.1086/118116

Hunter, C., & Qian, E. 1993, Monthly Notices of the Royal Astronomical Society, 262, 401, doi: 10.1093/mnras/262.2.401

Jeans, J. H. 1915, Monthly Notices of the Royal Astronomical Society, 76, 70, doi: 10.1093/mnras/76.2.70

Kamann, S., Husser, T. O., Brinchmann, J., et al. 2016, Astronomy and Astrophysics, 588, A149, doi: 10.1051/0004-6361/201527065

Kamann, S., Husser, T. O., Dreizler, S., et al. 2018, Monthly Notices of the Royal Astronomical Society, 473, 5591, doi: 10.1093/mnras/stx2719

King, I. R. 1966, The Astronomical Journal, 71, 64, doi: 10.1086/109857

Lanzoni, B., Dalessandro, E., Ferraro, F. R., et al. 2007, The Astrophysical Journal, 668, L139, doi: 10.1086/522927

Lanzoni, B., Mucciarelli, A., Origlia, L., et al. 2013, The Astrophysical Journal, 769, 107, doi: 10.1088/0004-637X/769/2/107

Lightman, A. P., & Shapiro, S. L. 1977, The Astrophysical Journal, 211, 244, doi: 10.1086/154925

Lin, D. N. C., & Tremaine, S. 1980, The Astrophysical Journal, 242, 789, doi: 10.1086/158513

Lynden-Bell, D. 1960, Monthly Notices of the Royal Astronomical Society, 120, 204, doi: 10.1093/mnras/120.3.204

—. 1962a, Monthly Notices of the Royal Astronomical Society, 124, 1, doi: 10.1093/mnras/124.1.1

—. 1962b, Monthly Notices of the Royal Astronomical Society, 123, 447, doi: 10.1093/mnras/123.5.447

Madau, P., & Haardt, F. 2015, The Astrophysical Journal, 813, L8, doi: 10.1088/2041-8205/813/1/L8

Magorrian, J., Tremaine, S., Richstone, D., et al. 1998, The Astronomical Journal, 115, 2285, doi: 10.1086/300353

Mann, C. R., Richer, H., Heyl, J., et al. 2019, The Astrophysical Journal, 875, 1, doi: 10.3847/1538-4357/ab0e6d

Merritt, D. 1985, The Astronomical Journal, 90, 1027, doi: 10.1086/113810

—. 2013, Dynamics and Evolution of Galactic Nuclei (Princeton University Press)

Meylan, G., & Heggie, D. C. 1997, Astronomy and Astrophysics Review, 8, 1, doi: 10.1007/s001590050008

Mezcua, M. 2017, International Journal of Modern Physics D, 26, 1730021, doi: 10.1142/S021827181730021X

Michie, R. W. 1963, Monthly Notices of the Royal Astronomical Society, 125, 127, doi: 10.1093/mnras/125.2.127

Miller, M. C., & Hamilton, D. P. 2002, Monthly Notices of the Royal Astronomical Society, 330, 232, doi: 10.1046/j.1365-8711.2002.05112.x

Miocchi, P. 2007, Monthly Notices of the Royal Astronomical Society, 381, 103, doi: 10.1111/j.1365-2966.2007.12165.x

Miocchi, P., Lanzoni, B., Ferraro, F. R., et al. 2013, The Astrophysical Journal, 774, 151, doi: 10.1088/0004-637X/774/2/151

Osipkov, L. P. 1979, Soviet Astronomy Letters, 5, 42

Paynter, J., Webster, R., & Thrane, E. 2021, Nature Astronomy, 5, 560, doi: 10.1038/s41550-021-01307-1

Peebles, P. J. E. 1972, The Astrophysical Journal, 178, 371, doi: 10.1086/151797

Peterson, C. J., & King, I. R. 1975, The Astronomical Journal, 80, 427, doi: 10.1086/111759

Plummer, H. C. 1911, Monthly Notices of the Royal Astronomical Society, 71, 460, doi: 10.1093/mnras/71.5.460

Portegies Zwart, S. F., & McMillan, S. L. W. 2002, The Astrophysical Journal, 576, 899, doi: 10.1086/341798

Qian, E. E., de Zeeuw, P. T., van der Marel, R. P., & Hunter, C. 1995, Monthly Notices of the Royal Astronomical Society, 274, 602, doi: 10.1093/mnras/274.2.602

Schmidt, M. 1963, Nature, 197, 1040, doi: 10.1038/1971040a0

Schwarzschild, K. 1916, Abh. Konigl. Preuss. Akad. Wissenschaften Jahre 1906,92, Berlin,1907, 1916, 189

Sérsic, J. L. 1968, Atlas de Galaxias Australes

Sesana, A., Gair, J., Berti, E., & Volonteri, M. 2011, Physical Review D, 83, 044036, doi: 10.1103/PhysRevD.83.044036

The LIGO Scientific Collaboration, the Virgo Collaboration, & the KAGRA Collaboration. 2025, GW231123: A Binary Black Hole Merger with Total Mass 190-265 M$\odot$, arXiv, doi: 10.48550/arXiv.2507.08219

Tremaine, S., Richstone, D. O., Byun, Y.-I., et al. 1994, The Astronomical Journal, 107, 634, doi: 10.1086/116883

Tremou, E., Strader, J., Chomiuk, L., et al. 2018, The Astrophysical Journal, 862, 16, doi: 10.3847/1538-4357/aac9b9

Trenti, M., Ardi, E., Mineshige, S., & Hut, P. 2007, Monthly Notices of the Royal Astronomical Society, 374, 857, doi: 10.1111/j.1365-2966.2006.11189.x

van der Marel, R. P., & Anderson, J. 2010, The Astrophysical Journal, 710, 1063, doi: 10.1088/0004-637X/710/2/1063

Van Hese, E., Baes, M., & Dejonghe, H. 2011, The Astrophysical Journal, 726, 80, doi: 10.1088/0004-637X/726/2/80

Vasiliev, E. 2018, Agama Reference Documentation, arXiv, doi: 10.48550/arXiv.1802.08255

Vesperini, E., & Trenti, M. 2010, The Astrophysical Journal, 720, L179, doi: 10.1088/2041-8205/720/2/L179

Wang, J., Bose, S., Frenk, C. S., et al. 2020, Nature, 585, 39, doi: 10.1038/s41586-020-2642-9

White, R. E., & Shawl, S. J. 1987, The Astrophysical Journal, 317, 246, doi: 10.1086/165273

White, S. D. M. 1981, Monthly Notices of the Royal Astronomical Society, 195, 1037, doi: 10.1093/mnras/195.4.1037

Wu, X.-B., Wang, F., Fan, X., et al. 2015, Nature, 518, 512, doi: 10.1038/nature14241

Zocchi, A., Bertin, G., & Varri, A. L. 2012, Astronomy & Astrophysics, 539, A65, doi: 10.1051/0004-6361/201117977

Zocchi, A., Gieles, M., & Hénault-Brunet, V. 2016a, in Star Clusters and Black Holes in Galaxies across Cosmic Time, Vol. 312, eprint: arXiv:1501.05262, 197–200, doi: 10.1017/S1743921315007802

Zocchi, A., Gieles, M., & Hénault-Brunet, V. 2017, Monthly Notices of the Royal Astronomical Society, 468, 4429, doi: 10.1093/mnras/stx316

—. 2019, Monthly Notices of the Royal Astronomical Society, 482, 4713, doi: 10.1093/mnras/sty1508

Zocchi, A., Gieles, M., Hénault-Brunet, V., & Varri, A. L. 2016b, Monthly Notices of the Royal Astronomical Society, 462, 696, doi: 10.1093/mnras/stw1104